

120  
9-28-92 JS(2)

DOE/BC/14443-12  
(DE92001063)

**A FIELD LABORATORY FOR IMPROVED OIL RECOVERY**

**Final Report**

**By**  
**Alvin F. Hildebrandt**  
**John McDonald**  
**Elmond Claridge**  
**John Killough**

**Performed Under Contract No. FG22-89BC14443**

**University of Houston**  
**Houston, Texas**

---

**Bartlesville Project Office**  
**U. S. DEPARTMENT OF ENERGY**  
**Bartlesville, Oklahoma**

## DISCLAIMER

This report was prepared as an account of work sponsored by an agency of the United States Government. Neither the United States Government nor any agency thereof, nor any of their employees, makes any warranty, express or implied, or assumes any legal liability or responsibility for the accuracy, completeness, or usefulness of any information, apparatus, product, or process disclosed, or represents that its use would not infringe privately owned rights. Reference herein to any specific commercial product, process, or service by trade name, trademark, manufacturer, or otherwise does not necessarily constitute or imply its endorsement, recommendation, or favoring by the United States Government or any agency thereof. The views and opinions of authors expressed herein do not necessarily state or reflect those of the United States Government or any agency thereof.

This report has been reproduced directly from the best available copy.

Available to DOE and DOE contractors from the Office of Scientific and Technical Information, P.O. Box 62, Oak Ridge, TN 37831; prices available from (615)576-8401, FTS 626-8401.

Available to the public from the National Technical Information Service, U.S. Department of Commerce, 5285 Port Royal Rd., Springfield, VA 22161.

DOE/BC/14443-12  
Distribution Category UC-122

A FIELD LABORATORY FOR IMPROVED OIL RECOVERY

Final Report

DOE/BC/14443--12

By

DE92 001063

Alvin F. Hildebrant  
John McDonald  
Elmond Claridge  
John Killough

September 1992

Work Performed Under Contract No. FG22-89BC14443

Prepared for  
U.S. Department of Energy  
Assistant Secretary for Fossil Energy

Rhonda L. Patterson, Project Manager  
Bartlesville Project Office  
P. O. Box 1398  
Bartlesville, OK 74005

Prepared by  
University of Houston  
4800 Calhoun  
Houston, TX 77204-4792

**MASTER**

## TABLE OF CONTENTS

	<b>Page</b>
Table of Contents	iii
List of Figures	iv
Abstract	1-2
Executive Summary	3-7
Site Selection, Seismic Reservoir Definition, High Resolution Surface Seismic (Subtask #1), and Crosshole Seismic Tomography. (Subtask #5) Dr. John McDonald	8-19
Figures 1-6	20-22
Reservoir Rock Structure Determination (Subtask #2), and Simulations of Recovery Processes in Typical Depositional Environments (Subtask #4). Dr. Elmond Claridge	23-43
Figures 7-17	44-54
Developing an Evaluation of Local Flood Efficiency in Different Parts of the Demonstration Reservoir (Subtask #3). Dr. John Killough	55-76
Figures 18-37	77-95
Appendix I: Final Oil and Gas Reservoir Candidate List	96-100
Appendix II: Data on Seventy Six West Field	101

## LIST OF FIGURES

### Discussion 1: Dr. John McDonald

#### **Site Selection, Seismic Reservoir Definition, High Resolution Surface Seismic, and Crosshole Seismic Tomography. (Subtasks #1 & 5)**

	<b>Page</b>
Figure 1: Location of Seventy Six West oil field, site for Field Experiments	20
Figure 2: Oil Production Maps showing Test Well Sites	20
Figure 3: One-Dimensional P-wave Tomogram Between Wells 62-15 and 62-23	21
Figure 4: Bender Data Traces Showing Arrival Times and Relative Amplitudes of Propogated Pulses	21
Figure 5: Variation of Mean Frequency Versus Well Offset for the Bender, Sparker, and Airgun	22
Figure 6: Two-Dimensional P-wave Tomogram Between Wells 62-15 and 62-23	22

### Discussion 2: Dr. Elmond Claridge

#### **Reservoir Rock Structure Determination, and Simulations of Recovery Processes Typical Depositional Environments. (Subtasks #2 & 4)**

	<b>Page</b>
Figure 7: Coastal Barrier Bar Sandstone Reservoir Model	44
Figure 8: Alluvial Point Bar Sandstone Reservoir Model	45
Figure 9: Structure, Seventy Six West Field,, Subzone B	46
Figure 10: Net Sand Map, Subzone B	47
Figure 11: Structure, Seventy Six, West Field, Subzone C	48
Figure 12: Net Sand Map, Subzone C	49
Figure 13: Seventy Six, West Field, Simulation Grid (10 Acre Grid Blocks)	50
Figure 14: Computer Simulation, Primary/Secondary Recovery	51
Figure 15: Pilot 1/4 Five-Spot, Continued Waterflood	52
Figure 16: Computed Oil Recovery and Water Cut Curves for Continued Waterflooding and for a CO <sub>2</sub> - WAG EOR Process With 228 SCF of CO <sub>2</sub> (3% Mol) per Barrel of Water, for a Pilot Test	53

Figure 17:	Comparison of Computed Oil Recovery Curves for a Pilot CO <sub>2</sub> - WAG Flooding Process With Different CO <sub>2</sub> Concentrations in the Injected Stream	54
------------	--	----

**Discussion 3: Dr. John Killough**

**Developing an Evaluation of Local Flood Efficiency in Different Parts of the Demonstration Reservoir. (Subtask #3)**

		<b>Page</b>
Figure 18:	Parallel Computing with Globally Shared Memory	77
Figure 19:	Parallel Computing with Distributed Memory	78
Figure 20:	Flow Chart for Typical Compositional Simulator	79
Figure 21:	Flow Chart for Compositional Simulator with i860 Work Distribution	80
Figure 22:	Schematic Showing the Initial Parallelization	81
Figure 23:	Schematic Showing the Final Parallelization	82
Figure 24:	Schematic of the Domain Decomposition Algorithm	83
Figure 25:	Domain Decomposition Gridblock Communication	84
Figure 26:	Comparison of Block Jacobi DD with Various Techniques for Interface Estimates	85
Figure 27:	The Real Compositional Model Showing Active Cells and Load Imbalances for Each Processor	86
Figure 28:	Schematic of OSMG Technique	87
Figure 29:	Miscible Displacement - Unit Mobility Ratio Concentration Contour Lines	88
Figure 30:	OSMG Method	89
Figure 31:	Effect of Heterogeneity	90
Figure 32:	Boundaries of No Normal Flow	91
Figure 33:	Concentration Contour Lines Miscible Displacement	92
Figure 34:	Semi-variogram for Five Layers of Real Field Permeability Data	93
Figure 35:	Miscible Displacement-Real Field Data Contour Lines	94
Figure 36:	iPSc/2 Speedups for OSMG Method	95

## ABSTRACT

The purpose of Annex III of the Memorandum of Understanding, undertaken by the Houston Petroleum Research Center at the University of Houston, was to develop a field laboratory for research in improved oil recovery using a Gulf Coast reservoir in Texas. The participants: (1) made a field site selection and conducted a high resolution seismic survey in the demonstration field, (2) obtained characteristics of the reservoir, (3) developed an evaluation of local flood efficiency in different parts of the demonstration reservoir, (4) used diverse methodology to evaluate the potential recovery of the remaining oil in the test reservoir, (5) developed cross-well seismic tomography, and (6) will transfer the learned technologies to oil operators through publication and workshops. This abstract is an overview of these tasks.

Each of the research sections listed above are stand-alone works which, when consolidated, give a unique picture of the positive results accomplished with a synergistic approach to the problems of improved oil recovery. The tasks of site selection, high resolution seismic survey, and cross-well seismic tomography were the areas of research of Dr. John McDonald, Department of Geosciences and Director of the Allied Geophysical Laboratories. Dr. Elmond Claridge of the Department of Chemical Engineering, performed the tasks of obtaining the characteristics of the chosen reservoir and, using diverse methodology, evaluating potential oil recovery. The task of Dr. John Killough Department of Chemical Engineering, was the development of high performance computing for improved oil recovery. The report is in order by investigator and, therefore, their tasks. In addition, a more detailed abstract and summary accompanies the discussion of tasks by the individual investigators.

Task one consisted of field site selection and high resolution seismic survey of the demonstration field, and task five considered developing cross-well tomography. High resolution surface and crosshole seismic data have been collected using several energy sources in a shallow, clastic reservoir in south Texas. Results show that a piezoelectric cylindrical bender is not an optimum energy source at typical well spacings in a poorly consolidated environment such as the Seventy Six West field. For a tomographic data set recorded between wells spaced 600 ft, the signal-to-noise ratio was very low and cross-correlation with the input sweep did not readily produce interpretable data records. In a second experiment an airgun was used to successfully record high resolution surface and crosshole data. A one-dimensional P-wave velocity tomogram was constructed using the high resolution surface data. Also, a two-dimensional P-wave

velocity tomogram was constructed from the crosshole data. These tomograms agree well with a sonic log from a nearby well.

Under task two, obtaining reservoir rock characteristics, and task four, simulations of recovery processes for this reservoir, a general study of the effect of reservoir type on enhanced oil recovery processes by use of computer simulation for two types of reservoir the alluvial point bar and the off-shore barrier bar, was performed. The result of this study was to show that the opposite trend of the horizontal permeability with depth for these two types results in improved oil recoveries when the process is one with a less dense fluid injected and/or produced and the permeability is highest at the bottom, and vice-versa. Since this effect is opposite for primary recovery and for a waterflood or for a waterflood and a miscible gas flood or a steam flood, the normal alternating process sequence in either type of reservoir is to give alternating higher and lower recoveries.

It appears that the most likely process which could be used in the Seventy Six West field, which is at shallow depth (1200-1300 feet) and is nearing flood-out with water, is immiscible CO<sub>2</sub> flooding. The results of the simulations are encouraging, in that oil recoveries of 11-12% of original oil in place were calculated with CO<sub>2</sub> requirements which are low by comparison with miscible floods. It is recommended that immiscible CO<sub>2</sub> flooding be pursued.

Over the past fifteen years high performance computing has had a significant impact on the evolution of numerical predictive methods for improved recovery from hydrocarbon reservoirs. The complexity of reservoir simulation models has led to computational requirements that have consistently taxed the fastest computers. The work of task three, development of high performance computing, discusses how current state-of-the-art parallel architectures have been investigated to allow models which more closely approach realistic simulations while emphasizing accuracy and efficiency of the models. Two modeling approaches have been investigated on several different parallel architectures. The first approach involves the porting of existing commercial software to parallel MIMD shared and distributed machines. The second approach considers a novel reformulation of the numerical solution which emphasizes parallel efficiency. Both techniques have been shown to exhibit high parallel efficiencies on a distributed memory parallel computer ( the Intel Supercomputer Systems 860 ) for both real and hypothetical data. These simulation techniques were applied to the prediction of hydrocarbon recovery from the Seventy Six West field. Results showed the validity of predictions using other approaches.

## EXECUTIVE SUMMARY

The Seventy Six West field in Duval county, Texas, was chosen as the demonstration field as part of task one for this project. High resolution surface seismic data and crosshole data were recorded in this producing oil field in south Texas. For task five of the project, developing cross-well seismic tomography, a P-wave velocity tomogram was constructed from crosshole first arrival times for a well spacing of 496 ft using an airgun as the energy source . RVSP data were also recorded using the airgun and geophones in shallow surface holes. Frequencies from 70 to 150 Hz were recorded. These RVSP data were used to construct a one-dimensional tomogram of the interwell region between two wells separated by 1215 ft.

A tomogram produced from the airgun data shows good correlation with a nearby sonic log even though the frequency content of the data is low (70 to 150 Hz) for crosshole data. The airgun is capable of higher frequency output but it appears that problems with the source well contributed to the lowered frequencies.

Tomograms were produced by performing "big" iteration loops consisting of raytracing through a starting velocity model, performing inversion on the traveltimes residuals, and updating the velocity model for the next iteration. The raytracing algorithm is based on work by Moser, 1991 and the inversion uses SVD for the zeroth iteration and constrained LSQR for subsequent iterations.

Correlation results from data acquired with the bender in another crosshole experiment were very good over the full angular range. However, results show that a piezoelectric cylindrical bender is not an optimum energy source at typical well spacings in a poorly consolidated environment such as the Seventy Six West field. We expected results from experiment 4 to be at least as good if not better than results from bender 3; however, this was not the case.

For tasks two and four of the project, obtaining the reservoir characteristics for the Seventy Six West field and utilizing this data for potential improved oil recovery, two principal lines of research were performed, both by use of computer simulation of reservoir oil recovery processes. The first of these concerned a study of primary, secondary, and tertiary oil recovery processes in two main geologic types of oil reservoir rock formations - (a) those formed from ancient alluvial (river bank) sand bars, and (b) those formed from ancient off-shore barrier sand bars (like Galveston Island). The second study concerned a specific oil field in Duval County, Texas - Seventy Six West field - in which the Texas State Land Office holds the mineral rights to over half of the field. This field was chosen for geophysical

and simulation studies because the state was able to provide access to the field for the geophysical studies which are described elsewhere in this report. This field is also one of the series of geologic type fields which were selected by the Texas Bureau of Economic Geology for study as part of a different project called the State Lands Energy Resource Optimization (SLERO) project, hence, data were available from this source on field and rock properties, which could be used in the simulation studies of this particular field. It is of the off-shore barrier-bar type, but its stratigraphy is complicated by the presence of several such bars, displaced laterally and vertically, by a stream mouth, and by sands washed over the top of the bars by storms into the lagoons behind. Such complications in stratigraphy are the rule rather than the exception.

The first study showed the influence of the different vertical trends of horizontal permeability in the alluvial sand bars and in barrier bars - highest permeability at the bottom in the alluvial bars, and highest permeability at the top in the barrier bars - on the oil recovery behavior in primary recovery by pressure depletion, in secondary recovery by waterflooding, and in tertiary recovery by CO<sub>2</sub> flooding, or by steam flooding in the case of heavy oils. Three oil viscosity levels were employed, and so the results reflect the behavior of a variety of crude oils in these reservoir types.

In the primary recovery phase, the alluvial bar type showed much higher oil recovery than the barrier bar type. However, in a waterflood started in each case during primary depletion at a point when the pressure had declined from the initial pressure to about 1100 - 1300 psi, the barrier bar type showed better performance. In a subsequent CO<sub>2</sub> tertiary flood, the additional oil recovery was slightly better for the alluvial point bar type. This was also the case for steam drive, in which only the most viscous oil was assumed to be present. The results accord with the realization that with low density fluids being produced or injected as drive fluids, the better oil recovery is obtained with a permeability profile from high at bottom to low at top, while the reverse is true for an injected fluid more dense than reservoir oil, namely water.

In the study of the Seventy Six West field, a history match was first performed with a three-dimensional grid-block plan covering the entire reservoir plus the aquifer to the southeast. The aquifer size was varied to obtain the observed behavior of the field, namely, that pressure depletion occurred despite partial pressure support from the aquifer, and a secondary gas cap was generated on the high side of the field, to the northwest. A waterflood was started about halfway through the life of the field (to date) and this helped to maintain pressure so as to provide a minimum level of well productivity. Nearly all of the initial dissolved gas had been produced during primary depletion so that the remaining oil contains very little natural

gas. Current average pressure is only a little over 100 psi, versus nearly 600 psi initial. The water cut (from the waterflood) has risen to a relatively high level but the current oil recovery is over 46% of the original oil in place - a relatively high level for primary plus secondary, which can be attributed to the relatively low level of remaining oil saturation in the gas cap, as compared to the waterflood residual oil saturation in the rest of the reservoir. Additional oil recovery is estimated at 4% of the original oil in place. However, this still leaves 1/2 of the original oil in place. Attention was therefore placed on what might be accomplished by a tertiary recovery process. For this purpose, a one-acre pilot test area was selected around one of the better wells. It was assumed that four production wells would be drilled in a five-spot pattern around this well, which would be converted from a producer to an injection well.

The possible choice of enhanced oil recovery processes is limited by the shallow depth of this field, which limits injection pressures to only a little over 500 psi. This is insufficient to obtain miscibility with CO<sub>2</sub> or with any hydrocarbon mixture containing very much natural gas in admixture with LPG. Chemical flooding methods were considered to be too expensive (surfactant-polymer) or to have too little prospect of additional oil (polymer alone). However, there are a few examples reported in the petroleum engineering literature of immiscible CO<sub>2</sub> floods in which sizable additional oil recoveries - up to 10% of original oil or more - were obtained. These were generally at 1000 psi or higher, but it was decided to explore this possibility at the 500 psi level by computer simulation using a 10x10x6 grid simulation model. It was found that best results are obtained, as indicated by the prior publications, by joint injection of water with the CO<sub>2</sub> at such ratios that the excess CO<sub>2</sub> over the amount which would dissolve in the water at the pressure level of 500 psi assumed to be maintained in the pilot area would be in about a 1:1 volume ratio to the water. Much of this excess CO<sub>2</sub> then dissolves in the oil, swelling it somewhat and much reducing its viscosity. These two effects lead to development of an oil bank which is driven by the water to the producing wells. In these simulations with different water:CO<sub>2</sub> ratios, the extra oil recovery reached 10-11% of original oil in place. It is therefore suggested that investigation of the possibility of using this method of extra oil recovery be continued.

The work done on task three, development of computing techniques to evaluate improved oil recovery methods, has demonstrated that a highly efficient parallel model can be generated for a commercial n-component, three-phase, equation-of-state reservoir simulator in a distributed memory parallel computer. A linear equation solver using multigrid, domain decomposition, and z-line corrections can be efficiently parallelized. For a hypothetical case this solver showed performance comparable to serial solutions. In parallel, the solver was significantly faster than serial solvers. For two simulations

involving compositional data, the parallel model performed at computation rates comparable to mainframe supercomputers.

A numerical technique has been developed, that permits the analysis of flow in heterogeneous porous media down to a length scale from a few feet to a few tens of feet with great efficiency.

This method of Operator Splitting on Multiple Grids, for an example of flow in heterogeneous porous media, has been successfully implemented on both Intel Hypercubes, i.e., the 386-based iPSC/2 and the RISC-based iSS/860. An overall parallel efficiency of about 93% was obtained on a 32-node i860 Hypercube.

The modeling techniques described above were used to validate the results of E. Claridge given in tasks two and four for waterflooding and immiscible carbon dioxide injection recoveries for the Seventy Six West field. The first stage of the modeling consisted of matching the results for both waterflooding and immiscible carbon dioxide injection. The 10x10x8 three-dimensional model was reconstructed for the VIP-Comp model. Simulation results closely matched those of Claridge. The validity check of the simulations was performed by a twenty-seven fold refinement of the grid which had been used by Claridge. The 30x30x24 grid was first used to perform waterflood simulations. The results showed that there was little or no effect of grid refinement for the waterflood. Oil recovery for both cases was virtually identical. The simulation for the immiscible carbon dioxide injection case presented a significant modelling challenge. The extremely fine grid caused significant instability problems resulting in extremely small timesteps. Fortunately, the speed of the model calculations allowed the simulations to be performed in a reasonable timeframe. Results for the fine-grid, immiscible carbon dioxide case showed a slight degradation in recovery of about 3%. The reason for this reduction in recovery was that the gravity override of the injected gas could be better captured with the fine detail of the vertical layering. Nonetheless, these results validate those of Claridge; that is, immiscible carbon dioxide injection may result in a significant improvement in oil recovery for the field. Several questions remain to be answered, however. First, better data must be obtained for the field to replace that data which was estimated in this study. Second, the economics of the process should be further investigated with emphasis on pattern spacing, injection rates, and carbon dioxide availability.

Future work planned in the seismic research area includes a project designed to resolve a stratigraphic anomaly by using a combination of two types of seismic data: high resolution 3-D surface seismic and crosshole data. The anomaly occurs in the Cole "C" sands between a producing well and a dry hole. Available surface seismic data shows a loss in reflector continuity corresponding to a loss of production in

the cole "C" sands between the wells. Work proposed is to conduct a high resolution 3-D survey over the anomalous zone and process and interpret the results. In addition, two new holes would be drilled between the present wells to allow recording crosshole seismic data. The tomograms produced from the crosshole data would be used to tie to the 3-D surface data to provide a complete interpretation of the stratigraphic anomaly.

Work planned in reservoir simulation and computerization research involves the implementation of more efficient, but equally parallelizable, domain decomposition and multigrid algorithms. Load balancing issues must be further investigated. The operator splitting method in three-dimensions appears a natural progression of the work toward the solution of more realistic situations.

Technology transfer of these results, as well as discussion of future research programs extending from these findings, is underway. Dr. John McDonald will be making a number of presentations at upcoming meetings organized by the Texas Independent Producers and Royalty Owners association (TIPRO). The first meeting is scheduled for September 1992 and attendance is expected to be over 400.

**Subtask #1: Site Selection, Seismic Reservoir Definition, and High Resolution Surface Seismic**

**Subtask #5: Crosshole Seismic Tomography  
(Dr. John McDonald, Principal Investigator)**

**ABSTRACT**

High resolution surface and crosshole seismic data have been collected using several energy sources in a shallow, clastic reservoir in south Texas. Results show that a piezoelectric cylindrical bender is not an optimum energy source at typical well spacings in a poorly consolidated environment such as the Seventy Six West field. For a tomographic data set recorded between wells spaced 600 ft, the signal-to-noise ratio was very low and cross-correlation with the input sweep did not produce interpretable data records. In a subsequent experiment an airgun was used to record high resolution surface and crosshole data. A one-dimensional P-wave velocity tomogram was constructed using the high resolution surface data. Also, a two-dimensional P-wave velocity tomogram was constructed from the crosshole data. These tomograms agree well with a sonic log from a nearby well.

**Site selection:**

Due to difficulties with a major oil company for the use of one of their fields for our experiments, discussions were completed with the General Land Office Commissioner for use of a state owned field: Seventy Six West field in Duval County, Texas. The location of this field can be found on the Freer NW quadrangle of the USGS topographic series. The field covers sections 61, 62, 63, 64, 80, 81 and 86 and is located some 4 miles WNW of Freer, Texas (Figure 1).

Production is mainly from the Jackson-Yegua sands at a depth of about 1350 ft. Average daily production for the field is about 165 bbl per day. Experiments have targeted the Frio Sandstone present in the eastern half of the field. Compressional velocities at this depth range from 5000 to 7000 feet per second. These poorly consolidated sediments present a "worst case" for transmitting seismic energy. Well logs show that sandstone thickness ranges from 17 to 26 ft between wells 62-9 and 62-19(1). The petrophysical characteristics of the Frio Sandstone are comparable to those of the producing Cole sandstones.

Geological and geophysical data pertaining to the field were assembled. The producing Cole sands are tabular sandstones of Eocene age. It is estimated that these reservoirs will have only produced about 38% of the oil in place at abandonment, making them particularly good candidates for improved oil recovery.

We worked closely with Mike Speed, the operator for the General Land Office. In addition, we subcontracted to the Bureau of Economic Geology (BEG) and the the Southwest Research Institute (SwRI). Under the surface

seismic program, Vibroseis CMP lines originally collected for Mobil in the late 1970's were made available by Clinton Manges' office and several lines have been reprocessed in the Allied Geophysical Laboratories (AGL) at the University of Houston.

**High resolution surface measurements:**

A total of five field trips to the Seventy Six West field were completed. The trips involved coordination with the General Land Office, the Bureau of Economic Geology, Southwest Research Inc., Omnitech Inc., and with the field operator. The dates and duration of the experiments are as follows:

Experiment 1	May, 1990	30 hours
Experiment 2	June, 1990	60 hours
Experiment 3	December, 1990	80 hours
Experiment 4	April, 1991	200+ hours
Experiment 5	August, 1991	200+ hours

Note: no surface seismic measurements were made during the first three experiments.

Experiment 4-

During the fourth experiment, we attempted to record high resolution surface seismic data by using a downhole energy source. This experiment took place in December, 1990. The energy source used was the piezoelectric bender and receivers were commercially available "marsh" phones. Twenty four high frequency receivers were spaced at equal intervals between wells 62-9 and 62-19 (Figure 2). The receivers were placed at the bottoms of shallow holes drilled to a competent rock layer. A fan of data was collected using the depth range 20 to 740 ft. In addition, a three-component accelerometer was placed close to the source well to record the near-field source signature as well as provide detailed velocity information.

The high resolution data or RVSP (Reversed Vertical Seismic Profile) data were recorded using an EG&G 2401 seismograph. This system could record all 24 channels simultaneously in IFP (instantaneous floating point) format. Initially, an EG&G 1225 system with 12 channel capability was used; however, the system is restricted to fixed gain amplifiers with a maximum gain of 66 dB. Because of the relatively low output of the bender, it was felt that the enhanced capabilities of the 2401 system would be more beneficial. RVSP data were recorded using a field stack of 64. A stack test was performed comparing data stacked 64, 128, and 256 times.

Experiment 5-

A fifth experiment was completed in September, 1991. High resolution surface seismic data of two types were collected:

- 1) standard VSP and RVSP and
- 2) CMP reflection measurements.

The standard VSP data were recorded using a Vibroseis energy source; RVSP data were recorded using an airgun as a downhole energy source. The CMP reflection data as well as the VSP data were recorded with the

Vibroiseis energy source operating in a high frequency mode from 40 to 160 Hz. Following is a summary of surface data recorded:

well to surface (RVSP):

- 62-15 to geophones between 62-15 and 62-23
- 62-15 to geophones between 62-15 and 62-18

surface to well (VSP):

- vibrator 500 ft west of 62-18
- vibrator 450 ft west of 62-15
- vibrator 450 ft east of 62-23

surface to surface (CMP):

- vibrator between 62-15 and 62-23; geophones between 62-15 and 62-23.

## **Results:**

### Experiment 4-

Analysis of the RVSP data from experiment 4 showed little or no recognizable signal. This was not completely unexpected considering the energy output of the source and the characteristics of the near-surface geology.

The accelerometer data which was recorded near the source well displayed complex dispersion with the source signature increasingly dispersed with the increase in propagation distance. There appeared to be reverse dispersed waves overprinted by normally dispersed waves. This was in addition to arrivals through the steel casing in well 62-9, water column, and casing generated surface waves. Spectral analysis indicated predominant frequencies around 650 and 1200 Hz, with energy attenuation at increasing offset.

### Experiment 5-

The data set from experiment 5 provide a valuable opportunity to analyze seismic data of different types. Exploration seismic data can be broadly categorized into three types:

- 1) data recorded with seismic energy passing through the near surface weathering layer twice,
- 2) data recorded with the energy passing through the near surface layer once, and
- 3) data recorded without traversing the near surface layer.

Data of the first type correspond to CMP reflection data. The second type of data is represented by VSP and RVSP data. Both of these data types were recorded. Data of the third type is represented by crosshole data.

Data quality for the RVSP data from experiment 5 was variable, but acceptable. This contrasts with RVSP data recorded from experiment 4 which was of such poor quality that it could not be used.

We have been able to construct a one-dimensional (i.e. layered) P-wave velocity tomogram from the surface data recorded between wells 62-15 and 62-23 (Figure 3). This was done by using the RVSP data which were recorded by geophones at the surface. This one-dimensional tomogram correlates well with the sonic log from 62-30.

Processing of the VSP and CMP data sets is still in progress.

### **Subtask 5: Crosshole Seismic Tomography**

#### **Introduction:**

Crosshole tomography has been shown to be useful for producing high resolution, interwell images of seismic velocity structure<sup>(2,3,4)</sup>. Small scale physical modeling results have shown that anomalies as small as two-thirds of the dominant wavelength can be resolved<sup>(5)</sup>. A piezoelectric bender is a currently available downhole energy source that can generate seismic energy from 500 to 5000 Hz <sup>(6)</sup>. Used in shallow, clastic lithology with an average compressional velocity of approximately 6000 ft/sec, resolution of 7 ft requires transmitted frequencies of 600 Hz or higher.

#### **Laboratory work:**

Laboratory work was conducted using scaled physical models to simulate cross borehole tomography. Some of the existing mounting and positioning equipment had to be redesigned to accomplish this.

Calibration tests were conducted to select the size and style of transducers most suitable for the work. The goal was to scale field measurements in the range of 400-4,000 Hz to the range of 40,000-400,000 Hz in the laboratory. Measurements made through a uniform block of material were successfully inverted to obtain a constant velocity field free of artifacts.

Two graduate students worked as research assistants on the project. Their task was to build models, collect data, and write the software programs to invert the measurements and interpret the results. Calibration tests of laboratory transducers and materials were successfully completed. A number of materials were identified that covered the range of density and velocity necessary to simulate typical reservoirs. Two students were recruited and trained in the use of the laboratory equipment.

Simulated crosshole data can now be successfully collected free of positioning artifacts.

#### **Geology:**

With the help of the Bureau of Economic Geology, all of the available geological data were assembled and analyzed. Diane Hyatt of the General Land Office had completed an M.S. thesis on the Seventy Six West field

which was an invaluable source<sup>(7)</sup>. Well logs were interpreted at the Jackson-Yegua sand and cross sections developed in both the strike and dip directions. A facies map of the field was produced and interpreted in light of the depositional environment. Maps were also constructed for production and the water/oil ratios.

Our experimental work has concentrated on the most productive area of the field, section 62, and around the most productive well, 62-9. Initial experiments were aimed at the producing Jackson-Yegua sands but subsequent experiments have been directed at the shallower Frio sand. Experiments have targeted a Frio sandstone that occurs in the eastern half of the Seventy Six West field. Although non-productive in this field, the Frio sandstone is a prolific producer along the Texas Gulf Coast. The Frio sandstone at Seventy Six West field is up to 40 ft thick and was deposited in narrow, dip-oriented, mixed-load to bed-load fluvial channels. Sandstone isopachs illustrate a strongly developed tributary pattern reflecting migration of the channels across a gently sloping, muddy floodbasin. Sandstone thickness between the experimental wells 62-7, 62-9, and 62-19 ranges from 17 to 26 ft and the trend of the sandstone at this location defines the edge of a meander loop.

Petrophysical characteristics of the Frio sandstone such as sediment composition and degree of cementation and compaction are comparable to those of the producing Cole sandstones in the underlying Jackson-Yegua Group. The averages for Frio sandstones state wide are 31% porosity and 1300 md permeability; comparable numbers for the Cole sands in the Jackson-Yegua are 31% porosity and 1000 md permeability. The initial experiments on the Frio sandstone are therefore directly applicable to subsequent experiments on the oil productive Cole sandstones.

#### **Data Collection:**

The following section summarizes the data collection activities by experiment number.

##### Experiment 1-

For the first experiment, well 62-19 was selected as the source hole because it was closest to the highest production in the field. Offset receiver holes were chosen in both the dip and strike directions (62-19 to 62-7 in the dip direction, and 62-19 to 62-9 in the strike direction). Data from these first experiments had very low signal-to-noise ratio and were essentially uninterpretable.

The first experiment utilized the bender as an energy source. The receiver system consisted of a single element, high frequency hydrophone. Source depths ranged from 710 to 1390 ft below the surface. Receiver depths ranged from 820 to 1312 ft. The bender is a low energy source and stacking is required to obtain a record with acceptable signal-to-noise ratio. The number of repetitions varied from 16 to 1000 and data were recorded

using both bursts and sweeps. Experiment 1 was the only experiment that recorded data from the depth of the producing Cole sands at approximately 1350 ft. Subsequent experiments targeted the Frio sand at a depth of 530 ft. This provided increased angular coverage by being able to place the source and receivers below the zone of interest.

#### Experiment 2-

Two downhole sources were used in the second experiment: the bender and an airgun. Based on poor results from experiment 1, it was decided to decrease the hole spacings from the 600 plus ft offsets of the first experiment. Two shallow test holes, GH-1 and GH-2, were used in addition to the operating oil wells 62-9 and 62-19. The 700 ft test holes were drilled between 62-9 and 62-19 which provided offsets of 50, 200, 400, and 600 ft. The experimental sites were cleared of mesquite for an area of about 10 acres around the five holes used in the experiments.

An airgun was used in addition to the bender source. Excellent signals were received from the airgun at all offsets and in all formations, with frequencies up to 300 Hz. Good signals were received at 1000 Hz at all offsets using the bender source in a formation with a velocity of approximately 7000 ft/sec. In formations with lower velocities, the bender signal was indistinct.

#### Experiment 3-

Prior to experiment 3, modifications were made to the bender to improve its radiation pattern and the number of elements in the receiver system was increased to three. This modified bender was used for a set of experiments concentrating at the 600 ft offset. Data were collected from a series of fans which had geometry similar to that planned for recording the full tomographic data set. A variety of stack numbers and signal types was used. In addition to the experiment at the 600 ft offset, tests were also made at the 200 ft offset. Data quality at this offset was excellent for both burst and sweep data.

Additional data were recorded using the airgun and the sparker. Airgun data were recorded at the 600 ft offset only. The airgun produced strong signal but results were not reliable because of difficulties with the time zero transducers.

In addition to the airgun and bender, an arc discharge tool commonly called the sparker was used. The energy output of the sparker is less than that of the airgun but more than that of the bender. Data sets consisting of five fans were recorded at the 200 ft offset. Final failure of the power supply prevented data collection at the 600 ft offset. Spectral analysis of the 200 ft offset data showed most of the transmitted energy concentrated in the frequency range 600 to 800 Hz.

#### Experiment 4-

The fourth experiment consisted of collecting a full crosshole data set using the bender. The bender was further modified with the addition of a second

active element. In addition, the downhole voltage supplied to the tool was increased by a factor of two. Data from 1224 raypaths were recorded with maximum angular coverage of 61 degrees. Crosshole data fans were recorded with source positions from 40 ft below the surface to 740 ft incrementing by 20 ft. Receiver positions were at depths from 40 to 700 ft also in increments of 20 ft giving 1224 possible raypaths. An upsweep 50 ms in length was used with a start frequency of 500 Hz and ending frequency of 2000 Hz. The total record length was 350 ms. Source repetition for all crosshole data was 250 times. Recording time for one source/receiver position was approximately 9 minutes and total field time was 11 days.

#### Experiment 5-

A fifth experiment was completed in the Seventy Six West field during the period from latter August to early September, 1991. Crosshole data were recorded as well as surface, VSP, and RVSP data.

The goal of experiment 5 was to improve the signal-to-noise ratio of the recorded signal. Southwest Research Institute had recently completed design of an improved arc discharge device which we hoped to use. This is an impulsive source with a significantly greater power output than the piezoelectric bender. However, the tool was still in the field test stage and was not available for use in our tests.

Plans for experiment 5 were to collect data suitable for imaging the producing Cole sandstones. Numerous constraints severely limited the number of wells that could be used for data acquisition:

- i) Production wells could not be used for any attempts to deepen wells because of potential damage to the producing formation.
- ii) The number of existing wells that had sufficient depth for the experiment was very small.
- iii) The well spacing between a number of potential wells was too large.
- iv) There were very few wells with sufficiently large inside diameter.

Subject to these constraints, the wells chosen for data acquisition were the pair 62-15 and 62-23. The source well was 62-15 and the receiver well was 62-23; interwell spacing was 1215 ft. With this long offset, we felt that the only energy source with any chance of success was the airgun. A receiver string consisting of 24 hydrophone elements with 20 ft spacing was used to record the seismic signals. Data were to be recorded from 7215 unique raypaths. The maximum source depth was 1290 ft and the maximum receiver depth was 2160 ft. Coverage of interwell space was skewed toward the receiver well but still covered the target zone of the Cole sandstones.

Numerous difficulties were experienced in the course of completing experiment 5. Most of the problems were associated with the source well, 62-15. This was an abandoned and plugged well which had to be "unplugged" before it could be used for data collection. As such, the

condition of the casing and cement bonding could not be determined before hand. The airgun was configured at its maximum volume of 160 cubic in (maximum energy output) which had been used successfully in similar environments with well spacing approaching 1215 ft. However, after looking at numerous data records, no direct arrivals were observed.

Because of these problems, a closer well, 62-18, was quickly prepared for use as a receiver well. The well spacing from 62-15 to 62-18 was 496 ft. A crosshole data set was collected between these wells consisting of 65 source levels and 53 receiver levels to give 3445 possible raypaths. Even at this closer well spacing and with the high energy output of the airgun, only 60% of the shots were interpretable.

### **Results:**

All data processing was done on a Convex 210 computer using DISCO version 8.0. Data were transcribed into standard SEG Y format for portability and ease of access.

Data recorded using the bender in all experiments had the problem of cross-feed equal in length to the input signal beginning at 0 ms. At larger horizontal offsets or wide angular coverage this is not a problem, but at short offsets, the desired signal can be buried within the cross-feed. This can occur, for example, when the sweep length used is 50 ms. A first arrival time of less than 50 ms will then be contaminated with cross-feed. The cross-feed originates from the proximity of the amplifiers (used to supply power to the tool) to the data acquisition system. The solution requires another field vehicle to isolate the two systems.

A technique used to enhance the signal-to-noise ratio was horizontal stacking. That is, for data collected with the three element receiver system, output from each of the three elements was summed into a single, stacked trace. The receiver element spacing is 2 ft. Calculations showed that the difference in arrival times of the energy from element 1 to element 3 based on different average velocities and maximum raypath length was less than the resolution of the recording system.

### Experiment 1-

Initial experiments with the SwRI bender at the depth of the Jackson-Yegua sand were less than successful; it was found that the source signal was not coupling to the formation. Further experiments were directed at the Frio sandstone at a depth of about 530 ft. Measurements were made with input frequencies up to 2000 Hz at offsets ranging from 50 to 600 ft. These measurements are summarized in an SwRI Report "High Resolution Seismic Tomography Measurements Using The Cylindrical Bender Source" by J. H. Bangs et. al. A description of the first four field trips and experimental results can be found in the 60th Ann. Internatl. Meeting, 1991 SEG Expanded Abstracts, 371-374, by C. A. Link et al.

### Experiment 2-

Results from experiment 2 demonstrated the higher energy output of the airgun. The airgun is a relatively high powered source and only a single firing was required to transmit a strong signal at an offset of 600 ft. Transducers attached to the tool provided time zero signals. With a single firing, the airgun produced distinct first arrivals at the furthest offset of 600 ft. Volume configuration of the airgun was 50 cubic inches.

The bender produced clear, usable signals at horizontal spacings of 50 ft and 200 ft. When it was used at the 600 ft offset, good signal was observed at only the 550 ft source and receiver depth position, even for a stack of 500. At an offset of 50 ft, a common receiver gather at a depth of 420 ft with source depths from 320 to 520 ft indicated a relatively narrow source radiation pattern.

The data collected during experiment 2 clearly show that very high frequency (over 1,000 Hz) seismic energy can be recorded at offsets to 600 ft in poorly consolidated, clastic sediments in an operating oil field. This is information which has heretofore been unavailable in the public domain. This was reconfirmed in experiment 4.

### Experiment 3-

The goal of the third experiment was to determine the most suitable source for collecting a data set for producing a tomogram. In addition to testing the airgun and bender, an arc discharge tool was also tried. Horizontal offsets used were 200 ft and 600 ft.

A comparison of downhole sources was made from data collected during experiment 3. The airgun was the most powerful but with the lowest frequency content. The sparker was intermediate in power and frequency content but failed catastrophically during the course of the field work. The bender gave the highest frequency output but the lowest power level. The decision was made to use the bender to collect a full crosshole data set in the fourth experiment.

Spectral analyses of airgun data showed a dominant frequency of about 200 Hz at the 600 ft offset. A spectral analysis of bender data clearly displayed attenuation of higher frequency as horizontal offset increased.

A graph showing the variation of frequency with offset for the downhole sources used is shown in Figure 5.

### Experiment 4-

Spectral analyses of the bender data set from experiment 4 showed transmitted energy with a dominant frequency of about 900 Hz. This was an increase in frequency compared to results from the third experiment. However, this increased frequency was not accompanied by an increase in power so that the data recorded were actually lower in signal-to-noise ratio than the data for experiment 3.

Because of the low signal-to-noise ratio of the crosshole and RVSP data, we were not able to pick first arrival times. A great deal of effort was directed at developing picking algorithms able to distinguish recorded seismic signal from background noise; however, the algorithms are effective only if the signal-to-noise ratio of the data is above a certain threshold. Unfortunately, this was not the case for the data recorded in experiment 4.

The study of the near-field data recorded with the three-component accelerometer clearly showed dispersion effects that contributed to the poor results of the cross-correlation process.

#### Experiment 5-

Processing of the data from experiment 5 has concentrated on the crosshole data recorded between well 62-15 and 62-18. We have been able to produce a P-wave velocity tomogram based on a model cell size of 20 by 31 ft even though the frequency of the data was generally low ranging from 70 to 150 Hz (Figure 6). The tomogram produced from this data can be characterized as low resolution; however, correlation with a sonic log from a nearby well is good. In the tomogram, a high velocity zone occurs at a depth of about 530 ft. This correlates with the depth of the Frio sandstone.

In addition to the two-dimensional tomogram, it was possible to construct a one-dimensional (i.e. layered) P-wave velocity tomogram from the RVSP data set recorded for the long well spacing (1215 ft). The tomogram layer thickness is 40 ft and was constructed by using the RVSP data which were recorded by geophones at the surface. This one-dimensional tomogram also correlates adequately with the sonic log from 62-30.

The most likely explanation for the low frequency data recorded in experiment 5 is that the source well, 62-15, was in such poor condition that there was poor or no coupling to the lithology. Evidence to support this comes from observation of data records showing better signal propagation from certain portions of the well than others which did not appear to be geology related. Also, the well was "making" water as it was being used.

### **SUMMARY**

High resolution surface seismic data and crosshole data were recorded in a producing oil field in south Texas. A P-wave velocity tomogram was constructed from crosshole first arrival times for a well spacing of 496 ft using an airgun as the energy source. RVSP data were also recorded using the airgun and geophones in shallow surface holes. Frequencies from 70 to 150 Hz were recorded. These RVSP data were used to construct a one-dimensional tomogram of the interwell region between two wells separated by 1215 ft.

We believe that the addition of a second active element to the bender may have contributed to the poor quality of the data set acquired in experiment 4. Correlation results from data acquired with the bender in experiment 3 were very good over the full angular range. We expected results from experiment 4 to be at least as good if not better than results from bender 3; however, this was not the case.

A tomogram produced from the airgun data shows good correlation with a nearby sonic log even though the frequency content of the data is low (70 to 150 Hz) for crosshole data. The airgun is capable of higher frequency output but it appears that problems with the source well contributed to the lowered frequencies.

Tomograms were produced by performing "big" iteration loops consisting of raytracing through a starting velocity model, performing inversion on the traveltimes residuals, and updating the velocity model for the next iteration. The raytracing algorithm is based on work by Moser, 1991 and the inversion uses SVD for the zeroth iteration and constrained LSQR for subsequent iterations.

#### **ACKNOWLEDGEMENTS**

This research is supported by the U.S. Department of Energy under Grant No. DE-FG05-89ER14058, and by a Texas Mou-Annex III under Grant No. DE-FG07-89BC1443 to the University of Houston. Research at the Bureau of Economic Geology and at the University of Houston is also partially supported by the State Lands Energy Resources Optimization Program under Contract No. EORPA-7. This research would not have been possible without the cooperation of Garry Mauro, the Texas Land Commissioner, and the help of Don Petty and Peter Boone of the GLO. The airgun was provided by Omnitech Inc.; Southwest Research Institute developed the bender and arc discharge tool.

Douglas Hamilton of the BEG has been responsible for developing the geological framework for the geophysical research. Joe Bangs of SwRI has been the engineer responsible for conducting the initial crosshole field experiments and for further subcontracting drilling and wireline services. The field experiments and the processing of the data were under the direction of Todd Jones and Curtis Link of the Allied Geophysical Laboratories (AGL). Hua-Wei Zhou and Jiri Jech of the AGL are responsible for the raytracing and inversion software; Jorge Mendoza developed the automatic first arrival picking algorithm. CMP lines originally collected for Mobil in the late 1970's were reprocessed in the AGL at the University of Houston by Bob Engels and Lisa Buckner under the direction of Dan Ebrom.

## REFERENCES

1. Hamilton, D., Personal comm., Bureau of Economic Geology, University of Texas, Austin.
2. Bregman, N.D., Bailey, R.C., and Chapman, C.H., 1989, Crosshole seismic tomography, *Geophysics*, vol. 54, no. 2, 200-215.
3. Harris, J.M., Lazaratos, S., and Michelena, R., 1990, Tomographic string inversion: 60th Interntl.. Mtg. SEG, Expanded Abstracts, 82-85.
4. Justice, J.H., Vassiliou, A.A., Singh, S., Logel, J.D., Hansen, P.A., Hall, B.R., Hett, P.R., and Solanki, J.J., 1989, Acoustic tomography for monitoring enhanced oil recovery, *The Leading Edge*, vol. 8, no. 2, 12-19.
5. Balch, A.H., Chang, H., Hofland, G., Ranzinger, K., and Schneider, W.A. Jr., 1990, Seismic cross-borehole imaging of the near surface using tomography and prestack migration in elastic physical models: 60th Interntl.. Mtg. SEG, Expanded Abstracts, 133-136.
6. Balough, W.T., and Owen, T.E., 1988, New piezoelectric transducer for hole-to-hole seismic applications: 58th Interntl.. Mtg. SEG, Expanded Abstracts, 155-157.
7. Hyatt, D.B., 1990, The geology of the Seventy Six West Field, Duval County, Texas: M.S. thesis, University of New Orleans.

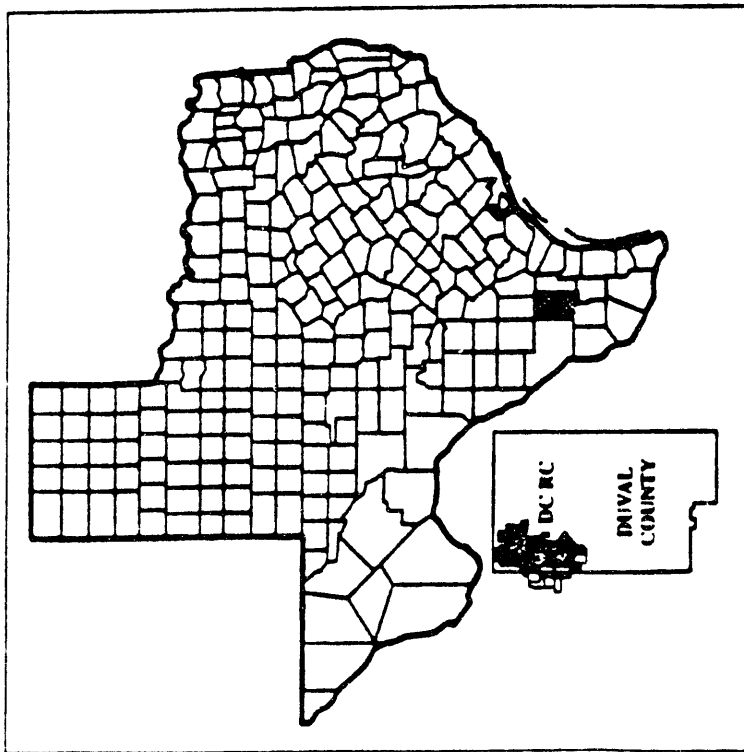


Figure 1. Location of Seventy-Six West oil field in Duval County, Texas: site for field experiments.

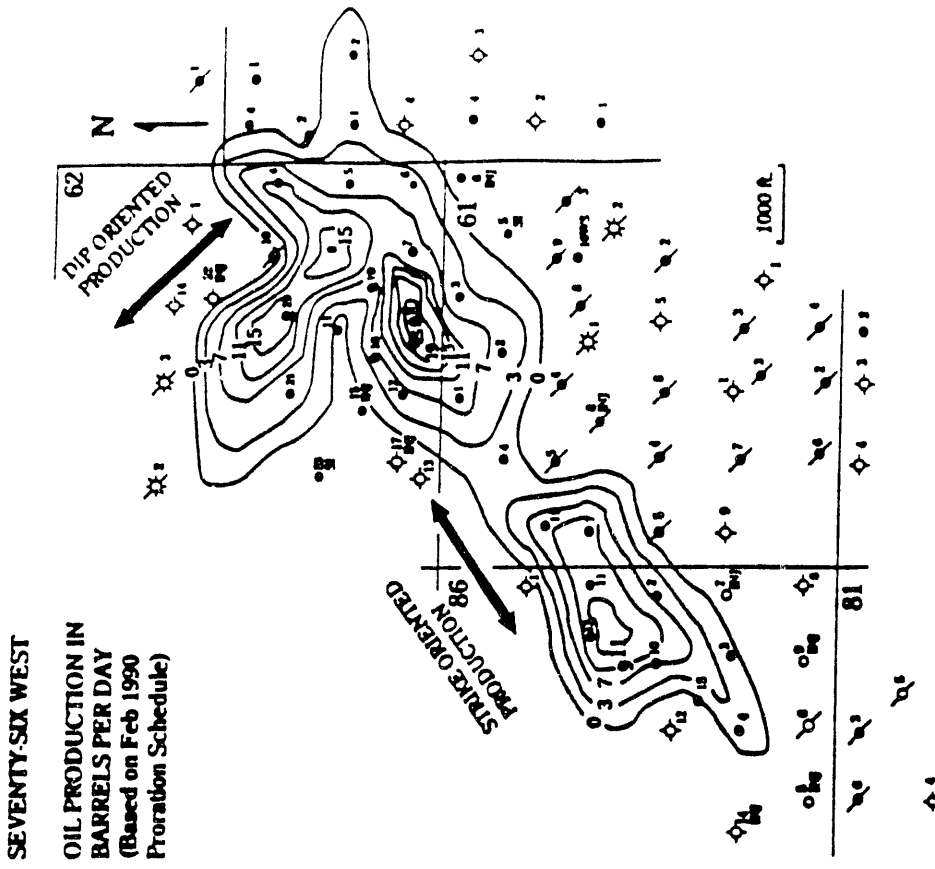


Figure 2. Oil production map showing location of test wells: section 62 nos. 7, 9, 15, 18, 19, and 23.

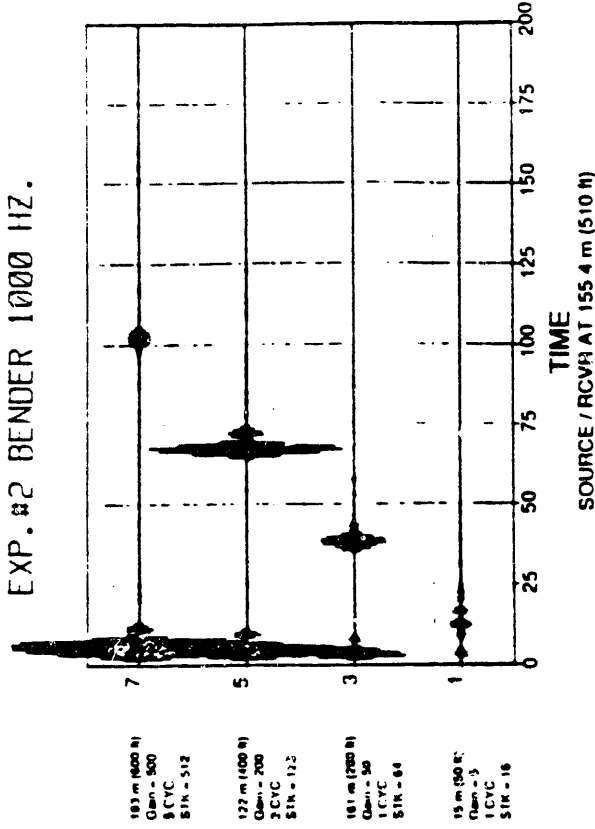


Figure 4. Bender data traces showing arrival times and relative amplitudes of propagated pulses. Input signal to bender is 1000 Hz sinusoid. Number of cycles, signal gain, and number of field stacks is shown to the left of each trace. (High amplitude pulse at  $t = 5$  to 10 ms is instrument crossfeed.)

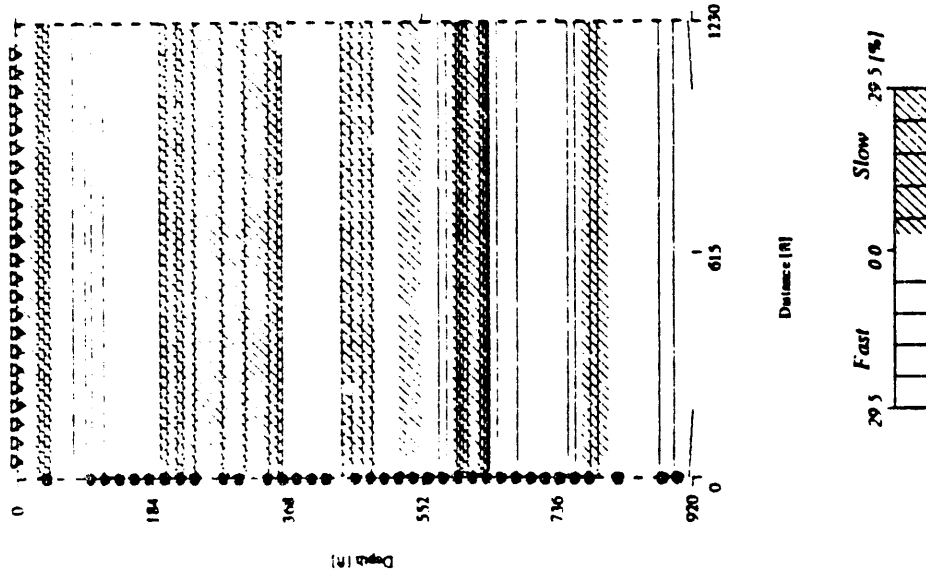


Figure 3. One-dimensional P-wave velocity tomogram between wells 62-15 and 62-23. The Frio sandstone is at approximately 530 ft. Velocity values are plotted as percentage difference from background velocity = 6950 ft/s.

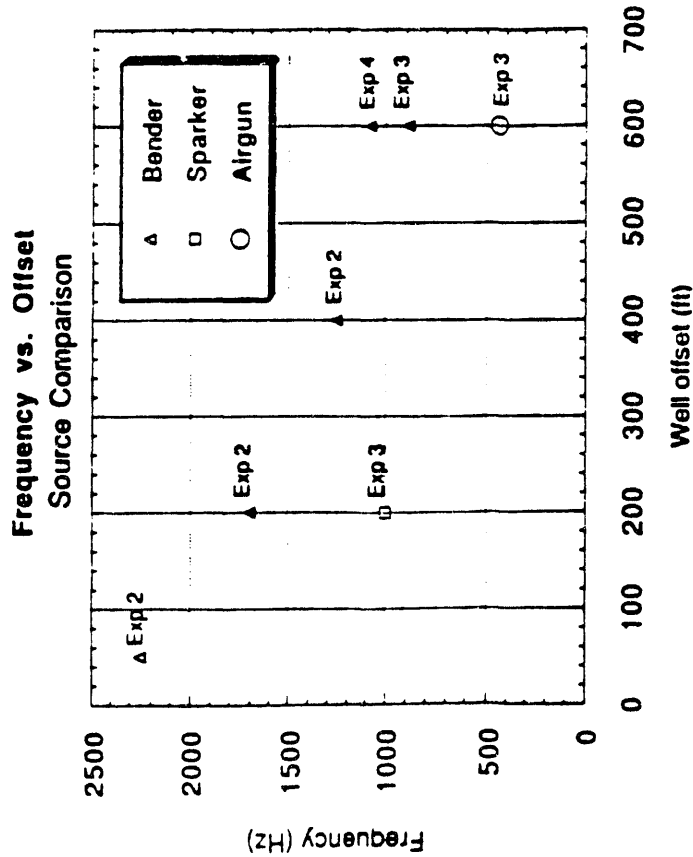


Figure 5. Graph showing variation of mean frequency versus well offset for the bender, sparker, and airgun.

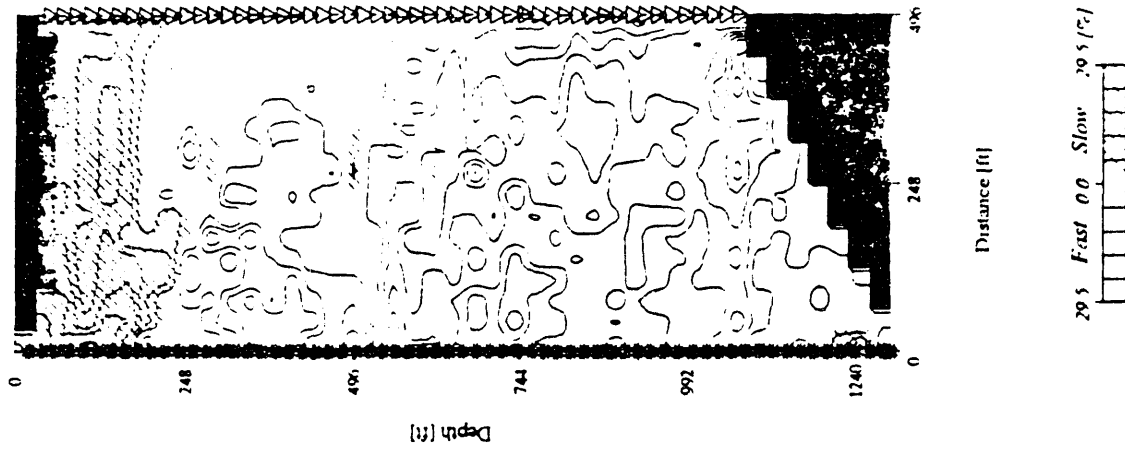


Figure 6. Two-dimensional P-wave velocity tomogram between wells 62-15 and 62-18. The Frio sandstone is at approximately 530 ft. Velocity values are plotted as percentage difference from background velocity = 6950 ft/s.

**Subtask 2: Reservoir Rock Structure Determination, and  
Subtask 4: Simulations of Recovery Processes in Typical  
Depositional Environments  
(E. L. Claridge, Investigator)**

**Abstract**

Under these subtasks, a general study of the effect of reservoir type on enhanced oil recovery processes was performed by use of computer simulation for two types of reservoir: the alluvial point bar and the off-shore barrier bar. The result of this study was to show that the opposite trend of the horizontal permeability with depth for these two types results in improved oil recoveries when the process is one with a less dense fluid injected and/or produced and the permeability is highest at the bottom, and vice-versa. Since this effect is opposite for primary recovery and for a waterflood or for a waterflood and a miscible gas flood or a steam flood, the normal alternating process sequence in either type of reservoir is to give alternating higher and lower recoveries.

In line with other subtasks, attention was shifted from the first oil field chosen for those tasks to the substitute Seventy Six West field and under these subtasks to study by computer simulation the possibilities for enhanced oil recovery. It appeared that the most likely process which could be used in this field, which is at shallow depth (1200-1300 feet) and is nearing flood-out with water, is immiscible CO<sub>2</sub> flooding. The results of the simulations are encouraging, in that oil recoveries of 11-12% of original oil in place were calculated with CO<sub>2</sub> requirements which are low by comparison with miscible floods. It is recommended that this possibility be pursued.

**Discussion**

It was originally intended, under Subtask 2, to carry out studies of the pore structure of different kinds of rocks using the university's X-Ray Computed Tomography apparatus. Dr. Harry Deans, who was one of the investigators connected with this project, began studies under this section. However, he transferred from the University of Houston to the University of Wyoming in the fall of 1990, and these studies were not completed at that time. In addition, the original oil field that was to be used for this project was made unavailable by Exxon. The field that was used for this project, the West Seventy Six field, was not suitable for a pore structure study. A request to change the project to accommodate these changes was submitted to the D.O.E. Project Manager, Mr. Robert Lemmon, and was subsequently approved.

Under Subtask 4, this author had initiated studies of the influence of the characteristics of reservoir rocks resulting from their mode of deposition on their behavior in oil recovery processes. A computer simulation of two

of the major reservoir types, as exemplified by relatively simple models which had first been presented in a geology training course and were later published in the Journal of Petroleum Technology<sup>(1,2)</sup> by well-known geologic experts was employed. These were the alluvial point bar type and the coastal barrier bar type. This part of the work is reported below. It was decided after Dr. Deans left to combine Subtasks 2 and 4 and report the results obtained in this author's study under the combined heading. Later a computer simulation study was initiated of the Seventy Six West field, since this had become the target of the geophysical studies under other Subtasks in this project. Results of this study are also reported here, following the results of the alluvial point bar and coastal barrier bar study.

### **Depositional Models (Alluvial Point Bar and Coastal Barrier Bar)**

Generally, actual oil reservoirs containing the coastal barrier bar depositional types also contain many complicating structural aspects, such as multiple layers of the given type on top of each other, possibly with some other types adjacent or intermixed, with shale layers in between, and with slump-faults separating different parts of the reservoir from each other. The simple structures studied in this part of the work give guidance as to the influence on primary, secondary, and tertiary oil recovery processes of the vertical permeability trends in the barrier-bar and alluvial-deposit portions of such complex reservoirs. The work is described in detail in a Master's Thesis by David Hanauer<sup>(3)</sup>.

The characteristic difference between alluvial and off-shore bars is the opposite trend of horizontal permeability in the vertical direction. In the alluvial deposits, the coarsest sands are at the bottom of any given vertical sequence, and successively finer sands are deposited on top, until the deposit is capped by a layer (or layers) of mud. The latter turns into practically impermeable shale over geologic time, and since such a deposit is generally laid down on top of earlier layers, each with its layer of shale on top, derived from previous periods when the meandering river was in the same vicinity within its valley, each sequence also has a shale layer at the bottom. Hence, each sequence repeats the same vertical sequence of large sand particles with corresponding high permeability at the bottom, grading to fine and very fine sand particles and corresponding low permeability at the top.

By contrast, the trend of horizontal permeability with height is the opposite in barrier bars. In such bars, the direction of building is from near the shore outward. Fine sands and mud lie on the bottom, and as the bar is gradually built outward by sands carried downstream and out into the sea by flooding rivers emptying into the sea, coarser sands deposit first (on top of the previous finer sands) while more fine sand is carried further from the shore before it settles to the bottom. As the bar builds upward, the coarsest sands are deposited on top of the barrier bars. During the quiet periods of

river flow, fine sand and mud is carried to a lesser distance and in much lower amount, so that lagoons containing silt and mud form behind the barrier bars. Furthermore, tides carry some sand back into the lagoons through the river outlets between bars, and sea storms carry sand back both through such mouths and over the tops of the barrier bars. In addition to these short term effects over hundreds or thousands of years, periods of high and low sea level tend to alternate over longer periods, so that the coast line migrates seaward and then landward, with the result that older barrier bars become covered by mud carried farthest from shore by emptying rivers, or are partially eroded away when the sea retreats. Hence, the simple barrier bar model used in this part of the study serves to indicate the effect of the permeability trend in the vertical direction within each one of the barrier bars making up a typical complex reservoir. Similarly, the alluvial bar model used in this study shows the behavior of each sequence in a more complex reservoir containing many layers of which each is a given depositional sequence. The two simple models used in this study are shown in Figures 7 and 8.

The comparative behavior of these two types of deposits is discussed below in terms of their behavior in primary depletion, waterflooding, and CO<sub>2</sub> flooding, as well as steam flooding in the case of the most viscous of the three viscosity levels of reservoir crude oil studied. More details are given in Hanauer's study than will be included here; however, the most important results are shown below.

### **Simulation Results:**

For the primary production, secondary waterflood, and CO<sub>2</sub> miscible flood simulations, the computer simulation program used was the Multiflood Simulator of the consulting firm of Todd, Dietrich and Chase, Inc. (name now changed to TCA Reservoir Engineering Services). It was provided to this author (E.L. Claridge) under a contract limiting its use only to research and student instruction under this author's supervision at the University of Houston. For steam flooding simulations, the same firm's Volatile Oil Steam Flood Simulator was used, subject to the same restrictions.

### Primary Recovery

As mentioned, three levels of reservoir crude oil viscosity were used, labelled Light, Medium, and Heavy Oil. The reservoir oil composition in the simulator used for primary depletion, waterflood, and CO<sub>2</sub> flooding was represented by five hydrocarbon pseudo-components, or by three such components in the case of steam floods. In the five-component case, these were methane (CH<sub>4</sub>), ethane (C<sub>2</sub>H<sub>6</sub>), C<sub>3</sub>-C<sub>4</sub> (LPG, or LITE), C<sub>5</sub>-C<sub>10</sub> (gasoline, or MEDM), and C<sub>11+</sub> (non-volatile hydrocarbons at typical reservoir conditions, HVY). The mixture viscosities are calculated for any

given composition by volume-fraction weighting of the logarithms of the component viscosities. The viscosities were calculated for a reference pressure of 2000 psia for the mixed components LITE and MEDM for a typical composition of this carbon number range in a crude oil, and the same value was used in each case. The reservoir oil viscosities were varied between the three cases by changing the composition (less light components in the medium and heavy oil cases) and by arbitrarily assigning different values to the HVY component.

The three reservoir crude oil viscosities are as follow:

Light oil:	1.3 cp
Medium oil	43.8 cp
Heavy Oil	272.4 cp

The possible effect of infill drilling was studied by decreasing the pattern size for a given reservoir area to 1/4 the area per pattern. This did not introduce any heterogeneities which might in an actual case make the infill drilling results better. Without such heterogeneities, the only effect of pattern size reduction was to accelerate the process in time.

The primary recovery results for five-spot well patterns are as follow:

Table 1  
Primary Oil Recovery, % of OOIP

	<u>Single Pattern</u>		<u>4 Patterns</u>	
	<u>Alluv. Barrier</u>	<u>Barrier</u>	<u>Alluv. Barrier</u>	<u>Barrier</u>
Light Oil	43.7	18.2	41.9	18.8
Medium Oil	15.3	8.2	14.1	8.4
Heavy Oil	6.2	4.4	5.2	4.5

The marked difference between the recoveries for the alluvial point bar model and for the coastal barrier bar model is attributable to the relative recovery from the three top layers of the five-layer models, as shown by the remaining average oil saturations in the single pattern, light oil case in the following table:

Table 2  
Remaining Oil Saturations by Layers

	<u>Alluvial Bar</u>	<u>Barrier Bar</u>
Layer 5 (Top Layer)	0.19	0.25
4	0.25	0.39
3	0.45	0.68
2	0.84	0.84
1 (Bottom Layer)	0.83	0.84

## Secondary Recovery by Waterflooding

Normally, a waterflood of a pressure depletion type reservoir will be started before the reservoir approaches the abandonment pressure or abandonment oil rate. One reason for doing this is to avoid trapping the waterflood residual oil saturation, a crude oil which has shrunk because of the loss of dissolved gases. The trapped oil is essentially stock tank oil. If the waterflood is started at a higher pressure, much of the original content of dissolved gases will still be present in the oil trapped by the waterflood, and the stock tank oil content of the gas-swollen oil which is trapped by the waterflood will be less. Another reason is that it is undesirable to have to continue to operate the field after primary abandonment conditions have already been reached while waiting for the oil displaced by the waterflood to reach production wells. To simulate in these models the typical situation when a waterflood might be started, the water injection was begun when the reservoir had reached a pressure of 1100 to 1300 psia, declining from an initial pressure of 4000 psia.. The waterfloods were terminated at a 98% water cut. Results were as follow:

Table 3:  
Waterflood Oil Recoveries, % of OOIP

		<u>Single Pattern.</u>		<u>4 Pattern</u>	
		<u>Alluv.</u>	<u>Barrier</u>	<u>Alluv.</u>	<u>Barrier</u>
<u>Light Oil</u>	at start of water injection	22.0	12.5	22.0	12.5
	at 98% water cut	64.3	69.3	63.9	69.1
<u>Medium Oil</u>	at start of water injection	5.0	5.0	5.0	5.0
	at 98% water cut	50.5	55.4	44.6	55.4
<u>Heavy Oil</u>	at start of water injection	3.0	3.0	3.0	3.0
	at 98% water cut	32.8	34.3	24.7	33.4

The lower oil recovery for the four-pattern (infill-drilled) case is due to the higher flooding rate which smaller patterns made possible, and thus higher viscous force compared to gravity and capillary force. When the rate was reduced to the same rate as in the single pattern floods, the oil recovery in the four-pattern case increased by about 5% of OOIP.. Alternatively, at the same higher flow rates, the capillary pressures were increased by a factor of 5. Again the oil recoveries increased by about 5% of OOIP. This does not quite make up for the differences seen in the table, but verify that the results are due to much increased viscous force relative to the other two main forces, in the four-pattern cases. Hence, there can be an oil recovery penalty due to attempting to speed up the process too much. Another possible reason is that there may be too few blocks (only two) between injection and production well blocks in the four-pattern case, as compared to five blocks between in the case of the single patterns. Too few blocks allows earlier breakthrough of water and the oil bank is less well defined.

The effect of the ratio of vertical permeability to horizontal permeability was examined, for values of 0.1, 0.01, and 0.001, for the light oil case in the coastal barrier bar model. Oil recoveries were about 2% and 4% lower for the 0.01 and 0.001 ratio cases, compared to the values for 0.1 ratio.

Normal versus inverted five-spot patterns were examined. No significant differences were found.

Waterflood remaining oil saturations were typically higher in the top two layers of the alluvial point bar model than in the coastal barrier bar model, by 12 to 14%. This is due to the lesser extent of waterflood which had occurred in the low permeability layers at the top of the alluvial point bar reservoir at the time when the economic limit of 98% water cut was reached..

### Tertiary Oil Recovery by CO<sub>2</sub> Miscible Flooding

All of the tertiary CO<sub>2</sub> miscible floods were started at the 98% watercut point in the corresponding waterfloods. These were performed as 1:1 WAG (water alternating with gas) injection processes, with 0.4 hydrocarbon pore volume (HPV) of CO<sub>2</sub> and of water injected, then followed with straight water injection until again a water cut of 98% was reached. The extra oil recovered was thus clearly due to the injection of the 0.4 HPV slug of CO<sub>2</sub>, regardless of when in this tertiary process the extra oil was actually produced. Much of the extra oil is in fact produced after the injection of CO<sub>2</sub> has ceased and the final waterflood is taking place. The table on the next page gives a summary of results. Only the four-pattern configuration was used.

As shown in Table 4, the extra oil recoveries due to CO<sub>2</sub> flooding were quite modest as compared to the 10% to 15% extra oil recoveries reported for CO<sub>2</sub> - WAG floods in the petroleum literature. It is believed that this is principally due to the relatively efficient waterfloods which had been carried out in these models, but some of the tendency toward low oil recoveries may have been due to the use of the four-pattern well arrangement, with its too low a number of blocks between well blocks.

Table 4  
Tertiary CO<sub>2</sub> Flood Oil Recoveries, % of OOIP

		<u>Alluvial Bar</u>	<u>Barrier Bar</u>
<u>Light Oil</u>	at start of CO <sub>2</sub> injection	63.8	69.1
	at end of final waterflood	67.4	74.0
<u>Medium Oil</u>	at start of CO <sub>2</sub> injection	44.6	55.4
	at end of final waterflood	48.8	57.3
<u>Heavy Oil</u>	at start of CO <sub>2</sub> injection	24.7	33.9
	at end of final waterflood	25.0	35.3

## Steam Drive

The TDC Volatile Oil Steam Flood Simulator has only three oil components; the fourth component is water as liquid or steam. Two of the oil components are volatile, while the third is treated as non-volatile under the reservoir conditions. For this purpose, the methane and ethane components used in the prior simulations were combined and called GAS, the C<sub>3</sub>-C<sub>4</sub> component (LPG) was re-named LITE, and the previous MEDM and HVY components were combined and called OIL. Thus, the three oil components were GAS, LITE, and OIL. Steam flood simulations were carried out only on the Heavy Oil case. Steam was injected for ten years in all of the barrier bar cases, but in the case of the alluvial point bar model, steam was injected for seven to ten years. In all cases, steam was followed by cold water until a water cut of 98% was reached (if it did not occur before water was injected). A small amount of primary depletion was carried out (about 2.5% oil recovery) before steam injection in order to produce a small distributed gas saturation. This allowed much greater steam injection rates during early stages of the process. Steam injection pressure was 2000 psia and the steam quality was 70.8%. This gave a BTU content of 1000 BTU/lbm steam. This BTU content is used as a standard in the industry for normalizing steam injection at different quality and pressure. Only the four-pattern well configuration was used. Results are in Table 5:

Table 5:  
Steam Flooding Oil Recoveries, % of OOIP

	<u>Alluvial Bar</u>	<u>Barrier Bar</u>
7 Years steam + final waterflood	51.2	
8 " " " "	52.6	
9 " " " "	53.8	
10 " " " "	54.9	43.4(46.9*)

\* First value shown is for a 9x9x5 grid block model (same for a 9x9x4), while the value in parentheses is for a 13x13x4 grid block model, with more blocks between injectors and producers.

These results show what is commonly known: that steam will generally recover more oil than do cold processes when the oil is relatively viscous. What was unexpected was that the run for the barrier bar was longer than 100 years, although the first 40% OOIP recovery was obtained in 25 years. The runs for the alluvial bar were about 20 years long. The reason for the long recovery period for the coastal barrier bar was determined by running separately four portions of a 16x12x5 model, each portion 4 blocks long in the landward-seaward direction. The three portions landward had oil recoveries exceeding 50% and relatively short lives of about 20 years, but the fourth, seaward section, containing only the three lowest permeability layers (and mostly the two lowest, at the bottom) had a very long life (120

years) and an oil recovery of 42.2% of OOIP. When all portions are run together, this seaward portion contributes relatively little to the total recovery, but stretches out the last portion of the recovery curve over a very long time.

### **Conclusion**

The case where the higher permeability layers are at the bottom (alluvial point bar type) is generally more favorable for processes where a gas phase is injected, but the coastal barrier bar type with the lowest permeability at the bottom is better for a waterflood.

### **Seventy Six West Field Study**

It had originally been planned to carry out geophysical and other studies described in this project in the Friendswood field, southeast of Houston. However, the operator of this field placed financial burdens on the use of wells in the field for the purposes contemplated such that it was not considered possible for the project to bear these burdens. Hence, attention was given to selecting a suitable alternate field. A candidate was found in the Seventy Six West field, in that a major portion of this field was in state receivership as a result of a court judgement. It was found that the state land office would permit experimental work of the nature desired, in this field. A geologic study, embodied in an M.S. thesis by D.B. Hyatt<sup>(4)</sup>, was available; this was the basis of a publication by the same author<sup>(5)</sup> in 1990. The information in this M.S. thesis was used as the principal basis for the geometric model of the field which was used in the computer simulations.

This field had also been chosen as one of the example fields of a series of different depositional types to be studied in the State Lands Energy Resource Optimization (SLERO) program of the Bureau of Economic Geology. (BEG) Because of this, more data became available concerning the field than would otherwise have been available, since the previous owners of the mineral rights in this field had not furnished a significant amount of data concerning the field - no PVT data, no rock properties, no oil properties, etc.. Most of the SLERO data used came from a SLERO Report entitled "Final Oil and Gas Reservoir Candidate List," dated February 20, 1990. A more abbreviated report of reservoir properties, with general geologic maps appended, had been furnished at an earlier time by Ulises Ricoy of the BEG under contract with the Energy Laboratory of the University of Houston. These two sources plus some data from the M.S. thesis mentioned were used as the basis for rock and oil properties for the simulations. Appropriate pages from the SLERO report and from the Ricoy report are given in Appendix I. A much more detailed geologic study of the field has recently been presented in a paper given by D.S. Hamilton<sup>(6)</sup> at the 1991 Society of Petroleum Engineers' Annual Meeting in Dallas. This paper was not available at the time the simulation work reported here was performed.

The reservoir consists of two moderately thick to thin layers of relatively high permeability sandstone at a depth of about 1300 feet, called the Cole B and C sands. The permeable layers pinch out on the high side of the reservoir, on the northwest. It is approximately an elongated oval in shape, with the long axis from southwest to northeast. There were some indications of a small initial gas cap on the northwest side, but this is not certain (it was neglected in these simulations). The reservoir slopes gently to the southeast at an angle of about 1.5 degrees. The thesis gave maps of contours on the top surface and of the isopachous thickness of the two layers. These are shown as Figures 9 to 12.

A grid was chosen to form a rectangle 20 blocks long (southwest to northeast) and 11 blocks wide (southeast to northwest), and two layers thick (to represent the B and C sands), as shown in Figure 13. Each square block was ten acres in area, so that the block dimensions were 660 feet by 660 feet. A transparency was made of this grid so that it could be placed on the top surface and isopachous maps just mentioned. The depths to the top surface of each layer in each grid location were read from the top surface contour maps, and the thickness of each block in each layer was read from the contours on the isopachous thickness maps. These data were read in for the entire grid, except that where the block lay outside the reservoir boundary, zero thickness was read for each layer. A common porosity (30.7%) and permeability (1209 md) were read in for all grid blocks, since no data existed which would provide a basis for distributed values as compared to these average data.

A difficulty was immediately found with the porosity value. The volumetric content of the layers as given by the isopachous maps and the given porosity was about 75 million barrels of stock tank oil. A value of 10 million barrels of original oil in place was given by Ricoy's report. The SLERO report mentioned above gave (as of 1988) a value of original oil saturation of 78% and a current average oil saturation of 40%, with a total oil production to that date of 4.603 million barrels. This would indicate that the original oil in place was:  $(78/(78-40)) \times 4.603 = 9.45$  million barrels. The 10 million barrel value was adopted. This meant that the porosity value quoted in the data furnished us had to be revised downward. A value of 4.008% gave a value of 10 million barrels of original oil in place, hence this value was adopted. It did not seem unreasonable since in the M.S. thesis referred to, from which the layer thicknesses were obtained, it was mentioned that the layer thicknesses were derived from the electric logs rather than from whole core analyses, and that the thicknesses so derived included impermeable sands and conglomerate as well as permeable sandstone. The SLERO report mentions 15 feet of net pay out of 40 feet of gross pay. A ratio of net pay to gross pay of 0.13055, times the given porosity of 30.7%, would result in the porosity value of 4.008% which was used.

In Hamilton's SPE paper (6), the original oil in place is stated to be 25 million barrels. It is not apparent why this new value has appeared from the same source as the prior value of 10 million barrels reported to the Energy Laboratory. If the larger value is adopted, then the oil recoveries by primary and secondary processes would have to be multiplied by (10/25) or 0.4; thus, the last reported value of 46% of OOIP would become 18.4%. Water cuts are now high and secondary recovery is approaching completion; ultimate recovery would only reach 20% for the 25 million barrel OOIP basis.. This seems to the writer to be too low a value for the sum of primary and secondary recovery for this reservoir. Yet the value of 50% based on the 10 million barrel OOIP value also seems rather high.

For this study, it should be remembered that the value of 10 million barrels of stock tank oil originally in place has been used as the basis for calculating oil recovery percentages. However, it should be concluded that this statistic (OOIP) is subject to considerable doubt.

The aquifer on the southeast side is of unknown size. It was accounted for in the simulations by making the pore volume of the first line of blocks (that is, those blocks indicated to be present by the isopachous maps) some multiple of the volume calculated with the area, thickness, and corrected porosity mentioned above. These blocks were declared to contain only water (actually, with water saturations of 0.99999, implying oil saturations of 0.00001, since the computer program requires at least a tiny trace of oil phase to be present in any active grid block). Values of 10, 100, and 1000 were tried as the multiplying factor for these grid block volumes. If the aquifer were made too small, the producing wells died too soon, and not much water was produced along with oil during primary production, contrary to the field experience. On the other hand, if the aquifer were made too big, the water strongly invaded the reservoir and no secondary gas cap resulted, while wells watered out too soon and the observed oil recoveries at given stages of the process - that is, the recovery of about 31% at the time when significant water injection was started, and 46% by about 1988, were not matched; the calculated oil recoveries were too low. Evidently, the generation of a relatively large secondary gas cap, within which the oil recovery is higher than in the waterflood-invaded region, is necessary to obtain the reported recoveries. The factor of 100, while not giving an exact match to the observed recoveries, did seem to give the right behavior.

In the waterflood portion of the process, availability of water was not used as a limitation on injection rate; rather, water was injected with a 200 psi bottom-hole pressure, at injectivities proportional to the relative kh values for the various blocks where the injection wells were located.. After 20 years of the simulated waterflood process, the average reservoir pressure was 209 psia (somewhat biased by the aquifer block water pressures, which have a somewhat higher pressure than at the injection wells because of gravity head); this is considerably higher than the actual average pressure of

about 140 psig, and indicates too much water injection. This probably made the secondary gas cap somewhat smaller than the actual size, and the expected result of somewhat too low a calculated oil recovery did occur; it was 44% instead of 46%. Nevertheless, it did not seem very useful to attempt to fine-tune this simulation further, since the model did not incorporate many of the heterogeneities known to be present, and average data had been used for many properties which can be expected to vary from the average over the reservoir.

Figure 14 shows the simulated course of the primary depletion and waterflood over the years from 1954 (discovery year) until 2008. In 1992, the year in which the pilot simulation was started, the average oil recovery for the entire field is calculated to be 44% of OOIP. During primary depletion, from 1954 to 1972, the oil recovery obtained in the simulation was 31%. This corresponded to the recovery in 1967 reported by Ricoy. He assumes waterflooding from 1967 onwards. In the simulation, water injection at maximum rate was started at the point where the oil recovery was 31%, which in the simulation occurred in 1972 instead of in 1967. In 1988, Ricoy reports oil recovery as 4.6 million stb, or 46% of OOIP. In the simulation, after 21 years of waterflooding, the total oil recovery is slightly over 44%, thus the waterflood produced 13% instead of the 15% basis OOIP reported by Ricoy for this period of waterflooding.

#### **Pilot Area Simulator Model Description**

A principal value of the primary depletion and waterflood simulation was to give a reasonable value for the oil and water saturations in the region of Well No. 8 in Section 62, which had been tentatively selected as a proposed site for a possible enhanced oil recovery process pilot process, starting as of 1992. This is block  $i=16, j=8$ , containing Well No. 55 (out of 66 wells) in the primary depletion and waterflood simulation. After 20 years of waterflood (1992), the water saturation in the upper layer (B, 14 feet thick at this location) was 0.48818, while in the lower layer (C, 26 feet thick at this location) the water saturation was 0.53041; there was no gas phase present in either layer at this location. Using the thicknesses as fractions, the average water saturation was 0.51563, the average oil saturation was 0.48437 and the average oil recovery in these two layers at that location, based on 0.78 original oil saturation, was 37.90% of the OOIP at that location, compared to the field average of 44%, an estimated 47% at an economic limit of 98% water cut, and a maximum possible recovery of 55.13% by continuation of the waterflood to a water cut of 100%.

The pilot well pattern chosen was a one acre area surrounding Well 8. It was assumed that this well would be converted to an injection well, and four production wells would be drilled at the corners of a one-acre square, equidistant from Well 8. This pilot area was divided into quarters, and a quarter of the five-spot well pattern was represented for simulation purposes by a 10x10x6 grid. Thus, the length of a side of the grid blocks

was 10.4355 feet. Three layers of grid blocks were used for each reservoir layer (B and C), so as to include gravity segregation effects which might occur during a supplemental recovery process. Since the top layer was 14 feet thick, then each layer was 4.667 feet thick, while each layer in the lower C layer was 8.667 feet thick. The saturations of the B and C layers mentioned above were assigned to the three grid layers in each actual layer. It was assumed that water injection would be employed in surrounding wells as necessary to maintain a reservoir pressure of up to 500 psia in the pilot area, so that this pressure could be used as the bottom-hole pressure in the injection well.

A continued waterflood to 98% water cut was simulated in this pilot model. Results are shown in Figure 15. It can be seen that the water cut started at 96%, and at 98% water cut, the additional oil recovery was only 5.75% of OOIP, making a total of about 44% of OOIP recovery for this region. This is not unreasonable if the high gas cap oil recovery is responsible for the higher over-all field recovery.

#### **Choice of Supplemental Oil Recovery Process**

An in-situ combustion pilot test had been tried by Mobil in the southern extremity of the field. Stimulated oil production was obtained in a few wells, but the project was not continued further. If the net-to-gross sand ratio is as low as quoted in the SLERO report (15/40 feet) then the heat loss would be unfavorable for this process to be economic.

Polymer-thickened waterflooding was briefly considered. However, the main virtue of this process is to arrive at the economic limit of waterflood sooner (with less injection of aqueous fluid), and there is generally only a marginal increase in oil recovery over that of the ordinary waterflood, since the ultimate waterflood residual oil saturation is not altered. Since the waterflood process is already almost complete in this field, polymer flooding was not given further consideration.

Surfactant/polymer flooding has up to the present been considered to be uneconomic for oil prices less than about 1-1/2 times any given free market price of oil, so this process was not considered applicable.

The oil viscosity is stated in the SLERO report to be 30 centipoise (presumably stock tank oil viscosity, since a PVT report giving viscosity vs dissolved gas content or pressure is not available for this field). The reservoir oil viscosity is now close to the stock tank oil viscosity, since the current dissolved gas content of reservoir oil is stated to be 13 scf/stb and this much dissolved gas will not lower the viscosity very much (perhaps to 15-20 centipoise). Steam flooding is most appropriate when the oil viscosity is so high that waterflood recovery is low, and when the net-to-gross pay ratio is well above 1/2, further when the net pay is greater than ten feet; preferably as much as 50-100 feet. This reservoir does not fit that description.

The reservoir oil properties and waterflood behavior are more similar to those appropriate for a gas-injection type of supplemental oil recovery process. However, the shallow depth prevents the possibility of a miscible process with any hydrocarbons more volatile than propane (since the reservoir temperature is 103° F, at which the vapor pressure of propane is about 200 psia). Both ethane and carbon dioxide would require pressures in excess of 1000 psia for miscibility. A flooding process based on pure propane would be too expensive at current relative prices of crude oil and propane. Hence, the possibility of an economic miscible gas process is ruled out.

However, there are reports in the petroleum engineering literature of immiscible carbon dioxide flooding projects, in which water was injected along with the carbon dioxide<sup>(7,8,9,10)</sup>, and surprisingly high oil recoveries were observed, approaching those obtainable by miscible CO<sub>2</sub> flooding (10-15% of OOIP), in which water injection along with or alternated with CO<sub>2</sub> is a common practice... However, the pressure during the process was 850 psi in the Wilmington field case and 1050 psi in the Lick Creek case. In the Seventy-Six West field, it is considered that about 500 psi is the most that can be used in the pilot area without pushing a significant amount of oil up into the gas cap (for field-wide CO<sub>2</sub>-water flooding it would be desirable to fill the gas cap with water by direct injection into the gas cap, to avoid pushing an oil bank into the cap). For a much lower process pressure, it was not sure that similar oil recoveries could be obtained. Hence, it was considered necessary to simulate a pilot test to see what oil recoveries could be anticipated at this lower pressure.

The pilot was designed to be small in area so that results could be obtained and evaluated in a relatively short time (1-2 years). It is assumed that CO<sub>2</sub> could be supplied at any rate found to be desirable based on the results of the simulation study. It is assumed that the CO<sub>2</sub> can be injected at normal surface temperatures, together with or alternated with water (brine of current injection water salinity), at a bottom-hole pressure of 500 psi. In the Lick Creek and Wilmington field tests, the volume ratio of water and CO<sub>2</sub> at reservoir conditions was approximately 1:1. In the Lick Creek report, this is stated to be about the optimum ratio. It is not stated whether this is in excess of the amount of CO<sub>2</sub> which dissolves in the water or not. The article includes curves of solubility of CO<sub>2</sub> in brine and in crude oil versus pressure at the reservoir temperature. At 1000 psi, the indicated solubility of CO<sub>2</sub> in the water is about 85 scf per stb, or about 0.0114 mol fraction in the water phase. At 1000 psia and 118° F (the reservoir temperature) the volume of this dissolved CO<sub>2</sub> as a gas phase is about 4 cubic feet per pound mol (379.5 scf), or 0.16 barrel. The injection ratio for a 1:1 WAG ratio is stated to be 2 stb of water per mscf of CO<sub>2</sub>. Out of the 500 scf/stb injection ratio, therefore, 85 scf/stb would be dissolved and

415 scf/stb would be a free gas phase. This amounts to about 4.41 cubic feet or 0.785 barrel of gas phase per barrel of water. If we include the dissolved CO<sub>2</sub> volume as a gas phase, the total is 0.945 barrel of CO<sub>2</sub> as gas phase per barrel of water phase. Hence, the injection ratio as quoted does not correct for the amount of the injected CO<sub>2</sub> which dissolves in the water with which it is injected. With the correction, the ratio stated for water versus CO<sub>2</sub> is 1/0.785 or 1.274 barrel of water per barrel of free CO<sub>2</sub> gas phase at reservoir conditions, rather than a 1:1 volume ratio as stated. These calculations emphasize the need for deduction of the CO<sub>2</sub> which dissolves in the water from the injected CO<sub>2</sub> before calculating the ratio of water phase to the free CO<sub>2</sub> gas phase in the injected fluid stream mixture at reservoir conditions.

In any event, since the molar volume of CO<sub>2</sub> at low pressures is much greater than its volume at typical miscible flooding conditions, then a 1:1 volume injection ratio as is typically used in miscible flooding will amount to a much lower amount of CO<sub>2</sub> as scf per stb of water, at immiscible flooding conditions. Evidently, however, an optimum ratio if it exists is important to find, and may be a strong function of the reservoir pressure.

This ratio was, therefore, the variable which was investigated in the computer simulations of the one-acre pilot. The pressure was not varied. It is advantageous to have as high a pressure as possible, and a 500 psia level was chosen as feasible and about the highest that could be expected in this reservoir. At the 500 psia level, the solubility of CO<sub>2</sub> in the injection water is estimated to be (at 103°F reservoir temperature) about 100 scf/stb for pure water or about 73 scf/stb for 100,000 ppm salinity brine. The latter value was chosen as representative for this case. It amounts to 0.01 mol fraction of dissolved CO<sub>2</sub> in the injected mixture of water and CO<sub>2</sub>. In the simulator data input, the proportions of water and CO<sub>2</sub> in the injection stream, if injected simultaneously, are input as mol fractions.

While common practice is to inject water and CO<sub>2</sub> alternately (a typical interval might be two weeks to six months), it is supposed that the fluids mix in the reservoir. Because of gravity segregation, water tends to traverse the lower half of any reservoir cross-section while CO<sub>2</sub>, being less dense than water, tends to traverse the upper part of such a cross-section. For this immiscible flooding process, it is important to saturate the water which traverses the lower part of any cross-section with dissolved CO<sub>2</sub>, because the CO<sub>2</sub> in this carbonated water will transfer preferentially to the crude oil which it encounters. This results in swelling of the oil phase, thereby increasing its saturation and concomitantly its relative permeability. The CO<sub>2</sub> dissolved in the oil also reduces its viscosity, by a factor estimated to be two to three. These combined effects of swelling and viscosity reduction are responsible for a major part of the increased oil recovery.

In the upper part of the cross-section, where CO<sub>2</sub> preferentially tends to flow, it is helpful to have a sufficient water flow that the CO<sub>2</sub> as a gas phase is accompanied by water and by liquid oil phase. The interference of water phase and of oil phase with the flow of the gas phase by three-phase relative permeability effects can then hinder the rapid flow of free gas phase, and thereby reduce the extent to which CO<sub>2</sub> is produced without aiding oil recovery. While such excess CO<sub>2</sub> can (and should) be recycled by re-compression, drying and re-injection, this is an extra expense, for recycling costs about a quarter as much to a third as much as the purchased CO<sub>2</sub>. In general, in depleted oil fields, the produced CO<sub>2</sub> contains so little natural gas that it is not necessary to separate this component; the produced gas stream is suitable for re-injection. It is practically never possible to avoid the necessity for recycling, but it should be minimized as much as possible. In these simulations, the water and CO<sub>2</sub> were injected simultaneously, thereby ensuring that all of the injected water was saturated with dissolved CO<sub>2</sub>. The WAG (water/CO<sub>2</sub>) volume ratio was calculated with correction for the dissolved CO<sub>2</sub>, so that the ratio as given represents the ratio of water phase to free CO<sub>2</sub> gas phase. In these simulations, the run was pursued until the water cut reached 98% - the same terminal point as if the current waterflood were continued.. The results were evaluated on two bases: the extra oil recovery beyond what would have been obtained by the continued waterflood, basis OOIP, and the ratio of gross CO<sub>2</sub> (purchased plus recycle) and net CO<sub>2</sub> (purchased only) to extra recovered oil, as scf/stb. When the cost of purchased CO<sub>2</sub> and of recycled CO<sub>2</sub> are determined for a given case, and the value of the recovered oil is known, the economics of the process are largely determined. Usually, the gross ratio of CO<sub>2</sub> costs to market value of oil recovered must be no more than 1/2, to allow for operating costs, royalties, taxes, and profit.

### Simulation Results

The cases examined were those of 0.1, 0.03, 0.02, and 0.01 mol fraction of CO<sub>2</sub> in the injected mixture of water and CO<sub>2</sub>. The following table shows the results:

Table 6  
Simulation Results for Immiscible CO<sub>2</sub>/Water Floods

<u>Mol Fr. CO<sub>2</sub></u> <u>mol/mol</u>	<u>scfCO<sub>2</sub>/</u> <u>bbl H<sub>2</sub>O</u>	<u>Corr. WAG Ratio</u> <u>vol.water/vol.gas</u>	<u>CO<sub>2</sub>/EOR, mscf/st</u>		<u>Extra Oil EOR)</u>	
			<u>Gross</u>	<u>Net</u>	<u>stb</u>	<u>% OOIP*</u>
0.10	820.0	0.33	16.76	1.53	971.7	10.06
0.03	228.2	1.50	4.31	1.19	1136.7	11.77
0.02	150.6	3.00	3.26	1.22	1113.7	11.53
0.01	74.5	Infinite (CO <sub>2</sub> dissolved)	2.38	1.33	951.7	9.85
0.00	(No CO <sub>2</sub> ) -> 555.3 stb by continued waterflood = 5.75% of					

OOIP; the extra oil above is in addition to this amount.

\* Initial Oil In Place (prior to Primary Depletion) in the quarter-five-spot pilot area = 9661.6 stb.

In the case of the 0.03 mol fraction CO<sub>2</sub> run, a blowdown was simulated at the end of the normal process, bringing the reservoir pressure down from 510 psia, which was established in the initial pilot set-up, to about 22 psia. The previous simulation run had continued past the 98% watercut point to 98.33% and the oil recovery had increased from 11.77% to 12.05% of OOIP. The additional oil recovery due to this blowdown was 1.08% of OOIP. The CO<sub>2</sub> production reached 5188 mscf as compared to a total of 5243 mscf injected prior to the blowdown, hence recovery of the injected CO<sub>2</sub> was essentially complete at this point.

Figure 16 shows the course of this run with 0.03 mol fraction of CO<sub>2</sub> in the injected mixture of CO<sub>2</sub> and water, compared to the continued waterflood alternative. Figure 17 shows the oil recovery curves for all four runs, compared to continued waterflood, with the 98% water cut points marked. Note that the process takes longer, the less the CO<sub>2</sub> concentration, except for zero CO<sub>2</sub> content (continued waterflood). There is thus some advantage in using a higher CO<sub>2</sub> concentration, other factors being equal. In general, of the runs shown, the 3 percent (0.03 mol fraction) run seems the most advantageous. The process is completed in about 465 days. Thus, the results of the pilot test would be available within a reasonable time.

The 1371 mscf of CO<sub>2</sub> plus 20.9 mscf of natural gas which were present in the reservoir at the start of blowdown in this run provide gas lift for the 104 stb of oil and 2120 stb of water which were produced during blowdown. Total oil recovery at this point was 18.88% of OOIP in addition to the 37.90% recovered prior to the pilot operation, within the pilot area, or a total of 56.78% of OOIP. For this area, the prior recovery plus continued waterflood oil recovery would have totalled 43.65% of OOIP.

In any case, it would appear from these results that the optimum WAG ratio is about 1 to 2. For the WAG ratio of 1.5, net CO<sub>2</sub> ratio to extra recovered oil is the lowest of those shown, and the gross CO<sub>2</sub> to extra oil ratio is only about 4.3. These ratios are considerably less than the ratios generally observed in the higher pressure miscible CO<sub>2</sub> floods. At 1.19 mscf/stb net CO<sub>2</sub> to extra oil ratio, for the quarter five-spot studied, the purchased CO<sub>2</sub> would be 1353 mscf, and the recycled CO<sub>2</sub> would be 3546 mscf. If the latter cost 1/4 as much as the purchased CO<sub>2</sub>, then the cost of recycled CO<sub>2</sub> would be equivalent to that of 887 mscf of purchased CO<sub>2</sub>. The equivalent ratio of CO<sub>2</sub> at the purchase price to extra oil recovery is 1.97 mscf/stb. Even if the purchase price for the CO<sub>2</sub> was as high as \$4/mscf (which it might be if the CO<sub>2</sub> is delivered in tank trucks and stored at about 0° F), then the cost attributable to the CO<sub>2</sub> supply would be about \$8 per barrel of extra oil. This would probably meet the economic criterion of a

cost for the CO<sub>2</sub> supply of less than half of the market price for the crude oil.

Other pilot costs would comprise CO<sub>2</sub> storage and injection equipment, recycle compressor and dryer, pilot production well costs, conversion of surrounding wells to provide back-up water injection for confinement and pressuring-up of the pilot area, and a certain amount of loss of oil production from these converted wells. These would make the cost of the extra oil from this small pilot much higher than the market value of the 1100-1200 barrels of extra crude oil which is predicted to be recovered from the quarter-five-spot, or 4400-4800 stb from the entire five-spot (6600-7000 barrels gross, counting the continued waterflood oil production subtracted in calculating the extra oil).

Hence, the purpose of a pilot operation such as has been simulated would be to confirm the computer simulation, in anticipation of applying the process to the entire field. If the recovery from the entire field were the same as that calculated for the pilot area, the extra oil amounting to 13.13% of OOIP (basis 10 million stb) translates to 1.313 million barrels of extra oil. The market value of this much extra oil, based on an average market value of \$20/barrel, could be on the order of \$25 million.

Furthermore, as indicated by the inclusion of this field in the SLERO list, and by the discussion in Hamilton's paper<sup>(6)</sup>, this reservoir is approximately characteristic of a class of Texas reservoirs which originally contained on the order of about 3 billion barrels. For this extended resource, the Seventy Six West field could serve as a pilot operation to determine the economic feasibility of the extension of the immiscible CO<sub>2</sub> flooding process to many other fields of the same class. It is considered significant that an economic process for extra oil recovery for fields of this type seems to have been found, namely, immiscible CO<sub>2</sub> flooding

Extensive studies have already been made<sup>(11)</sup> to pinpoint CO<sub>2</sub> sources, and equipment has been developed for hauling CO<sub>2</sub> to fields for small-size projects (such as "Huff-and-Puff" single-well CO<sub>2</sub> stimulation treatments). The technology of handling CO<sub>2</sub> for such stimulations and for field-wide miscible CO<sub>2</sub> floods has already been established, so that no new technological problems are to be expected in applying CO<sub>2</sub> in lower pressure, immiscible floods.

### Summary

Under this portion of the project, two principal lines of research were performed, both by use of computer simulation of reservoir oil recovery processes. The first of these concerned a study of primary, secondary, and tertiary oil recovery processes in two main geologic types of oil reservoir rock formations - (a) those formed from ancient alluvial (river bank) sand bars, and (b) those formed from ancient off-shore barrier sand bars (like Galveston Island). The second study concerned a specific oil field in Duval County, Texas - The Seventy Six West field - in which the Texas State Land Office holds the mineral rights to over half of the field. This field was chosen for geophysical and simulation studies because the state was able to provide access to the field for the geophysical studies which are described elsewhere in this report. This field is also one of the series of geologic type fields which were selected by the Texas Bureau of Economic Geology for study as part of a different project called the State Lands Energy Resource Optimization (SLERO) project, hence, data were available from this source on field and rock properties, which could be used in the simulation studies of this particular field. It is of the off-shore barrier-bar type, but its structure is complicated by the presence of several such bars, displaced laterally and vertically, by a stream mouth, and by sands washed over the top of the bars by storms into the lagoons behind. Such complications of structure are the rule rather than the exception.

The first study showed the influence of the different vertical trends of horizontal permeability in the alluvial sand bars and in barrier bars - highest permeability at the bottom in the alluvial bars, and highest permeability at the top in the barrier bars - on the oil recovery behavior in primary recovery by pressure depletion, in secondary recovery by waterflooding, and in tertiary recovery by CO<sub>2</sub> flooding, or by steam flooding in the case of heavy oils. Three oil viscosity levels were employed, and so the results reflect the behavior of a variety of crude oils in these reservoir types.

In the primary recovery phase, the alluvial bar type showed much higher oil recovery than the barrier bar type. However, in a waterflood started in each case during primary depletion at a point when the pressure had declined from the initial pressure to about 1100 - 1300 psi, the barrier bar type showed better performance. In a subsequent CO<sub>2</sub> tertiary flood, the additional oil recovery was slightly better for the alluvial point bar type. This was also the case for steam drive, in which only the most viscous oil was assumed to be present. The results accord with the realization that with low density fluids being produced or injected as drive fluids, the better oil recovery is obtained with a permeability profile from high at bottom to low at top, while the reverse is true for an injected fluid more dense than reservoir oil, namely water.

In the study of the Seventy Six West field, a history match was first performed with a three-dimensional grid-block plan covering the entire reservoir plus the aquifer to the southeast. The aquifer size was varied to

obtain the observed behavior of the field, namely, that pressure depletion occurred despite partial pressure support from the aquifer, and a secondary gas cap was generated on the high side of the field, to the northwest. A waterflood was started about halfway through the life of the field (to date) and this helped to maintain pressure so as to provide a minimum level of well productivity, but nearly all of the initial dissolved gas had been produced during primary depletion so that the remaining oil contains very little natural gas. Current average pressure is only a little over 100 psi, versus nearly 600 psi initial. The water cut (from the waterflood) has risen to a relatively high level but the current oil recovery is over 46% of the original oil in place - a relatively high level for primary plus secondary, which can be attributed to the relatively low level of remaining oil saturation in the gas cap, as compared to the waterflood residual oil saturation in the rest of the reservoir. Additional oil recovery is estimated at 4% of the original oil in place. However, this still leaves 1/2 of the original oil in place. Attention was therefore placed on what might be accomplished by a tertiary recovery process. For this purpose, a one-acre pilot test area was selected around one of the better wells. It was assumed that four production wells would be drilled in a five-spot pattern around this well, which would be converted from a producer to an injection well.

The possible choice of enhanced oil recovery processes is limited by the shallow depth of this field, which limits injection pressures to only a little over 500 psi. This is insufficient to obtain miscibility with CO<sub>2</sub> or with any hydrocarbon mixture containing very much natural gas in admixture with LPG. Chemical flooding methods were considered to be too expensive (surfactant-polymer) or to have too little prospect of additional oil (polymer alone). However, there are a few examples reported in the petroleum engineering literature of immiscible CO<sub>2</sub> floods in which sizable additional oil recoveries - up to 10% of original oil or more - were obtained. These were generally at 1000 psi or higher, but it was decided to explore this possibility at the 500 psi level by computer simulation using a 10x10x6 grid simulation model. It was found that best results are obtained, as indicated by the prior publications, by joint injection of water with the CO<sub>2</sub> at such ratios that the excess CO<sub>2</sub> over the amount which would dissolve in the water at the pressure level of 500 psi assumed to be maintained in the pilot area would be in about a 1:1 volume ratio to the water. Much of this excess CO<sub>2</sub> then dissolves in the oil, swelling it somewhat and much reducing its viscosity. These two effects lead to development of an oil bank which is driven by the water to the producing wells. In these simulations with different water:CO<sub>2</sub> ratios, the extra oil recovery reached 10-11% of original oil in place. It is therefore suggested that investigation of the possibility of using this method of extra oil recovery be continued.

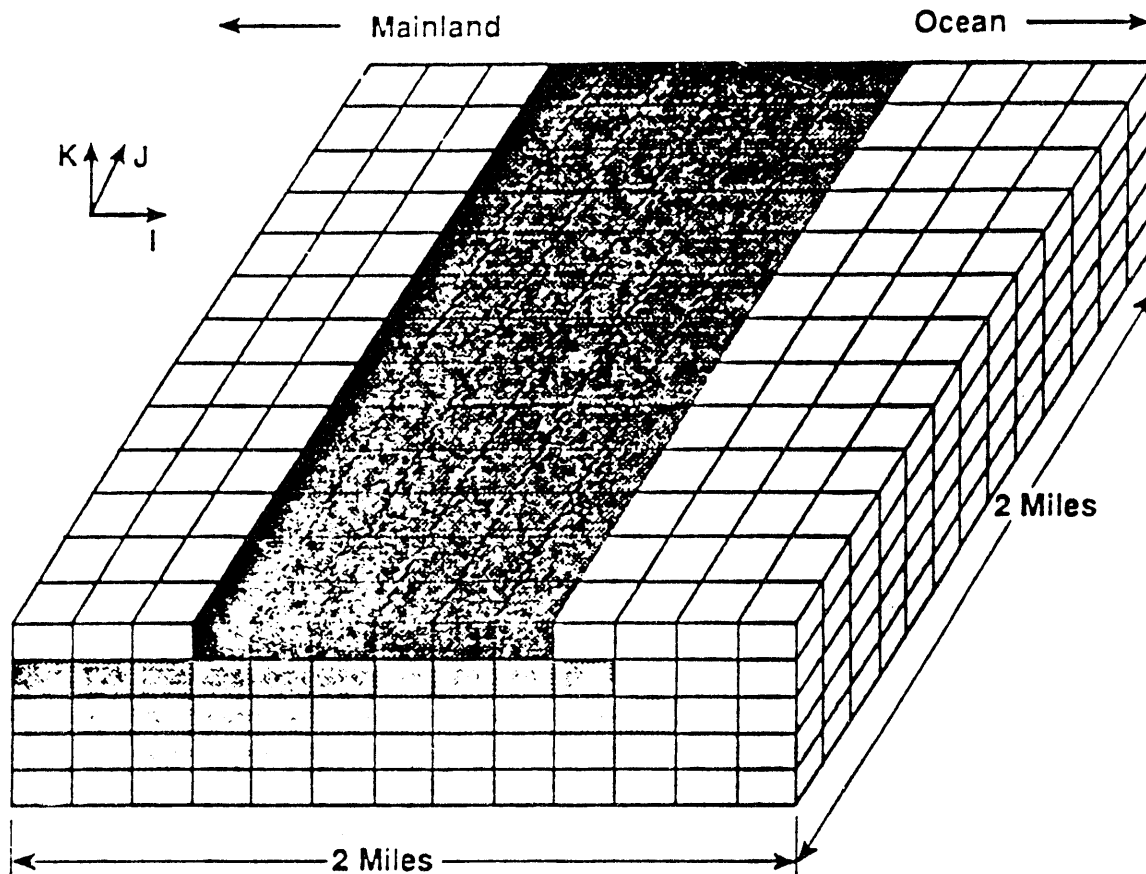
## Recommendations

1. As a matter of prudence, it is recommended that these simulation results be at least partially confirmed by some core flooding tests with similar type sandstone rock and with Seventy Six West field crude oil and water and CO<sub>2</sub> at the pressure and water/CO<sub>2</sub> ratios discussed above. Similar core flooding tests have already been carried out for the Wilmington field case (10), and these support the order of magnitude of the results reported here (15-20 saturation percent improved oil recovery, with 76-77 saturation percent initial oil in place in the cores). However, the Wilmington tests were run at 1000 psi, and the situation in the Seventy Six West field is such that only half that pressure can be used.
2. Should laboratory core flood data support these simulation results, then it is recommended that consideration be given by the Texas Land Office to carrying out a pilot test of the immiscible CO<sub>2</sub> flooding process in the Seventy Six West field.

## REFERENCES

1. Richardson, J.G., Sangree, J.B., and Sneider, R.M., "Meandering Stream Reservoirs." J. Pet. Tech. (Dec. 1987) pp. 1501-2.
2. Richardson, J.G., Sangree, J.B., and Sneider, R.M., "Coastal Barrier Reservoirs," J. Pet. Tech. (Sept. 1988) pp. 1127-8.
3. Hanauer, David, "Enhanced Oil Recovery Processes in Geologic Models," M.S. Theses, May 1988, University of Houston.
4. Hyatt, Diane B., "Geology of the Seventy Six West Field, Duval County, Texas," M.S. Thesis, May 1990, University of New Orleans.
5. Hyatt, Diane B., "Geology and Production Characteristics of the Seventy Six West Field, Duval County, Texas," Transactions of the Gulf Coast Association of Geological Societies, 40 (1990) pp. 305-318.
6. Hamilton, D. S., "Reservoir Heterogeneity at Seventy Six West Field, Texas: An Opportunity for Increased Oil Recovery From Barrier/Strandplain Reservoirs of the Jackson-Yegua Trend by Geologically Targeted Infill Drilling," SPE Paper 22672, presented at the 66th Annual Technical Conference of the Society of Petroleum Engineers, Dallas, October 6-9, 1991.
7. Durham, E.N. and Watson, J.A., "'CO<sub>2</sub> Field Injection Project Conducted by Phillips Petroleum Company - Ritchie Field, Union County, Arkansas," in *Target Reservoirs for CO<sub>2</sub> Miscible Flooding*, Contract No. DOE.MC/08341-17, U.S. DOE, Bartlesville, OK (Oct. 1980) II, p. 92.

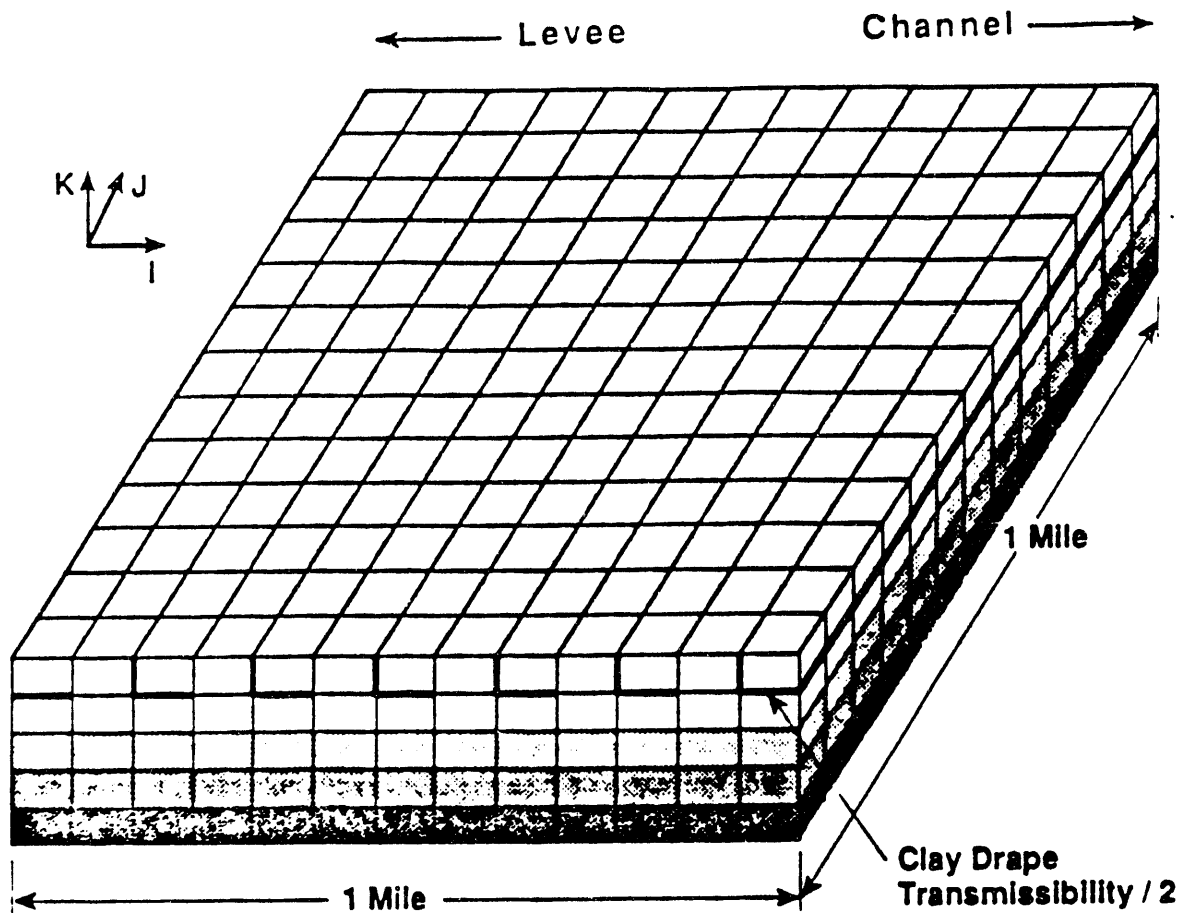
8. Reid, T.B. and Robinson, H.J., "Lick Creek Meakin Sand Unit Immiscible CO<sub>2</sub>/Waterflood Project," J. Pet. Tech. (Sept. 1981) pp. 1723-1729.
9. Saner, W.B. and Patton, J.T., "CO<sub>2</sub> Recovery of Heavy Oil: Wilmington Field Test," J. Pet. Tech. (July 1986) pp. 769-776.
10. Mayer, E.H., Earllougher, R.C. Sr., Spivak, Allan, and Costa, Alexander. "Analysis of Heavy-Oil Immiscible CO<sub>2</sub> Tertiary Coreflood Data," SPE Res. Eng. (Feb. 1988) pp. 69-75.
11. "Naturally Occurring Carbon Dioxide Sources in the United States - A Geological Appraisal and Economic Sensitivity Study of Drilling and Producing Carbon Dioxide for Use in Enhanced Oil Recovery," Gulf Universities Research Consortium Report No. 165 (Dec. 1978).



	Height ft	Permeability <sup>*</sup> md	Porosity %
	5	2700	28
	7	1400	28
	8	900	28
	11	225	25
	9	80	22

\* Vertical Permeability = Permeability /10

**Figure 7. Coastal Barrier Bar Sandstone Reservoir Model-Multiflood Simulator.**



	Height ft	Permeability <sup>*</sup> md	Porosity %
	13	100	23
	9	330	25
	8	750	27
	7	2000	27
	3	3000	26

\* Vertical Permeability = Permeability / 10

Figure 8. Alluvial Point Bar Sandstone Reservoir Model.

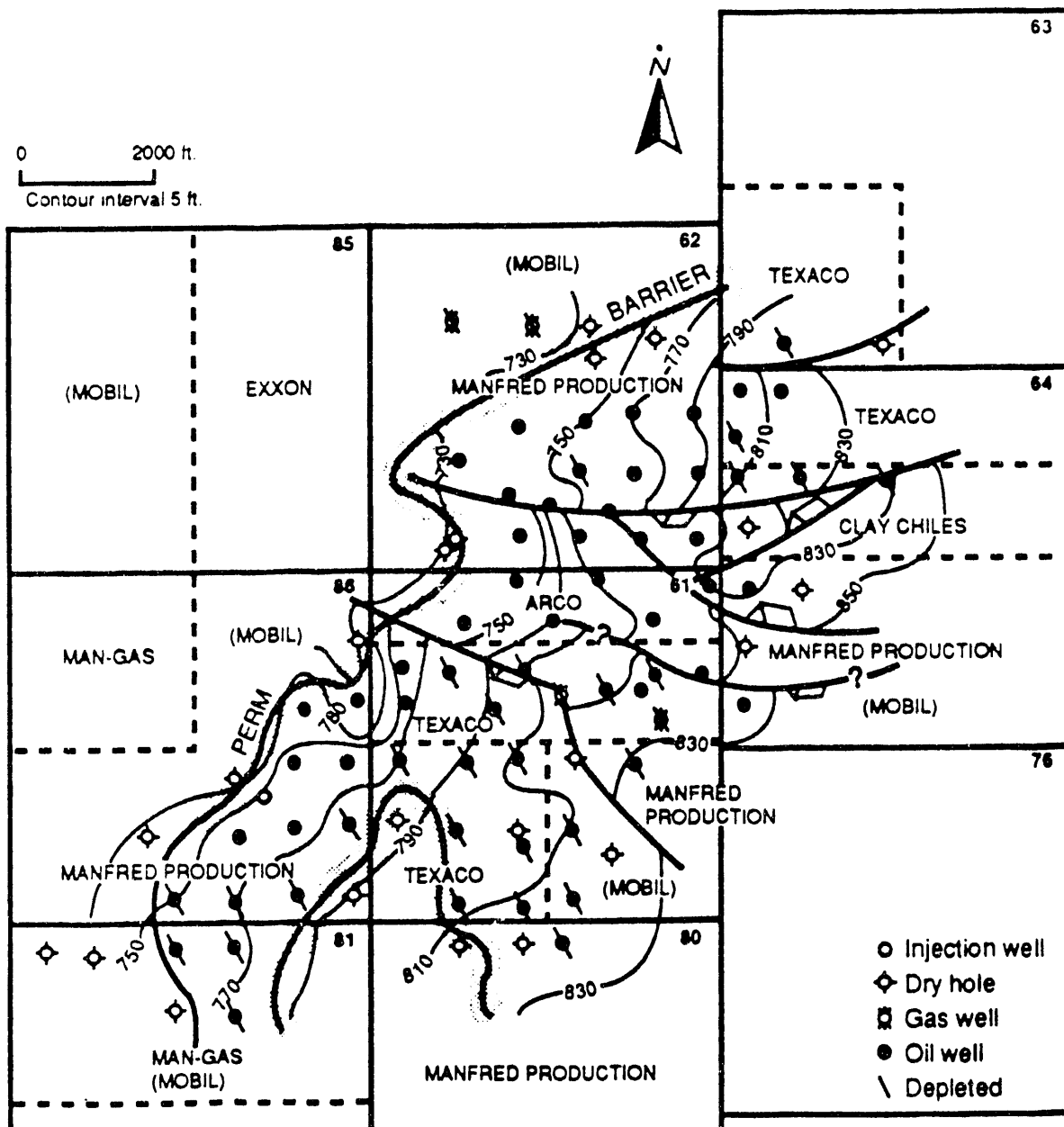


Figure 9. Structure, Seventy Six, West Field, Subzone "B".



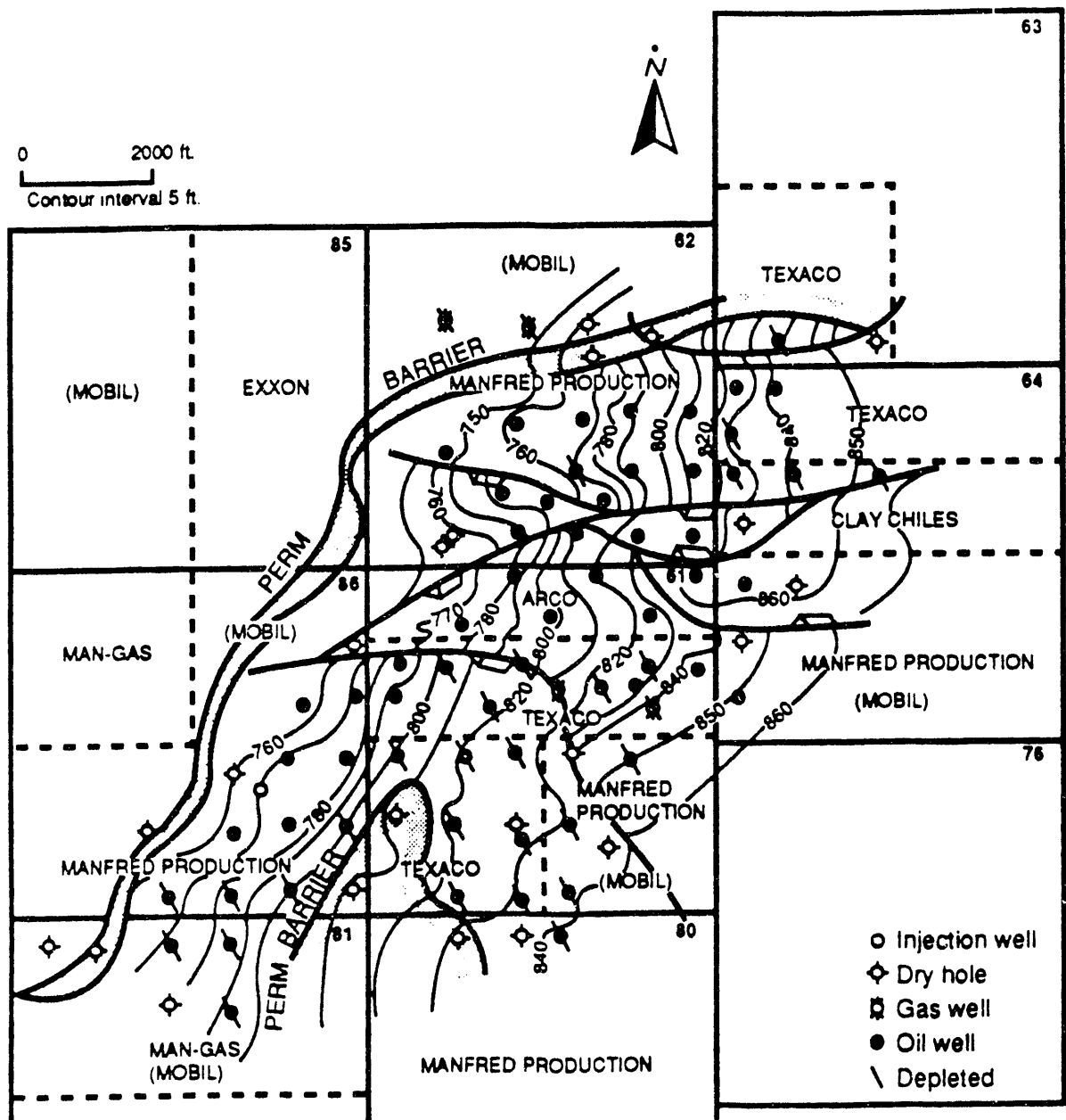


Figure 11. Structure, Seventy Six, West Field, Subzone "C".

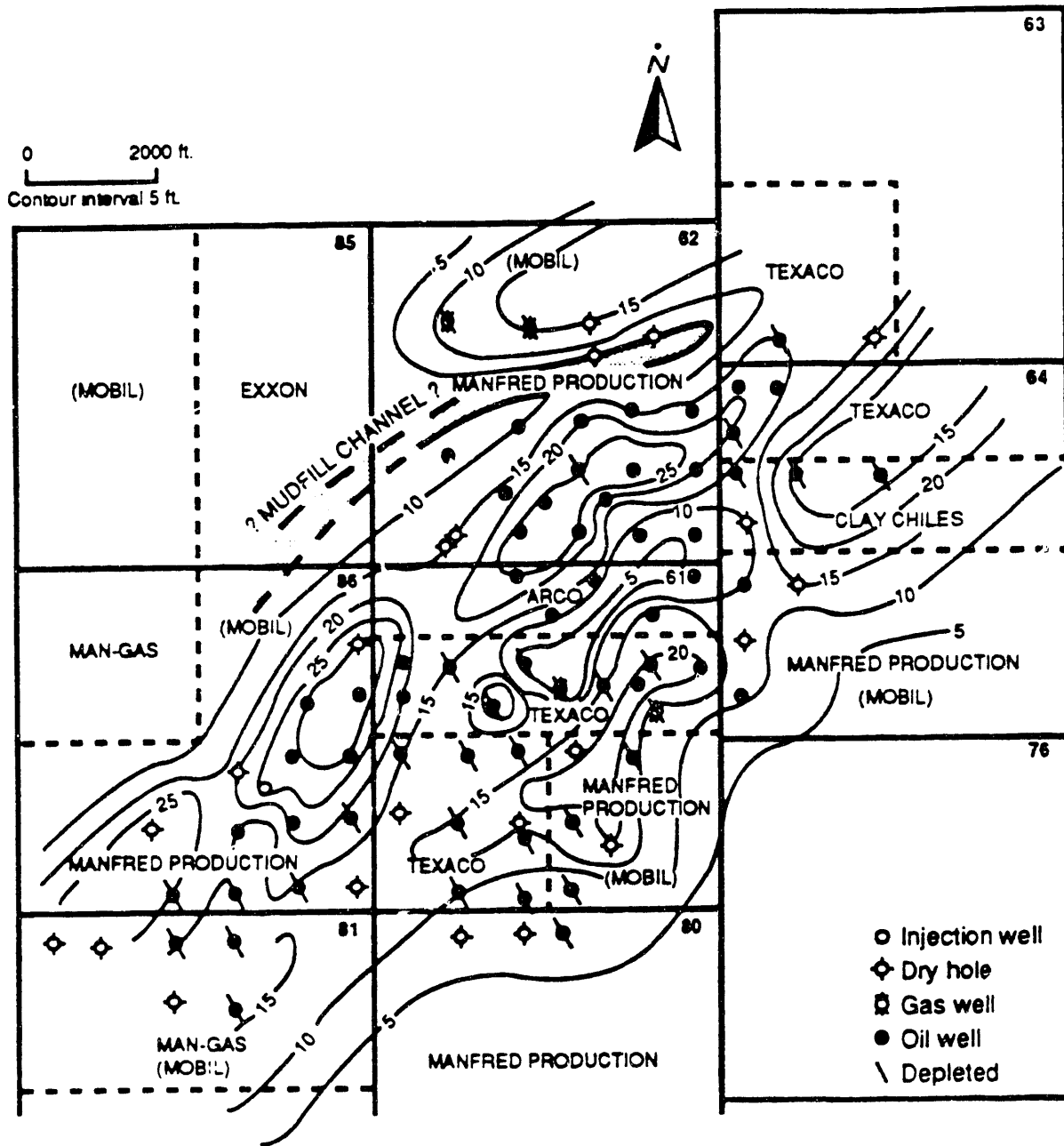
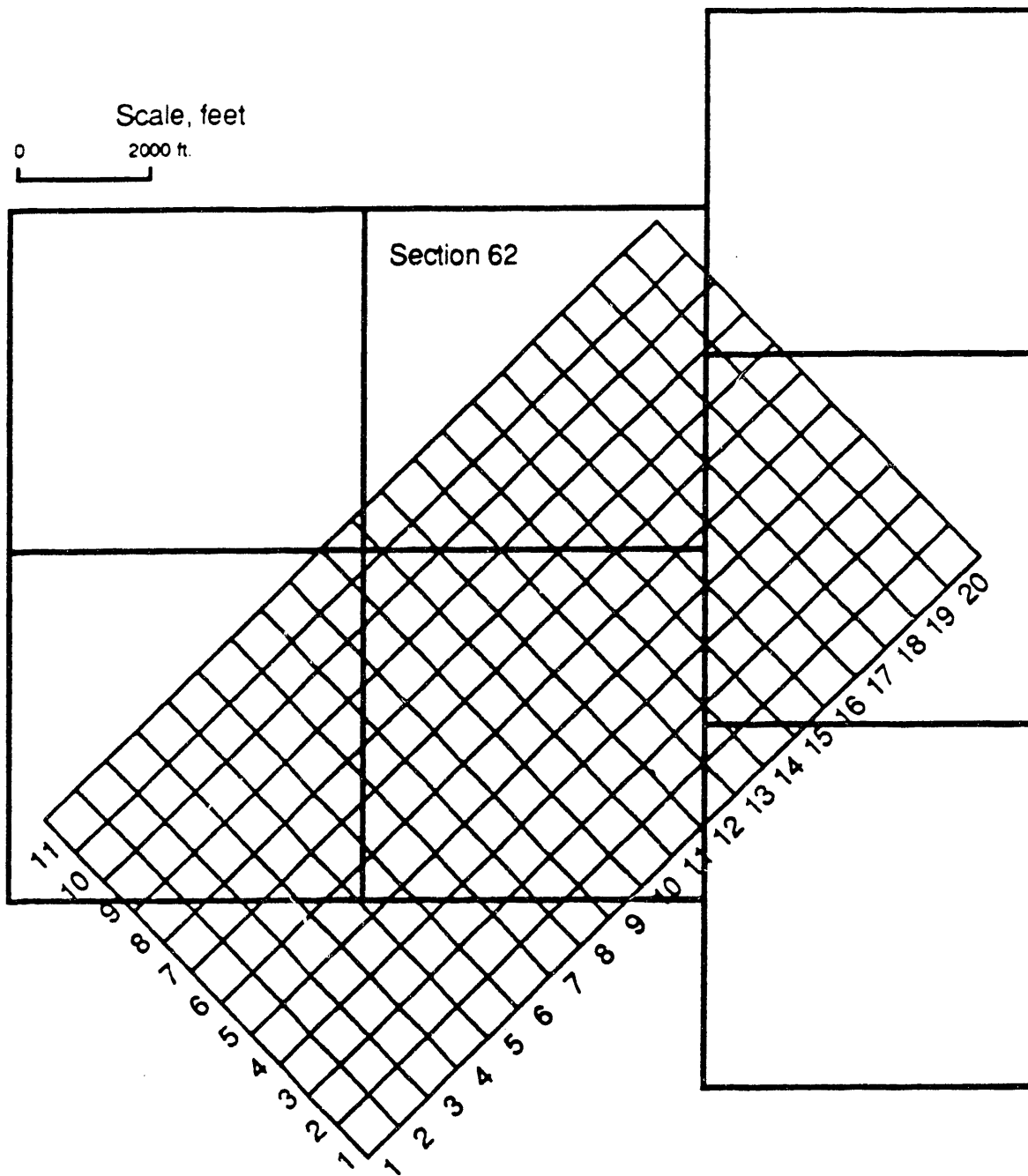


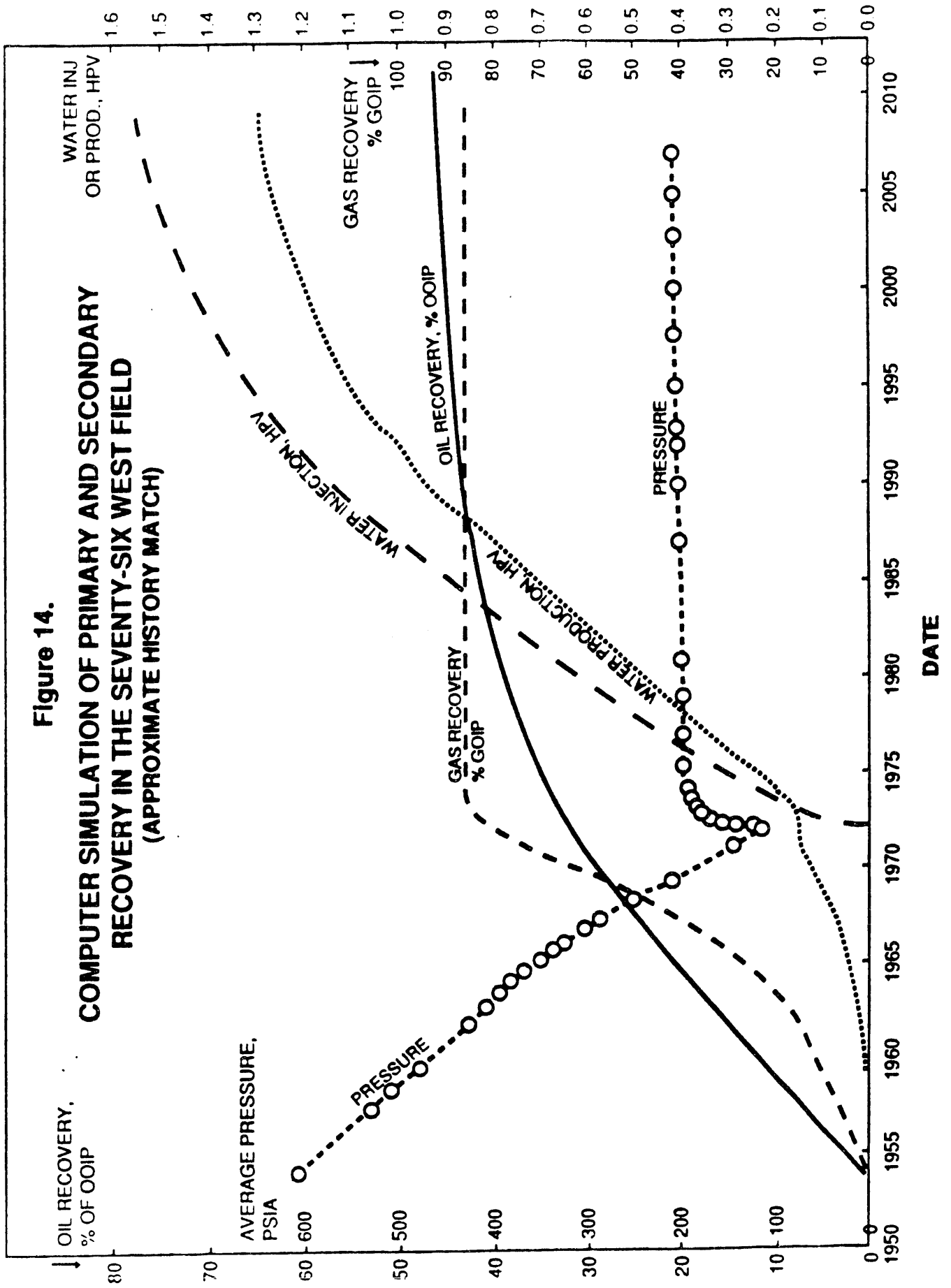
Figure 12. Net Sand Map, Subzone "C".



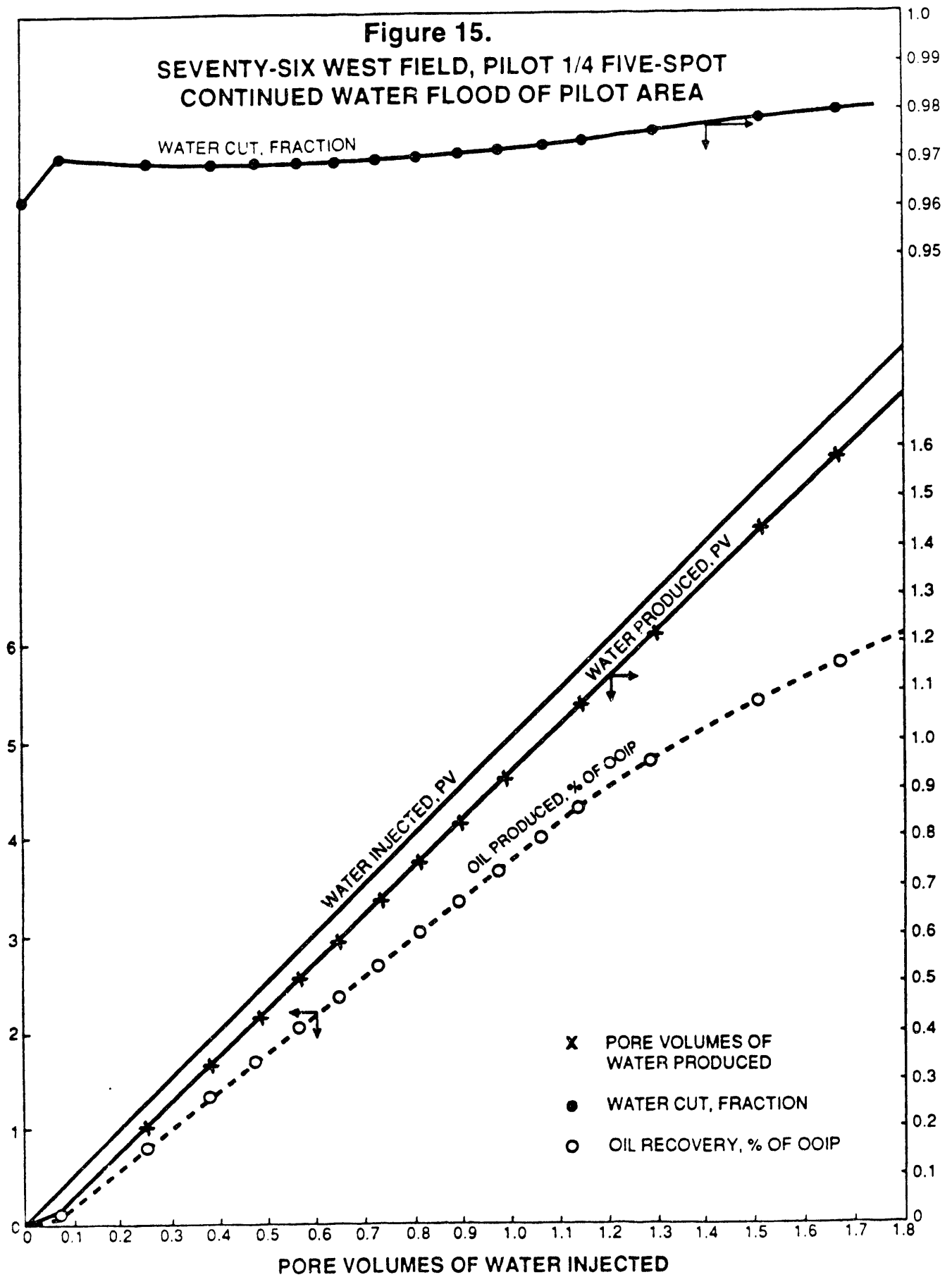
**Figure 13. Seventy Six, West Field, Simulation Grid  
(10 Acre Grid Blocks)**

Figure 14.

COMPUTER SIMULATION OF PRIMARY AND SECONDARY RECOVERY IN THE SEVENTY-SIX WEST FIELD (APPROXIMATE HISTORY MATCH)



**Figure 15.**  
**SEVENTY-SIX WEST FIELD, PILOT 1/4 FIVE-SPOT**  
**CONTINUED WATER FLOOD OF PILOT AREA**



**Figure 16.**  
**COMPUTED OIL RECOVERY AND WATER CUT CURVES**  
**FOR CONTINUED WATERFLOODING AND FOR A**  
**CO<sub>2</sub>-WAG EOR PROCESS WITH 228 SCF OF CO<sub>2</sub> (3% MOL)**  
**PER BARREL OF WATER, FOR A PILOT TEST**  
**IN THE SEVENTY-SIX WEST FIELD**

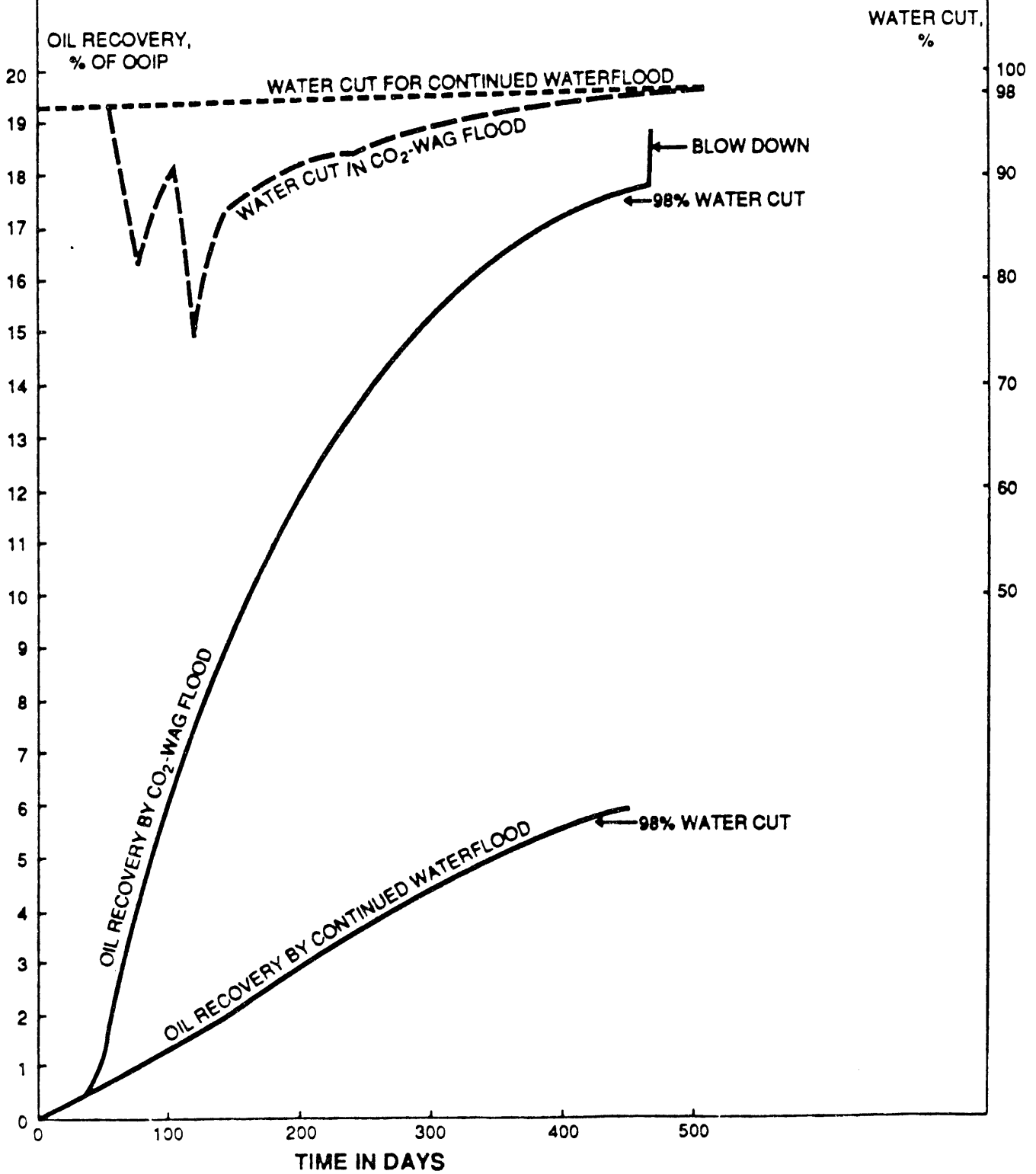
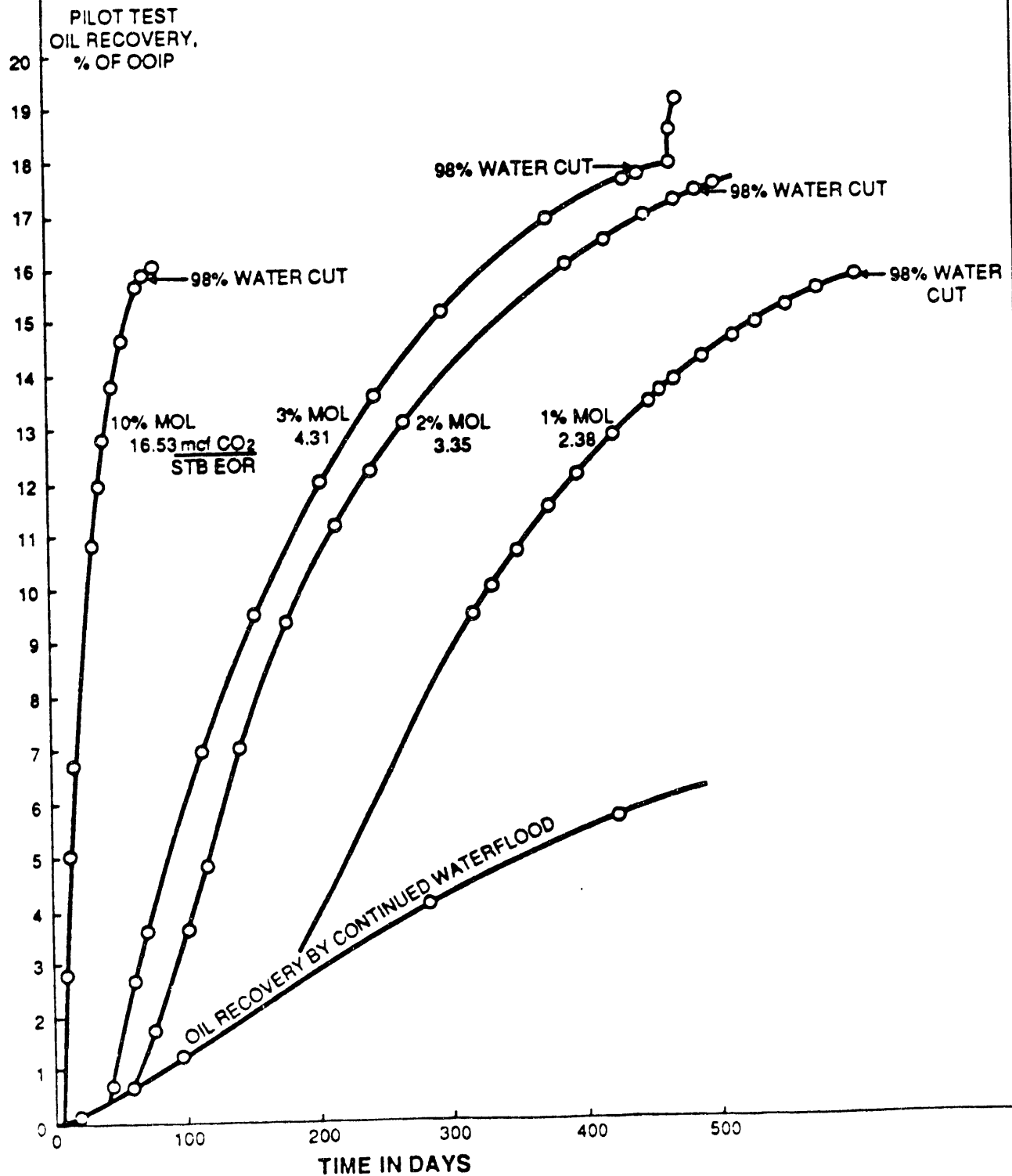


**Figure 17.**  
**COMPARISON OF COMPUTED OIL RECOVERY CURVES**  
**FOR A PILOT CO<sub>2</sub>-WAG FLOODING PROCESS IN THE**  
**SEVENTY-SIX WEST FIELD WITH DIFFERENT**  
**CO<sub>2</sub> CONCENTRATIONS IN THE INJECTED STREAM**



**Subtask #5: Developing an Evaluation of Local Flood Efficiency in Different Parts of the Demonstration Reservoir Utilizing Parallel Computing.**  
**(Dr. John E. Killough)**

**ABSTRACT**

Over the past fifteen years high performance computing has had a significant impact on the evolution of numerical predictive methods for improved recovery from hydrocarbon reservoirs. The complexity of reservoir simulation models has led to computational requirements that have consistently taxed the fastest computers. This work discusses how current state-of-the-art parallel architectures have been investigated to allow models which more closely approach realistic simulations while emphasizing accuracy and efficiency of the models. Two modeling approaches have been investigated on several different parallel architectures. The first approach involves the porting of existing commercial software to parallel MIMD shared and distributed machines. The second approach considers a novel reformulation of the numerical solution which emphasizes parallel efficiency. Both techniques have been shown to exhibit high parallel efficiencies on a distributed memory parallel computer ( the Intel Supercomputer Systems 860 ) for both real and hypothetical data. These simulation techniques were applied to the prediction of hydrocarbon recovery from the Seventy-Six West field. Results showed the validity of predictions using other approaches.

**INTRODUCTION**

Computer performance over the past decade has advanced significantly. These advances have been such that current single processor performance is limited by speed-of-light considerations. These limitations indicate that to achieve speedups greater than an order of magnitude above current technology, significant architectural changes must be employed. The emerging parallel computer architectures appear to be the most likely avenue for this advancement in computing.

Parallel computers have existed for several decades; however, it was only recently that architectures and languages have been such that these machines could be readily used for significant work. The parallel machines have three varieties: shared memory, distributed memory, and very long instruction word. The shared memory machines are characterized by computers such as the CRAY Y-MP 8/32, the IBM 3090 600S/VF, the Sequent Symmetry, and the ETA 10. The cpu's and memory are connected in a manner such that all memory is accessible by all CPU's. This is illustrated in Figure 18 showing a cross-bar like connection among the memory banks and CPU's. For the high-performance supercomputers such as the CRAY X-MP and IBM 3090, this global memory connection can be costly because of the requirement of rapid access to memory.

To overcome this difficulty, several distributed memory architectures have evolved. These are characterized by grids of less powerful CPU's connected in some fashion to each other for communication of data and synchronization. (See Figure 19) One of the most popular of these connections schemes is the hypercube topology. Two current machines employing this architecture are the N-CUBE and INTEL iSS/860. Each of these machines may have more than 100 processors. Both the N-CUBE and INTEL machines are multiple instruction, multiple data (MIMD) computers. Each CPU of the computer may execute different sets of instructions on different data. Another emerging distributed memory, massively parallel computer is the Connection Machine which is a single instruction, multiple data (SIMD) architecture with up to thousands of processors. All CPU's execute each instruction in lockstep with one another.

The very long instruction word computer such as the MULTIFLO and FPS 264 exploit local parallelism within a user's program. The compiler, by combining many parallel operations of the functional units of the machine into each instruction, can achieve significant speedups.

Several publications in the recent literature have dealt with the application of parallel computing to petroleum reservoir simulation in shared memory parallel environments. Scott, et al.,<sup>1</sup> investigated the parallelization of the coefficient routines and linear equation solvers for a black-oil model on a Denelcor HEP. Chien, et al.,<sup>2</sup> investigated compositional modeling in parallel on a CRAY X-MP 4/16. Barua and Horne<sup>3</sup> applied parallel computing using a non-linear equation solver for the black-oil case on the Encore Multimax. Killough, et al.,<sup>4</sup> looked at parallel linear equation solvers on both the CRAY X-MP and IBM 3090. Each of these applications involved the use of a shared-memory parallel computer. The question still remained as to whether a distributed memory architecture could be efficiently utilized for simulation of petroleum reservoirs.

More recently parallelization of reservoir simulators has been accomplished on distributed memory parallel computers. Work by van Daalen, et al.,<sup>5</sup> showed a speedup of a factor of forty on sixty processors on the Transputer-based Meiko computer. Wheeler and Smith<sup>6</sup> showed that black oil modeling could be performed efficiently on a hypercube. The application of compositional reservoir modeling to the distributed memory, message passing, INTEL IPSC/2 Hypercube was investigated by Killough and Bhogeswara<sup>7,8</sup>. The key issues in this parallelization involved the data structure of the program, message passing of data among processors, and development of parallel linear equation solvers for the model.

The need for high performance computing for the petroleum reservoir simulation model is dominated by the physics of the processes being investigated. The transport of multi-phase fluids in porous media is governed by a variety of complicated phenomena. In a typical underground flow problem, one identifies processes on a range of length scales, from the millimeter scale to the field scale, on the order of a few miles. Capillary

effects are important in the small scales and macroscopic effects like front coalescence and dispersion are important up to the largest scale.

With the introduction of Computer Tomography and Nuclear Magnetic Resonance techniques into the analysis of core samples of porous media, one can gain insight into the geological structure of the sample on the laboratory scale. Detailed three dimensional porosity maps for a core 4 in. in diameter and 12 in. long are now easily obtained. One can naturally incorporate this information, in the form of porosity and also permeability to model a displacement experiment through the core. Figure 3 shows results from a simulation using CT data on a scale of about one cubic millimeter. As shown by the fingering of the injected miscible fluid in the figure, the inclusion of fine-scale heterogeneities can significantly effect the displacement process.

The question of how to scale-up from this laboratory scale to the field scale is still open. However, a numerical scheme that can incorporate a description of the local heterogeneities as fine as possible, given the *state of the art computing*, represents a valuable tool in the development of scale-up schemes.

The goals of the research effort fall into two categories: the restructuring of existing commercial software and the development of novel formulations for the numerical solution of the partial differential equations associated with flow in porous media. For the commercial software the recent work has concentrated on improving the global data structure and linear equation solver of the model and applying the simulator to a problem involving real data. A novel formulation based on operator splitting on multiple grids has been developed which shows a high degree of parallel efficiency. The aim of this second portion of the research has been the development and implementation of a numerical procedure that can capture the influence of local heterogeneities on a length scale of 1 to 2 ft for a computational domain in the order of about 1,000 ft in two dimensions. The inherent parallel nature of the new formulation has been exploited to obtain high computational efficiencies. These efficiencies can in turn be utilized for the prediction of hydrocarbon recoveries from petroleum reservoirs in fine detail. An example of this approach is given at the end of the text.

### **ARCHITECTURE OF THE ISS/860**

Much of the development in this work has been performed on the INTEL ISS/860. The architecture of this computer is illustrated on the bottom of figure 19 for the case of sixteen ( $2^4$ ) processors. As shown in the figure for an n-dimensional hypercube with  $2^n$  processors, each processor has connections to n other processors. If these processors are numbered in a binary fashion, the nearest neighbors sharing connections differ by only one binary digit. Currently, the ISS/860 can have up to 128 processors with up to sixteen megabytes of memory for each processor. With vectorization each processor is capable of up to 60 double precision MFLOPS with the 40

MHz i860chip. This corresponds to about one-half of the speed of the Cray-1. Scalar performance for the i860 is about 2-3 MFLOPS.

The iSS/860 has two unique features which make it particularly useful for reservoir modeling. First, communication among processors does not require a knowledge of the hypercube topology to achieve efficiency. Through what is called a "direct-connect" scheme, messages can pass from one processor to any other processor in the system with only a few percent overhead for each connection which must be crossed. Data transfer rate is at 2.8 megabytes per second for message passing. Latency for each message setup is approximately 70 microseconds.

Second, the local memory size available for programs may be up to sixty-four megabytes. This allows an entire reservoir simulator of reasonable size to fit on a single node and makes model conversion less tedious.

### **THE COMMERCIAL SIMULATOR**

The commercial n-component, 3-phase, equation-of-state model VIP-COMP of Western Atlas Integrated Technologies was used as the basis for the parallelization. Although the model contains provision for fully-implicit capabilities, only the IMPES option has been investigated to date.

The model is based on the Young-Stephenson formulation<sup>9</sup>. Basically, this formulation involves the use of a Newton-Raphson iteration for the solution of the overall component material balances using an equation-of-state. The equation-of-state is used for calculation of both fugacities (K-values) and densities.

At each time-step a Jacobian is formed for each of the cells in the model. The unknowns for the Jacobian are the cell pressures, the mole fractions of the components, the overall hydrocarbon quantity, the water quantity, and the vapor fraction for each grid block in the model.

A pressure equation is derived for the IMPES case through a forward elimination of the Jacobian. After the solution of the linear equation for the pressures, back substitution then yields the values for the  $3n_c + 4$  unknowns at each grid block in the model. ( $n_c$  is the number of components in the model.)

A typical flow chart for the compositional reservoir model is shown in Figure 20. After input data such as reservoir description and well rates are read, rock properties (relative permeabilities) and PVT properties are evaluated (viscosities). Well rates are then distributed among the cells in the model. The Jacobian is then formed and the forward elimination is performed to yield the IMPES pressure equation. An iterative or direct linear equation solver is applied to this equation. After solution for the pressures, back substitution into the factored Jacobian yields the updated values for all variables.

## PARALLELIZATION OF THE MODEL

The first step in parallelization of the model was the profiling of the segments of the model to determine the portions which consumed the most CPU time. As shown on the flowchart in Figure 21 for 1792 cell version of the Third SPE Comparative Solution (described below), the majority of the i860 CPU time was spent in the formation of the Jacobian and the forward elimination process for the pressure equation (EQUATION SETUP). The PVT evaluations (flash), equation solution, and the variable update were next in order of computational work requirements with 11.4, 6.6, and 8.4 percent of the overall CPU time, respectively. Amdahl's law describes how much efficiency a parallel program can achieve:

$$\text{Speedup} = 1.0/(s+p/n)$$

where,

s = serial fraction of program work

p = parallel fraction of program work

For the case of medium grained parallelism of 32 processors, the maximum speedup for 5% serial overhead is 12.54. This indicates that almost all portions of the model must be parallelized to achieve large parallel computing efficiencies.

The initial goal of this work was to reduce the serial component to below 5% for the compositional model. To achieve this, all portions of the program were parallelized with the exception of the well routines. Input and output processing were assumed to be insignificant for most large-scale simulation problems. The validity of this last statement may vary depending on the graphics data requirements for the simulation.

### INITIAL STAGES OF PARALLELIZATION

The initial stages of the parallelization involved a proof-of-concept for the parallel model. First, the coefficient setup routines were parallelized since these were "perfectly" parallel and consumed the majority of the CPU time for the model problem. This initial parallelization showed that even with the unnecessary overhead of passing of initial data to the routines, greater than 97% parallel content of the algorithm was achieved (See reference 7.)

The next stage involved the parallelization of all routines in the model and the combination of these routines with a parallel linear equation solver. The steps in the parallelization are shown in figures 22 and 23. Each routine was made to perform in parallel separately with message passing between a master program and the slave programs as shown in Figure 22. This inefficient approach allowed the data structure of the parallel model to be developed so that solutions were identically the same as the serial results. Finally, all message passing between the master and slaves was

eliminated except for bookkeeping such as time step summaries, etc as shown in Figure 23. The initial parallel model had one major inefficiency in that the data structure for the linear solver was based on a domain decomposition approach as opposed to a serial decomposition used in the other routines of the model. Results for this overall parallel model are given in Table 1 (The test problem SPE#3 will be described later.):

Table 1  
Speedups of Parallel SPE#3 for iPSC/2 (80386)

	Number of CPU's			
	4	8	16	32
PVT	3.81	7.03	12.31	19.37
Rock Prop	3.91	7.64	14.51	26.74
Eq. Setup	3.52	6.52	11.08	17.54
Eq. Soln.	3.89	7.12	11.21	15.40
Total	3.77	7.40	12.87	20.51

Speedup for this table is defined as the time for serial execution divided by the time for the same program when executed in parallel. For thirty-two processors on the iPSC/2 80386/387 based computer, a speedup in excess of twenty was obtained.

Below are descriptions of the linear equation solver and the data structure which have been used to further improve the parallel compositional model beyond these initial results.

### THE PARALLEL LINEAR SOLVER

Our aim in this part of the work has been to develop a general purpose efficient and robust solver for all types of problems independent of the granularity of the computer architecture. This is a challenging problem since most often robust solvers may not be efficient and efficient solvers may not be robust enough for all types of problems. There is a factor of granularity which makes this even more complicated especially on distributed memory computers with up to 128 processors. On these machines the algorithm must be developed to minimize message passing overhead since each cpu has its own local memory and external data can only be obtained by message passing. This minimization of message passing overhead is much more important in the i860 based machine than the 386 based machine since the i860 CPU is more than an order of magnitude faster but the communication speeds are of the same order for the two computers.

Our approach has been to develop a somewhat complex preconditioner for a conjugate gradient residual type iterative methods such as ORTHOMIN(k).<sup>10</sup> This algorithm, which is based on the combined approach of domain decomposition and multigrid methods, consists of four steps:

Step 1. Solve a 2-dimensional subproblem resulting from Watt's<sup>11</sup> line correction using the multigrid technique.

Step 2. Perform Line Jacobi relaxation along the vertical direction with the updated residuals from the step 1.

Step 3. Use domain decomposition with either block Jacobi or red-black block Gauss-Seidel to obtain the subproblems and solve independently on different processors. The solution from steps 1 and 2 is used as the initial values for the boundaries of the subdomains. Subdomain problems are solved by RS/ILU(0)<sup>12</sup> or ILU(0)<sup>13</sup> iterative solvers usually with only 1-2 iterations.

Step 4. Use the solution obtained from the above three steps as the preconditioned solution for the ORTHOMIN(k) which acts as an overall conjugate gradient-like residual acceleration technique.

The basic idea of Watt's line correction technique in step 1 is to sum the residuals and the coefficients of the matrix in the given direction to obtain a lower dimensional subproblem the solution of which forces the sum of the residuals in the given direction to be zero. It has been proven empirically that this technique, when applied to the linear systems resulting from finite difference approximations, accelerates the convergence of the iterative methods. The Watt's method has been shown<sup>14</sup> to eliminate certain low frequency eigenvalues associated with eigenvectors aligned in the direction of the correction. In this algorithm line corrections are implemented in the z-direction. The 2-dimensional subproblem is obtained by summing the residuals and coefficients of the matrix in the z-direction. This 2-D problem keeps the same areal footprint as the original 3-D problem. Line correction is done only in the z-direction instead of all three x-,y- and z-directions to reduce message passing overhead.

The next obvious question to ask is how the 2-D subproblem is solved efficiently on distributed systems. The methods that were investigated are the various inherently parallel multigrid techniques<sup>15</sup>. The multigrid technique is a heuristic algorithm. Many variations of this technique can be obtained depending on how the various steps of this algorithm are approached. Two basic forms of the multigrid algorithm were investigated.

The first approach was to relax on the fine grid using a point Jacobi iterative method and to restrict the updated fine-grid residuals to the coarse-grid using simple injection for what is known as the restriction step.

Injection refers to the procedure of summing the fine grid residuals to obtain the residual for the associated coarse grid block. This procedure is performed recursively until the coarsest grid possible is obtained. In the examples below the coarsest grid is a 4x4 subgrid. The corrections obtained from the coarse grids are interpolated to finer grids using a piecewise constant interpolation operator  $I_k^{k+1}$  (where  $k$  is grid level and  $k=1$  refers finest grid and as  $k$  increases grid becomes coarser) which is the transpose of the restriction operator  $I_k^{k+1}$ . Point Jacobi relaxation is also done after interpolation to the finer grids. The coarse grid matrix  $A^{k+1}$  is obtained by a coarse grid Galerkin approximation (CGA) using restriction operator  $I_k^{k+1}$ , fine grid matrix  $A^k$  and interpolation operator  $I_k^{k+1}$  ( $= (I_k^{k+1})^T$ ) and this is represented as

$$A^{k+1} = I_k^{k+1} A^k I_k^{k+1} \quad (1)$$

This multigrid algorithm is known as the multigrid V-cycle.

The second variation of multigrid that was investigated is that of Dendy's BOXMG approach<sup>16</sup>. In this case interpolation and restriction is done with operator weighting and the coarse grid matrix is obtained by a Galerkin approximation. This leads a 9-point stencil on the coarser grids even though the finest grid is 5-point. In the previous approach a 5-point stencil is retained on all grid levels. For this work the 5-point stencil was used for all multigrid levels to reduce message passing overhead.

The solution obtained from this 2-D subproblem is projected into 3-dimensions. Line-Jacobi is then performed in the z-direction with the updated residuals from the Watt's correction. This part of the algorithm appears to distribute the Watt's solution more correctly when vertical heterogeneities exist and gives a better estimate of the planar subdomain interface values.

The solution thus far is used as the initial guess for the subdomain boundaries for a domain decomposition algorithm. The type of domain decomposition adapted in this work is known as the block domain decomposition (DD) with non-overlapping subdomains. These subdomains are obtained by either block Jacobi or red-black type domain decomposition. In this work both of these variations have been implemented. The block Jacobi DD technique is simplistic and results in some degradation as the number of subdomains (and processors) increases. The red-black block DD approach, obtained by dividing each subdomain of the block Jacobi DD method into red and black subblocks, is more robust for a given number of subdomains; however, because the level of parallelism for the red-black DD approach is one-half of the block Jacobi, the block Jacobi was found to be more efficient in parallel mode. For this reason results presented below are only for the block Jacobi DD method. Efficient solution of the subdomain problems is obtained by incomplete factorization with zero infill ILU(0) and orthomin acceleration.

Since memory in a distributed memory architecture is locally available to the cpus and not shared, the communication among the processors is done by message passing. An important step in implementation is identifying the parts of algorithm that require message passing and minimizing overhead due to this message passing. Initially, the original domain is split areally across the processors. Since the Watt's correction is done along the z-direction, the 2-dimensional subproblem has the same areal footprint as the 3-dimensional problem among the processors. The parts of the multigrid algorithm which require message passing are relaxation, residual update, coarse grid matrix evaluation (if the number of grid points in the x- or y-direction are not equal to  $2^n$  ), and interpolation. Figure 24 depicts the overall algorithm from the multigrid Watts' correction to the domain decomposition portion of the iteration.

For each portion of the multigrid algorithm, every processor must communicate with up to four processors which contain the neighboring grid information. The L<sub>2</sub> - norm is evaluated using an efficient global sum routine. Communication among the processors is done to update the residuals after the Line-Jacobi, once after the subdomain solution for block Jacobi DD and after both red and black subdomains for block red-black DD. The global sum routine is also used in ORTHOMIN(k) to evaluate the inner products. As will be shown below this technique yields an efficient parallel linear equation solution.

### **GLOBAL PARALLELIZATION OF THE MODEL**

The global parallelization of the model consisted of adapting the overall model data structure to match the linear equation solver areal domain decomposition data structure as shown in Figure 25. Only interface values are passed between processors for the calculation of coefficients and residuals. Asynchronous message-passing was used to reduce overhead for interprocessor communications. The message-passing consists of two steps: movement of data into buffers and the actual sending of the data. Through overlapping of these two steps some overhead reduction was observed.

### **THE EXAMPLE PROBLEMS**

Three example problems were used for the analysis in this work: a hypothetical, highly-heterogeneous, problem; a larger version of the SPE Third Comparative Solution<sup>16</sup>, and a set of data from a real compositional reservoir study.

The highly heterogeneous model is based on a 32x32x15 incompressible model with permeabilities which varied randomly by four orders of magnitude. Ten wells were placed randomly and completed in several layers throughout the model

The SPE Third Comparative Solution model was increased in size to a 16x16x7 grid. Grid block dimensions were reduced to maintain the same pore volume as the original problem. The layering of the model was obtained by splitting the first four layers of the original 7x7x4 problem. The injection and production wells were located at areal positions (1,1) and (13,13), respectively.

The final problem with real data represents a reservoir with both a volatile oil rim and a retrograde condensate gas cap. The field contains 150 feet of structure and average net pay of about 30 feet. The structure dips at approximately 100 feet per mile with the reservoir being bounded by faulting, stratigraphic trapping, and an oil-water contact. A severe composition gradient exists throughout this 22x29x5 model with approximately ten producing wells which were active during the period of simulation. Approximately 10% of the cells in the 3190 grid block, six hydrocarbon component, model are inactive (zero pore volume). The model also contains a large number of aquifer blocks with essentially no hydrocarbons. Permeabilities in the model vary areally by as much as two orders of magnitude.

## RESULTS

The highly heterogeneous problem was used as a test case for the parallel linear equation solver. To demonstrate the utility of the Watts' correction and the z-line Jacobi for the estimation of domain interface conditions, the solver was executed with only block Jacobi DD and compared to solutions with the correction and line Jacobi techniques. Figure 26 shows clearly the advantages of the use of the combined correction and line Jacobi solutions for interface estimates.

Solutions were performed in parallel and serial modes for comparisons of CPU and Wall Clock times. Results for all i860 times are based on the best scalar compiler optimization. Table 2 summarizes the results for the solver using block Jacobi DD with multigrid injection and z-line Jacobi. Speedup refers to the CPU time for the parallel case divided by the CPU time for the same code running on a single processor.

Table 2  
Speedups for Linear Equation Solver-iSS/860

	Iterations	CPU Time	Speedup
4 CPUs	12	5.99	3.75
8 CPUs	14	3.62	6.95
16 CPUs	17	2.52	12.19
32 CPUs	18	1.65	18.23

These results indicate that high parallel efficiency could be achieved for the domain decomposition solver. Analysis shows that the serial content due to message passing overhead is about 2-2.5%.

Unfortunately, parallel efficiency of the algorithm is not the only criterion by which to measure solver performance. A better criterion is a comparison of parallel solver performance with a good serial solver. This is especially important in light of the increase in the number of iterations with greater numbers of processors. For comparison with a serial algorithm, a Watts' corrected incomplete factorization with one level of infill was used (ILUC(1)). For a scalar computer this algorithm represents one of the better performing techniques for the solution of the equations resulting from heterogeneous models. Table 3 summarizes these results:

Table 3  
Speedups for Parallel Linear Solver Versus Serial

	Iterations	CPU Time	Speedup
Serial	17	16.93	-
4 CPUs	12	5.99	2.82
8 CPUs	14	3.62	4.67
16 CPUs	17	2.52	6.71
32 CPUs	18	1.65	10.26

Although somewhat lower speedups are obtained, the gains of the parallel algorithm over the serial solver are significant for numbers of CPU's ranging from 4-32. For the four domain case a serial version of the domain decomposition solver gave results that were about 30% less efficient than the ILUC(1) solver.

The parallel performance of the linear solver appeared to be good for a difficult problem; however, the question remained as to whether the solver could be used for simpler cases in which the physics dominated the problem such as the SPE Comparative Solution example. Below are summarized the results for two cases: the SPE Third Comparative Solution Problem and the real compositional simulation data.

The 16x16x7 model based on the Third SPE comparative Solution showed excellent parallel performance as summarized below in Table 4:

Table 4  
CPU Times for Parallel SPE#3 Simulations

	Number of CPU's				
	4	8	16	32	Serial
PVT	26.71	5.60	9.17	5.26	78.75
Rock Pr	2.46	1.21	0.62	0.35	9.59
Eq Set	106.31	49.43	24.37	12.76	441.54
Eq Soln	34.62	24.10	20.29	22.85	45.36
Update	9.71	4.65	2.33	1.21	37.21
Total	179.84	94.99	56.78	42.43	612.45

These raw CPU times indicate that the rock properties, equation setup, and update portion of the model were performing near ideal in parallel since the CPU times are in a ratio to the number of processors. The PVT properties portion of the model was not ideal due to the load balancing. As the compositions and pressures change during the course of the simulation different parts of the model require more CPU time for flash and phase boundary determinations. The real model data below demonstrates even better the problems associated with load balancing.

For a better comparison, the SPE#3 times are compared with the serial version of the unmodified compositional model in Table 5. Speedups are the serial times divided by the parallel wall clock time for the parallel simulation.

Table 5  
Speedups of Parallel SPE#3 Compared to Serial

	Number of CPU's				
	4	8	16	32	Serial
PVT	2.95	5.04	8.58	14.95	1.0
Rock Pr	3.90	7.93	15.47	27.40	1.0
Eq Set	4.15	8.92	18.12	34.60	1.0
Eq Soln	12.5	1.88	2.23	1.98	1.0
Update	3.83	7.97	15.97	30.75	1.0
Total	3.40	6.45	10.79	14.43	1.0

The speedup factors for the equation setup portion of the model appear to exceed the theoretical maximum. This anomaly can be explained by the reorganization of the flow coefficient calculations which was done in the parallel model. Originally the model had been organized to calculate flow coefficients in three passes - one for each direction of the grid. To make parallelization easier, a single pass through all grid blocks associated with a

CPU (node) of the hypercube was performed. This resulted in a slight improvement in program efficiency over the serial case. Similar results have been reported in the past in program restructuring for vectorization.

Overall, the performance for SPE#3 showed better than 50% parallel efficiency for all cases except 32 CPU's. For this problem the solver degradation significantly effected the results. For the 32 node case the wall clock time actually increased because of the increased number of iterations required. Further work may be necessary for this simpler problem to achieve better linear equation solver performance.

Summarized below in Table 6 are the results for the real data compositional study.

Table 6  
CPU Times for Parallel Real Data Simulations

	Number of CPU's				
	4	8	16	32	Serial
PVT	43.45	30.87	22.60	14.25	113.73
Rock Pr	1.28	0.69	0.38	0.20	3.08
Eq Set	57.16	30.50	14.75	8.64	174.79
Eq Soln	15.74	9.84	7.84	5.79	40.86
Update	5.07	2.66	1.44	0.75	19.15
Total	122.70	74.59	47.01	29.63	365.34

Parallel performance again appears to be good, but there are a few anomalies in the results. These can be better understood by considering the speedup data given in Table 7 below:

Table 7  
Speedups of Parallel Real Compared to Serial

	Number of CPU's				
	4	8	16	32	Serial
PVT	2.62	3.68	5.03	7.98	1.0
Rock Pr	2.41	4.46	8.10	15.40	1.0
Eq Set	3.06	5.73	11.85	20.23	1.0
Eq Soln	2.60	4.14	5.21	7.06	1.0
Update	3.78	7.20	13.30	25.53	1.0
Total	2.98	4.90	7.77	12.33	1.0

This simulation presents two separate problems which effect overall parallel performance. First, the void cells cause the load imbalance problem to appear in the equation setup and rock properties portions of the model. Second, the imbalance due to the flash solutions and phase boundary evaluations is more dominant since most of the cells must be flashed during the initial stages of production simulated here. Since the aquifer cells do not enter into these calculations, processors dominated by

aquifer cells are near idle for much of the period during the PVT evaluations. This difficulty of load imbalance is discussed more fully below.

To better evaluate these results simulations were extended to a year or more and compared with a mainframe supercomputer (a Cray X-MP 4/16 with 8.5 nanosecond clock). Results for the SPE#3 and Real Data cases are summarized in Tables 8 and 9:

Table 8  
CPU Times-Parallel Extended SPE#3 Simulations

	16-i860 CPU's	CRAY X-MP
PVT	19.45	17.01
Rock Prop	3.78	4.96
Eq. Setup	237.02	166.87
Eq. Soln.	106.25	42.37
Update	99.87	43.72
Total	466.37	274.93

Table 9  
CPU Times for Extended Real Data Simulations

	16-i860 CPU's	CRAY X-MP
PVT	111.03	204.01
Rock Prop	1.45	0.92
Eq. Setup	59.27	40.20
Eq. Soln.	33.36	18.58
Update	5.57	4.29
Total	210.99	268.06

For the SPE#3 problem the parallel model achieved a rate equal to 59% of the Cray. This corresponds to a computation rate of about 29.5 MFLOPS for the iSS/860. For the real problem the computation rate for the iSS/860 exceeded the Cray's by a factor of 1.27 . This corresponded to a computation rate of 33.36 MFLOPS for the sixteen parallel i860's. For these calculations the well computation time of about 5 seconds on the Cray was not included. Even in scalar mode on the i860 at about one-tenth of the Cray speed ( 50 seconds ), the conclusions are similar for the two cases if well calculations are included.

### LOAD BALANCING ISSUES

The real compositional model provides an excellent example of the difficulties associated with load balancing. The data contains approximately 10% void cells as well as a large number of aquifer cells. If the grid is divided as equally as possible among sixteen processors, then the active cell

count and work load for fifteen time steps appears as shown in Figure 27. For this example the active cells have little to do with the overall work distribution since all phase behavior calculations can be avoided in aquifer cells. An attempt was made at redistributing the workload by modifying the processor cell allocations. This redistribution of the workload resulted in an improvement in the computation time for the flash calculations (PVT), but this improvement was overshadowed by the tremendous skewness of the grid which resulted in significant increases in the coefficient setup and equation solution portions of the model as shown below in Table 10:

Table 10  
CPU Times for Real Simulations-Load Balancing  
16-i860 CPU's

	Original	Reallocated Grid
PVT	22.60	15.34
Rock Prop	0.38	0.87
Eq. Setup	14.75	31.44
Eq. Soln.	7.84	12.82
Update	1.44	3.20
Total	47.01	63.67

Several remedies to this difficulty are being pursued. An excellent possibility for balancing exists if only a few of the cells require a large amount of CPU time for flash calculations. In this case the cell unknowns can be redistributed among the processors at low cost, the flash can be calculated, and the resultant vapor and mole fractions replaced in other locations. Optimal load balancing for this case may require continual monitoring of the workload and periodic redistribution the grid.

### Implementation on Other Architectures

The parallelization discussed above has also been implemented in a parallel shared-memory MIMD environment on the IBM 3090/600J. This implementation involved a larger version of the real data problem. For the example speedups of greater than 5.0 for a six processor system were achieved. We are currently investigating the use of the SIMD, distributed-memory, Connection Machine CM-2 for reservoir simulation.

### Operator Splitting On Multiple Grids

The success of the parallelization of a commercial simulator led to the question as to whether an improved formulation could lead to even further parallel efficiencies. Underlying this development were two main concerns: the need to reduce the numerical dispersion introduced by a conventionally coarse finite difference discretization and the reduction of the computational effort needed for the pressure solution. The reduction of the numerical dispersion allows for a sharp definition of the concentration

or saturation fronts. With reduced dispersion it is possible to investigate both stable and unstable displacements including fingering due to viscous instabilities or to the local heterogeneities.

Basically, the method uses the IMPES procedure to numerically decouple the pressure equation from the species conservation equations. Then, a fourth order finite element method is used to solve the elliptic pressure problem on a coarse grid. This solution is projected to a fine grid of about 10,000 nodes inside each coarse grid element by a splines in tension technique, and the time stepping is performed on the fine grid. Whenever the pressure solution needs updating, the fine grid provides the current mobilities to the coarse grid for the building of the coefficient matrix for the pressure solver.<sup>17,18</sup>

To compute the pressure field at a particular time, one needs to solve the following elliptic problem,

$$\nabla \cdot \left[ \frac{K}{\mu^n} \cdot \nabla p^{n+1} \right] = 0 \quad (2)$$

where the superscripts  $n$  and  $n+1$  indicate quantities computed before and after updating the solution for the current time step,  $K$  is the permeability tensor of the porous medium,  $\mu$  the viscosity and  $p$  the pressure of the fluid phase.

In real applications, the apparently harmless pressure equation (2) will lead to an implicit and highly nonlinear elliptic or parabolic problem, particularly when phase behavior is incorporated into the modeling of multi-phase flows. The aim has been to develop a technique capable of analyzing a degree of heterogeneity as fine as possible. However, refining the discretization of the elliptic solver rapidly increases the computational cost making the whole task prohibitive.

To remove this bottleneck, the regularity of the elliptic operator can be exploited to obtain a numerical solution for the pressure on a coarse discretization by a fourth order finite element technique. This solution is then projected by an interpolation procedure to a fine grid, on which the time stepping is performed. If the pressure solution needs updating, a periodic restriction operation is performed from the fine to the coarse grid to recalculate the coefficient matrix for the discretized pressure equation. For a sufficiently acceptable coarse pressure solution, the degree of heterogeneity that can be incorporated into the fine grid solution allows for a detailed picture of the fluid dynamics of the problem.

Figure 28 shows a schematic of the grid levels for the solution to the pressure equation on the coarse grid and the time stepping on the fine grid. A typical case in this work has 64 to 100 coarse grid nodes and about 500,000 fine grid nodes.

## CASE EXAMPLES - RESULTS AND DISCUSSION

As a validation of the numerical technique, the simple problem of immiscible displacement with a unit mobility ratio on a quarter five spot was used. The example corresponds to a constant permeability of 1,000 mdarcys, an injection pressure of 2600 psia and atmospheric pressure at production. As a comparison, the same problem was solved using the standard central finite difference technique. Figures 29 (a) and (b) show the contour lines for the finite difference runs at 30 and 120 days, respectively. The grid in these runs is 50x50 evenly spaced. Figure 30 shows the results for this example problem using operator splitting on multiple grids. The pressure problem is solved on a grid of 10 by 10 by the collocation method and the species conservation equation is solved by a one point upstream weighting technique on a fine grid of 625 by 625. This gives a computational grid of nearly 400,000 points for the species equations and approximately 4,000 fine grid points in each coarse grid element. For a field of 1,000 by 1,000 feet the mesh spacing of the fine grid is 1.6 ft. The numerical dispersion is greatly decreased.

As a first example of heterogeneity, a case of flow in a medium of banded permeability is presented for the quarter five spot geometry. The input to this run is the same as the previous example with the exception of the permeability, which was arranged in five bands of equal width and alternating permeabilities of 1,000 mdarcys and 10 mdarcys in the x-direction. This makes the permeability around the wells the same as the previous example. Figure 31 shows the concentration contour lines obtained from the standard finite difference solution on a 50x50 mesh. The effect of the medium heterogeneity is apparent. The interaction between neighboring regions with a modest permeability ratio of 100 produces a tremendous numerical dispersion of the fronts.

The operator splitting approach in this case solves the pressure by the Galerkin formulation on an 8x8 nonuniform coarse grid. The species conservation equation is solved on a 626x626 fine grid. The boundaries of the coarse grid elements are everywhere coincident with lines of fine grid nodal points in this case. However, the implementation of the restriction from fine to coarse through the element integrals allows for nonoverlapping grid boundaries. Figure 32 shows the interpolated pressure solution for this problem along the diagonal between injection and production and both domain boundaries stemming from the source point. The interpolation was done by bivariate splines in tension with the appropriate tension factor to obtain a physical flow everywhere in the domain. Figure 33 shows three time instances of this displacement close to those of Figure 31. The numerical dispersion is greatly decreased in comparison to Figure 31 but the effect of the permeability contrast on the numerical dispersion of the method still noticeable here. A higher order finite difference discretization in space is a certain cure to this problem at minimal coding effort.

As an example of the power of the method to tackle flow situations with real data the problem of a miscible line drive over a large field that extends

a few miles miles in each direction is presented next. Figure 34 shows the permeability semi-variogram for this data, that was available in five layers. The correlation lengths for all five layers appears in the order of 1 mile. For this two-dimensional simulation layer 3 was chosen as the input, as it displays changes in permeability over more than two orders of magnitude (between a few mdarcys to about 400 mdarcys). The flow simulation is conducted in a line drive arrangement. Constant pressure is specified on both open sides, 2500 psia at injection and atmospheric pressure at production. The pressure equation is solved by Hermite-Galerkin on a coarse grid of 6 points in the direction of the general flow and 5 in the direction across the general flow.

Figure 35 shows the concentration contours for this displacement at two times. The cusping generated by a high permeability region on the left region of the domain near the entrance (figure 35-a) is apparent from the very beginning of the displacement. Also, there is a zero permeability region that produces a constriction of the flow. Figure 35-a shows the instant when the cusp is starting to go around the constriction. Figure 35-b corresponds to a time after the front has cleared this contraction zone. The remaining portion of the flow lags behind from the start due to a lower permeability distribution on that area.

Once again, the permeability contrast exaggerates the numerical dispersion and then it appears necessary to go to a higher order differencing scheme on the fine grid, although this is well known and adds virtually no complication to the code. The effect is more marked over areas where cusping is generated by high local Darcy velocities. The actual numerical output is less dispersed, however, than implied by the contour line plots as it was not possible to give the whole array of fine grid points to the contouring routine and therefore internal interpolation of this routine further spread the lines.

### **Parallelization of the Method**

The explicit feature of the various steps of the operator splitting on multiple grids method makes it readily parallelizable thus producing a scheme that yields not only high accuracy but also high computational efficiency.

Parallel tests were run on the 386-based iPSC/2 up to 8 CPU's and on the RISC-based iSS/860 up to 32 CPU's. Figure 36 shows the speed-ups obtained on the 386 machine, for 2, 4 and 8 CPU's. Speed-ups are shown for the building of the coefficient matrix, the interpolation, the time stepping and also for the whole OSMG cycle. The building of the coefficient matrix is well over 99% parallel-efficient up to the 8-node cube configuration. The interpolation step involves, as explained above, not only interior points of the subdomain but also a line of exterior nodes around it, obviously creating an overlapping of the tasks performed by the different processors. Understandably, a degradation is observed as the number of

CPU's increases. For example, the parallel efficiency of this step is 88.2% on 4 nodes and 82.1% on 8 nodes.

The time stepping with the asynchronous message passing strategy gives excellent parallel performances, e.g., 96.1% efficiency on the 8-node cube. This is substantially better than the result for the interpolation step, indicating that avoiding the message passing in the interpolation is detrimental. In this study, however, the fraction of the computational effort devoted to the interpolation is small so that the parallel performance of the whole OSMG cycle does suffer greatly because of this deficiency of choice. The overall parallel efficiency of the cycle is nearly 97% on 8 nodes and higher for smaller cubes.

Figure 36 shows the speed-up results for the i860 Hypercube up to a 32-node cube. The algorithm suffers a negligible degradation up to the cube of highest dimension. Again, the asynchronous message passing for the time stepping surpasses the parallel performance of the interpolation with subdomain overlapping, showing the high efficiency of this way of handling the message passing. For instance, the interpolation step shows parallel efficiencies of 82.4%, 77.3% and 72.1%, on 8, 16 and 32 processors, respectively. For the same three cube configurations, the parallel efficiencies for the time stepping are 96.7%, 91.5% and 83.1% and the values for the whole cycle are 98.5%, 96.6% and 93.3%.

## **CONCLUSIONS AND FUTURE DIRECTIONS OF THE RESEARCH**

This work has demonstrated that a highly efficient parallel model can be generated for a commercial n-component, three-phase, equation-of-state reservoir simulator in a distributed memory parallel computer. A linear equation solver using multigrid, domain decomposition, and z-line corrections can be efficiently parallelized. For a hypothetical case this solver showed performance comparable to serial solutions. In parallel, the solver was significantly faster than serial solvers. For two simulations involving compositional data, the parallel model performed at computation rates comparable to mainframe supercomputers.

A numerical technique has been developed, that permits the analysis of flow in heterogeneous porous media down to a length scale from a few feet to a few tens of feet with great efficiency.

This method of Operator Splitting on Multiple Grids, for an example of flow in heterogeneous porous media, has been successfully implemented on both Intel Hypercubes, i.e., the 386-based iPSC/2 and the RISC-based iSS/860. An overall parallel efficiency of about 93% was obtained on a 32-node i860 Hypercube.

Future work for this research involves the implementation of more efficient, but equally parallelizable, domain decomposition and multigrid

algorithms. Load balancing issues must be further investigated. The operator splitting method in three-dimensions appears a natural progression of the work toward the solution of more realistic situations.

## **APPLICATION TO THE SEVENTY SIX WEST FIELD**

The modeling techniques described above were used to validate the results of E. Claridge given in a companion report for waterflooding and immiscible carbon dioxide injection recoveries for the Seventy Six West field. The first stage of the modeling consisted of matching the results for both waterflooding and immiscible carbon dioxide injection. The 10x10x8 three-dimensional model was reconstructed for the VIP-Comp model. Simulation results matched closely those of Claridge. The validity check of the simulations was performed by a twenty-seven fold refinement of the grid which had been used by Claridge. The 30x30x24 grid was first used to perform waterflood simulations. The results showed that there was little or no effect of grid refinement for the waterflood. Oil recovery for both cases was virtually identical. The simulation for the immiscible carbon dioxide injection case presented a significant modelling challenge. The extremely fine grid caused significant instability problems resulting in extremely small timesteps. Fortunately, the speed of the model calculations allowed the simulations to be performed in a reasonable timeframe. Results for the fine-grid, immiscible carbon dioxide case showed a slight degradation in recovery of about 3%. The reason for this reduction in recovery was that the gravity override of the injected gas could be better captured with the fine detail of the vertical layering. Nonetheless, these results validate those of Claridge; that is, immiscible carbon dioxide injection may result in a significant improvement in oil recovery for the field. Several questions remain to be answered, however. First, better data must be obtained for the field to replace that data which was estimated in this study. Secondly, the economics of the process should be further investigated with emphasis on pattern spacing, injection rates, and carbon dioxide availability.

## **REFERENCES**

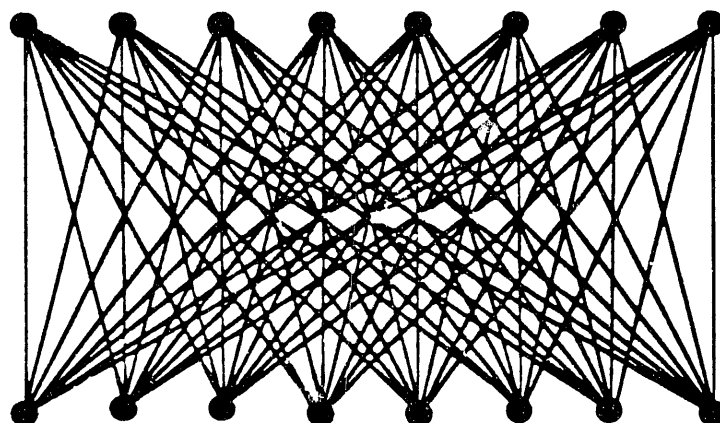
1. Scott, S. L., Wainwright, R. L., Raghavan, R., and Demuth, H., "Application of Parallel (MIMD) Computers to Reservoir Simulation", SPE 16020 presented at the 9th SPE Symposium on Reservoir Simulation, San Antonio, Texas, Feb 1-4, 1987.
2. Chien, M. C. H., Wasserman, M. L., Yardumian, H. E., and Chung, E. Y., "The Use of Vectorization and Parallel Processing for Reservoir Simulation", SPE 16025 presented at the 9th SPE Symposium on Reservoir Simulation, San Antonio, Texas, Feb. 1-4, 1987.
3. Barua, J., and Horne, R. N., "Improving the Performance Parallel (and Serial) Reservoir Simulators", SPE 18408 presented at the 10th SPE Symposium on Reservoir Simulation, Houston, Texas, Feb. 6-8, 1989.

4. Killough, J. E., and Wheeler, M. F., "Parallel Iterative Linear Equation Solvers: An Investigation of Domain Decomposition Algorithms for Reservoir Simulation", SPE 16021 presented at the 9th SPE Symposium on Reservoir Simulation, San Antonio, Texas, Feb. 1-4, 1987.
5. van Daalen, D. T., Hoogerbrugge, P. J., Meijerink, J. A., and Zeebraten, P. J. A., "The Parallelization of BOSIM, Shell's Black/ Volatile Oil Reservoir Simulator", *Proceedings of the First IMA/SPE European Conference on the Mathematics of Oil Recovery*, Oxford University Press, 1990.
6. Wheeler, J. A., and Smith, R. A., "Reservoir Simulation on a Hypercube", SPE 19804 presented at the 64th SPE Annual Conference and Exhibition, San Antonio, October, 1989.
7. Killough, J. E., and Bhogeswara, Rao, "Simulation of Compositional Reservoir Phenomena on a Hypercube", *Proceedings of the First IMA/SPE European Conference on the Mathematics of Oil Recovery*, Oxford University Press, 1990.
8. Killough, J. E., and Bhogeswaram Rao, "Simulation of Compositional Reservoir Phenomena on a Distributed Memory Parallel Computer", *Journal of Petroleum Technology*, November, 1991 ( to appear).
9. Young, L. C. and Stephenson, R. E., "A Generalized Compositional Approach for Reservoir Simulation," SPEJ (Oct. 1983), 727-742.
10. Vinsome, P.K.W., "Orthomin: An Iterative Method for Solving Sparse Banded Sets of Simultaneous Equations", SPE 5729 presented at the SPE 4th Symposium on Reservoir Simulation, Los Angeles, Ca., Feb. 1976.
11. Watts, J. W., "An Iterative Matrix Solution Method Suitable for Anisotropic Problems", SPEJ (March, 1971), 47-51.
12. Wallis, J. R., "Vectorization of Preconditioned Generalized Conjugate Residual Methods" in *Mathematical and Computational Methods in Seismic Exploration and Reservoir Modeling*, SLAM, 1987, 250-251.
13. Meijerink, J. A., and van der Vorst, H. A., "An Iterative Solution Method for Linear Systems of Which the Coefficient Matrix is a Symmetric M-Matrix", *Math. Comp.*, 31(1977), 148-162.
14. Watts, J. W., "A Method of Improving Line Successive Overrelaxation in Anisotropic Problems - A Theoretical Analysis", *Soc. Pet. Eng. J.* (April, 1973), 105-118.
15. Brandt, A., "Multi-Level Adaptive Solutions to Boundary-Value Problems", *Math. Comp.*, Vol. 31 (1977), 333-390.

16. Dendy, J. E., Jr., McCormick, S. F., Ruge, J. W., Russell, T. F., and Schaffer, S., "Multigrid Methods for Three-Dimensional Petroleum Reservoir Simulation", SPE 18409 presented at the Tenth SPE Reservoir Simulation Symposium, Houston, February, 1989.
17. Kenyon, D. E., and Behie, G. A., "Third SPE Comparative Solution Project: Gas Cycling of Retrograde Condensate Reservoirs", *JPT* (August, 1987), 1576-1584.
18. Dawson, C.N. and Wheeler, M.F., *An operator-splitting method for advection-diffusion-reaction problems*, MAFELAP Proceedings VI, J.A. Whiteman, ed., Academic Press, pp.463-482, 1988.
19. Rame´, M. and Killough, J. E., "A New Approach to the Simulation of Flows in Highly Heterogeneous Porous Media", SPE 21247 presented at the Eleventh SPE Symposium on Reservoir Simulation, Anaheim, California, February, 1991.

# PARALLEL COMPUTING WITH GLOBALLY SHARED MEMORY

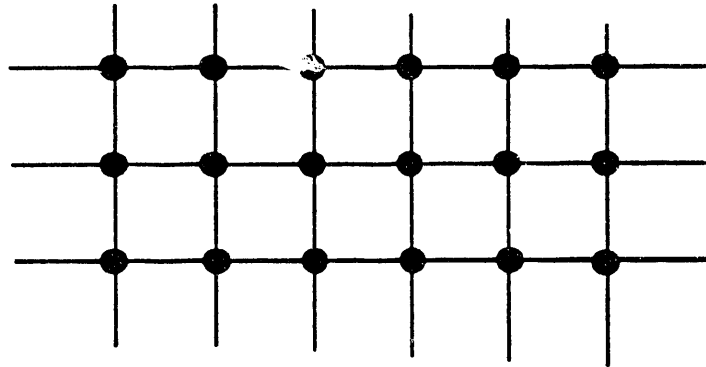
**PROCESSORS**



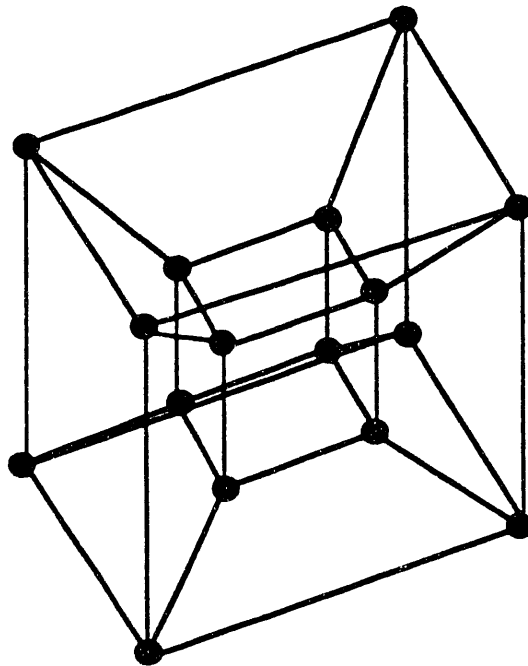
**MEMORY BANKS**

**Figure 18.**

# PARALLEL COMPUTING WITH DISTRIBUTED MEMORY



**GRID**



**HYPERCUBE**

**Figure 19.**

# FLOW CHART FOR TYPICAL COMPOSITIONAL SIMULATOR

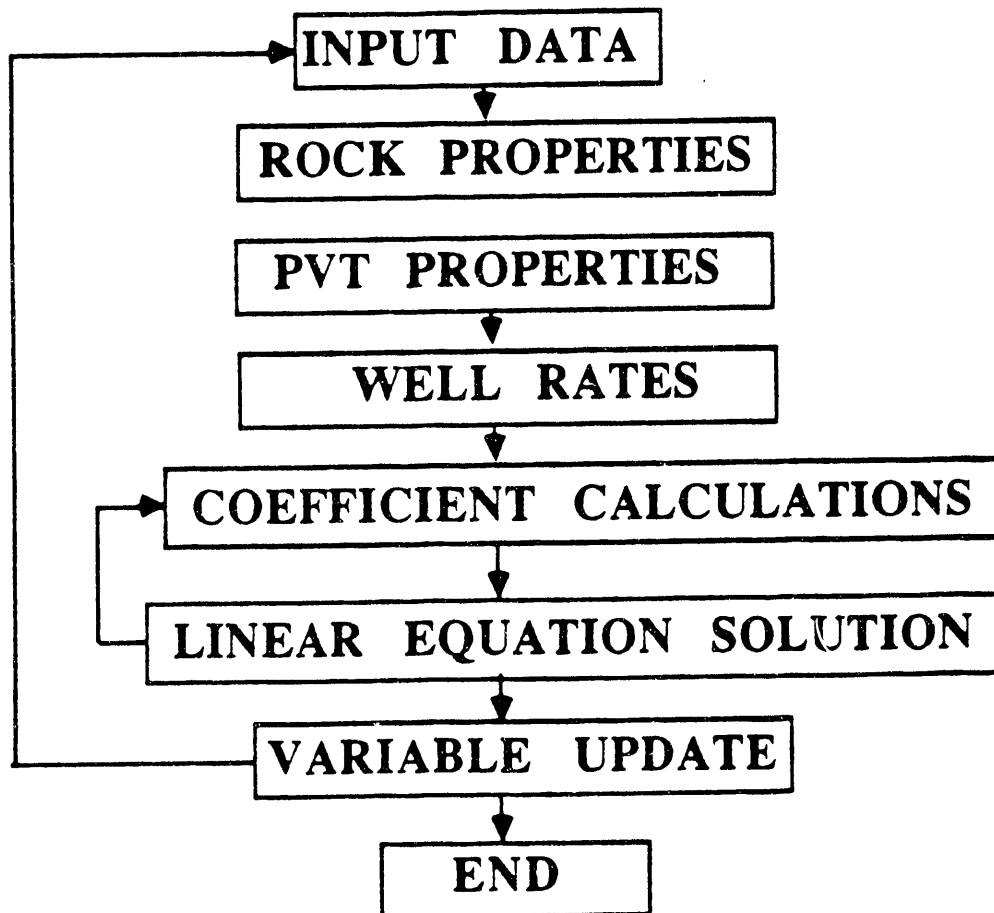


Figure 20.

# FLOW CHART FOR COMPOSITIONAL SIMULATOR WITH i860 WORK DISTRIBUTION

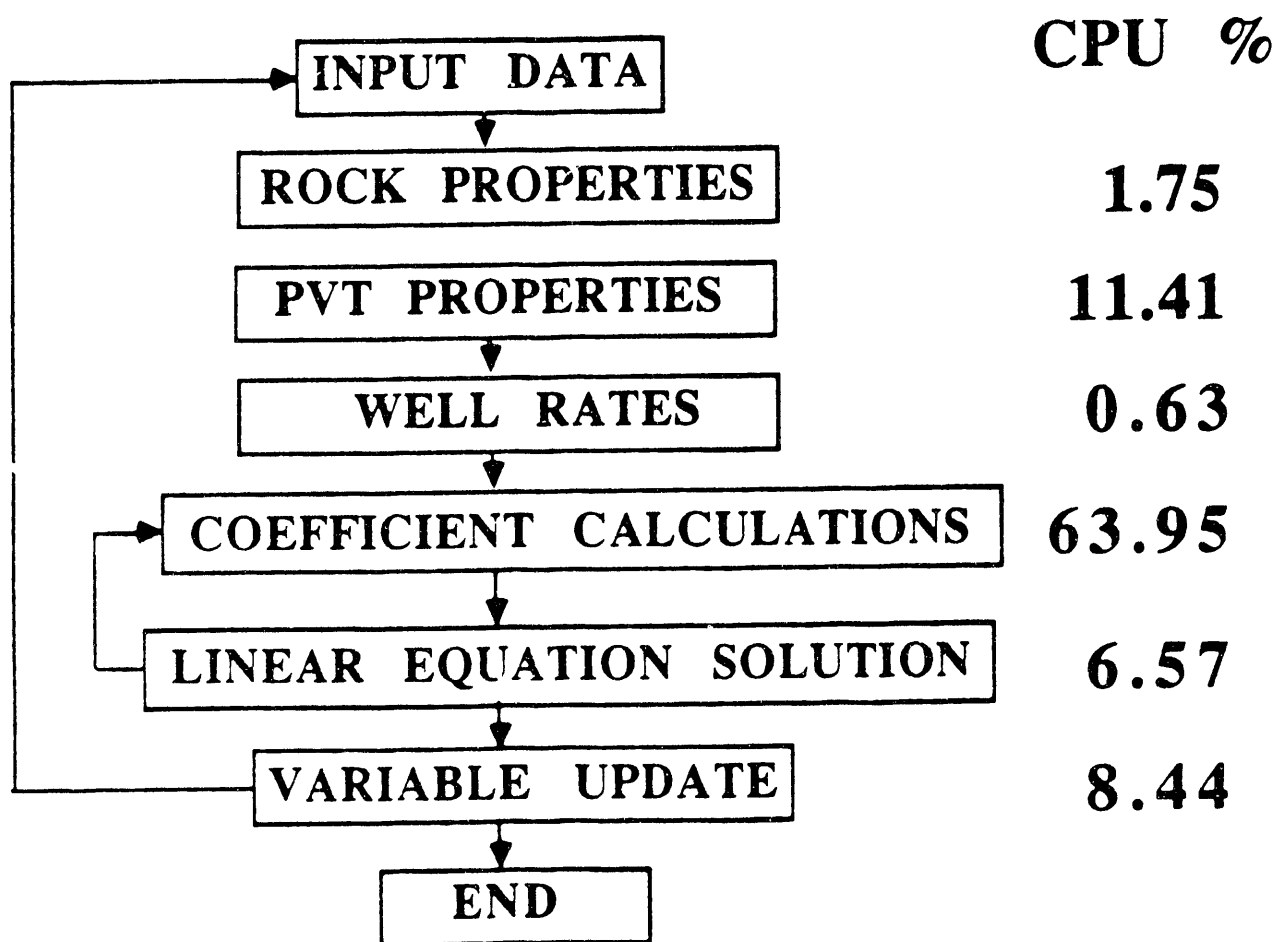


Figure 21.

# SCHEMATIC SHOWING THE INITIAL PARALLELIZATION

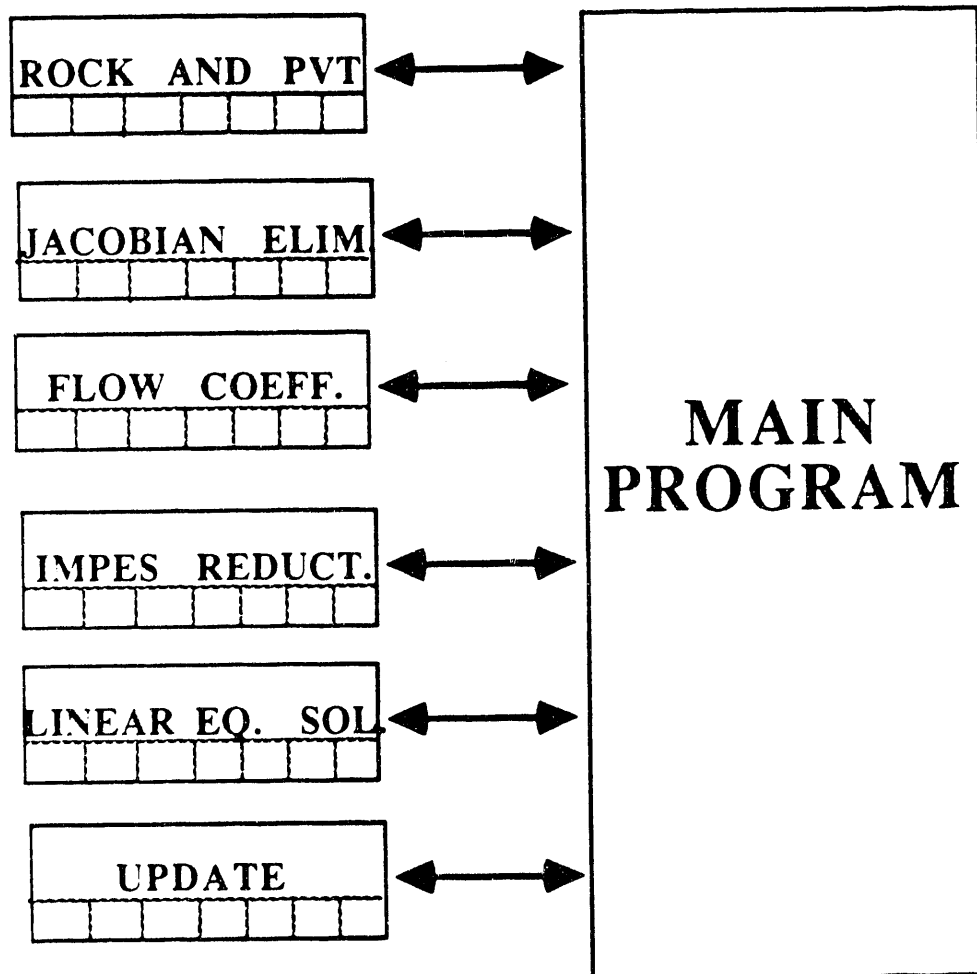


Figure 22.

# SCHEMATIC SHOWING THE FINAL PARALLELIZATION

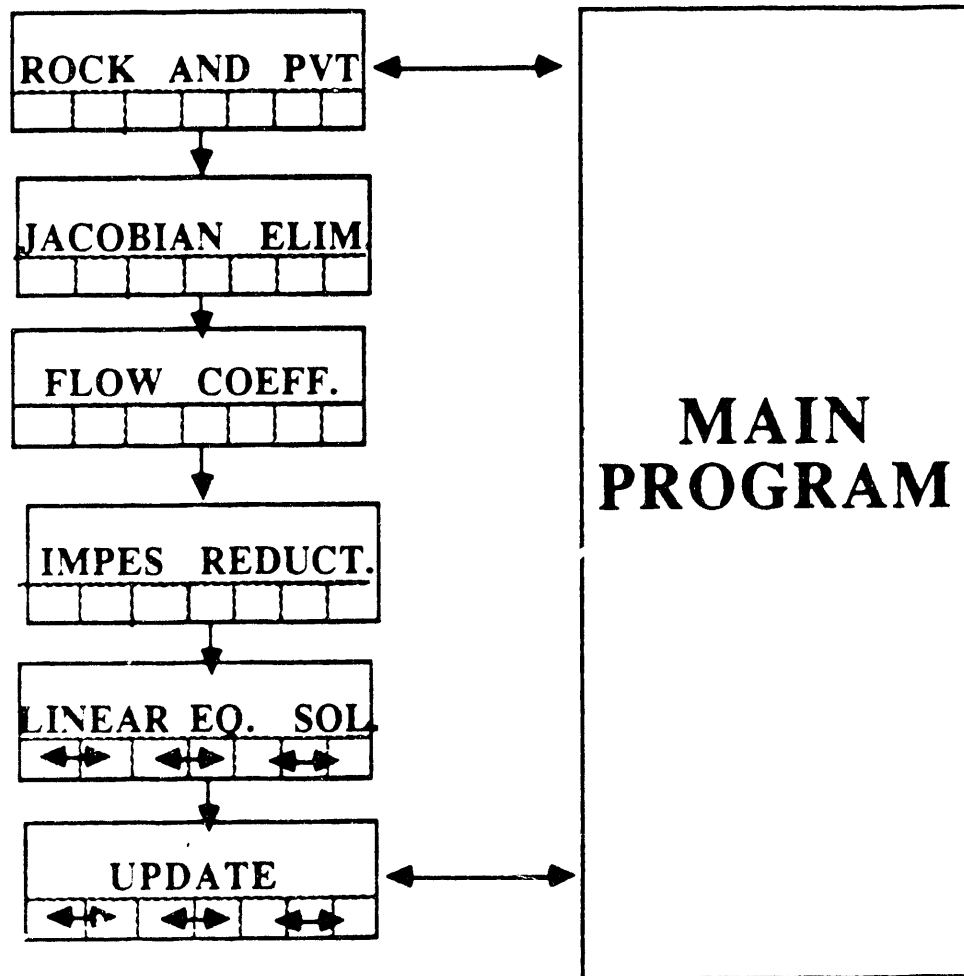


Figure 23.

# SCHEMATIC OF THE DOMAIN DECOMPOSITION ALGORITHM

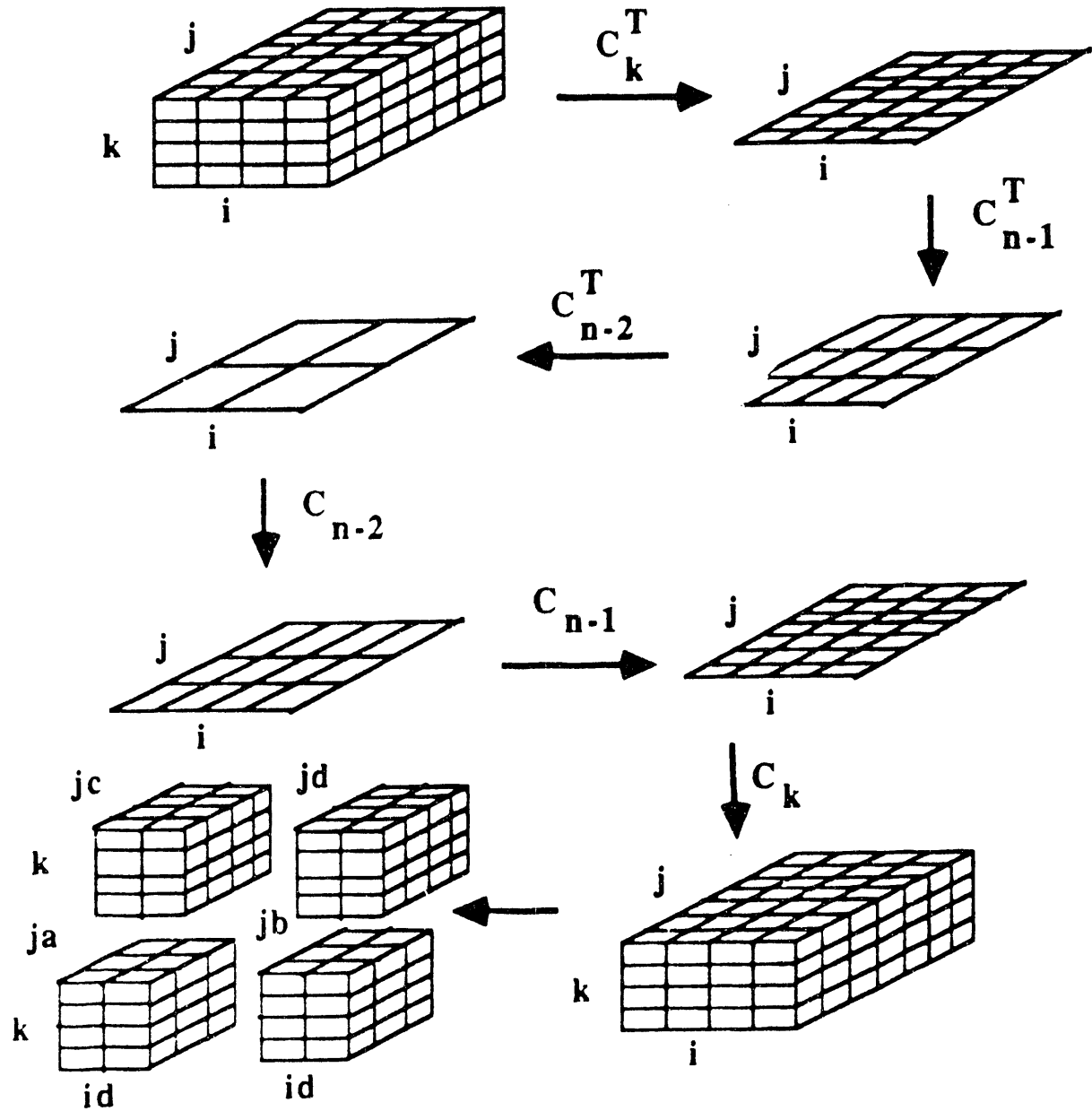
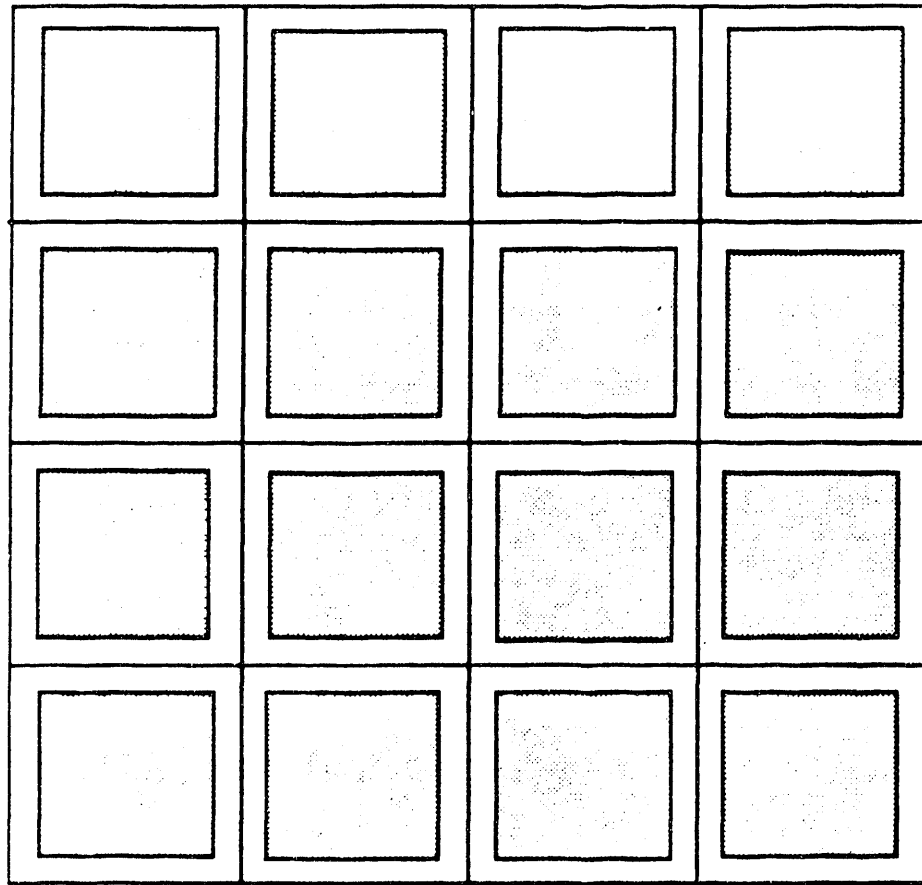


Figure 24.

# DOMAIN DECOMPOSITION WITH GRIDBLOCK COMMUNICATION



□ CELLS REQUIRING COMMUNICATION  
— PROCESSOR BOUNDARIES

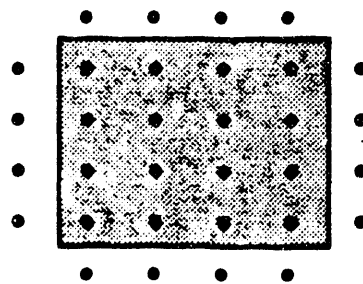
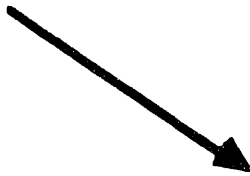


Figure 25.

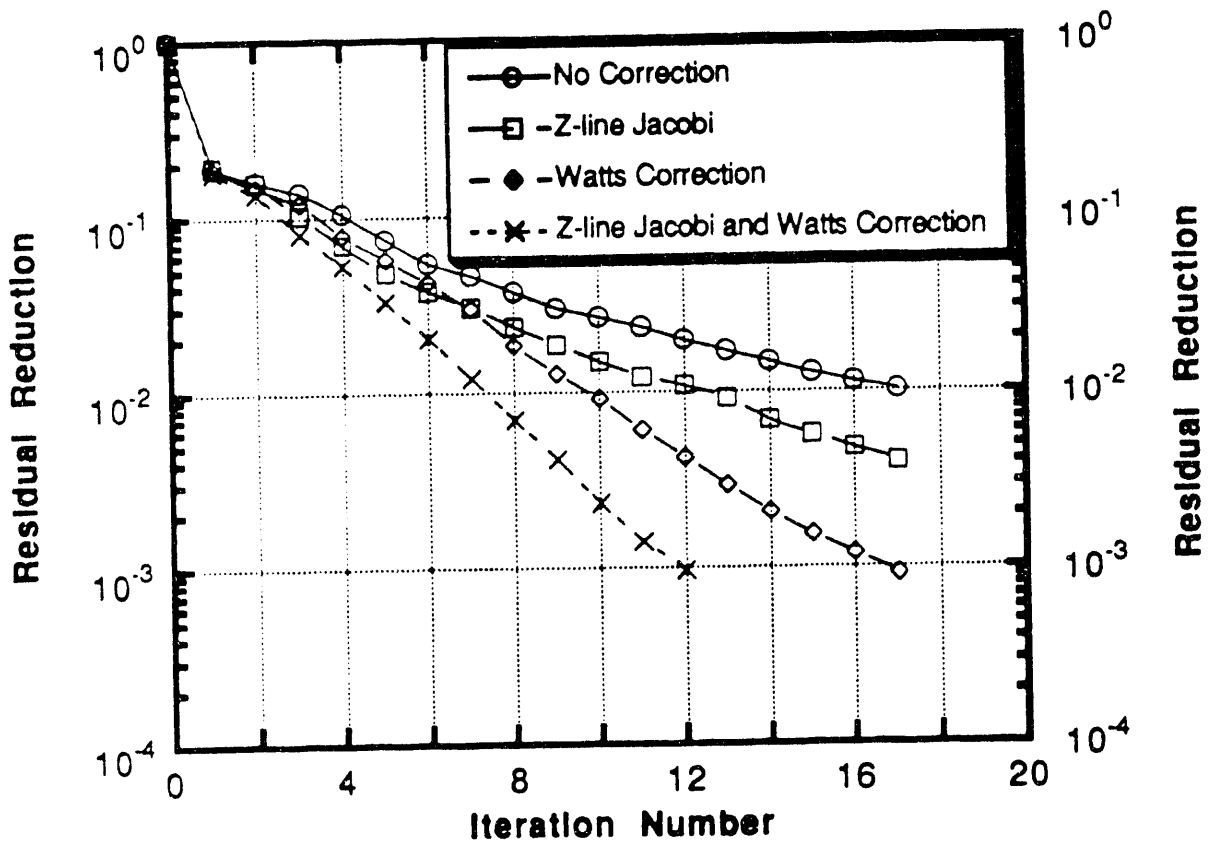


Figure 26. Comparison of Block Jacobi DD with Various Techniques for Interface Estimates

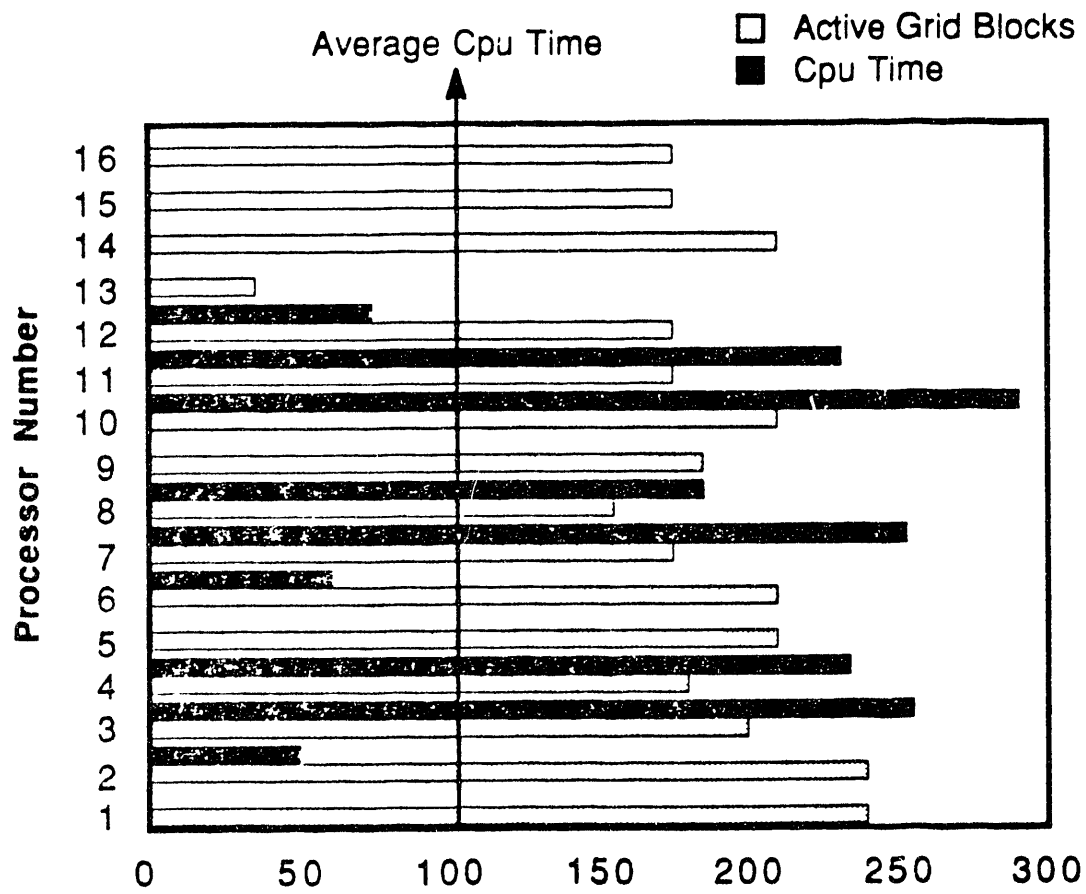
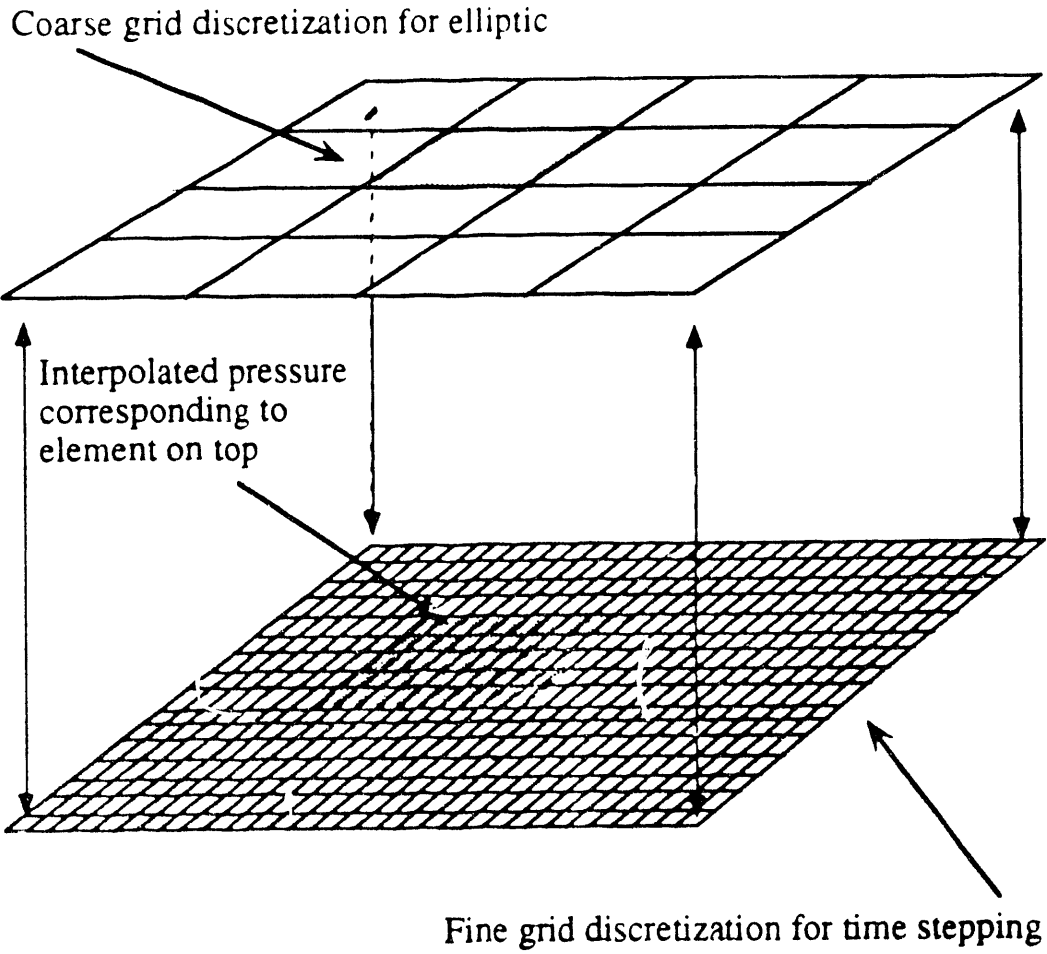


Figure 27. The real Compositional Model Showing Active Cells and Load Imbalance for Each Processor



**Figure 28. Schematic of OSMG Technique**

# Miscible displacement - unit mobility ratio Concentration contour lines

Finite difference on 50x50 grid

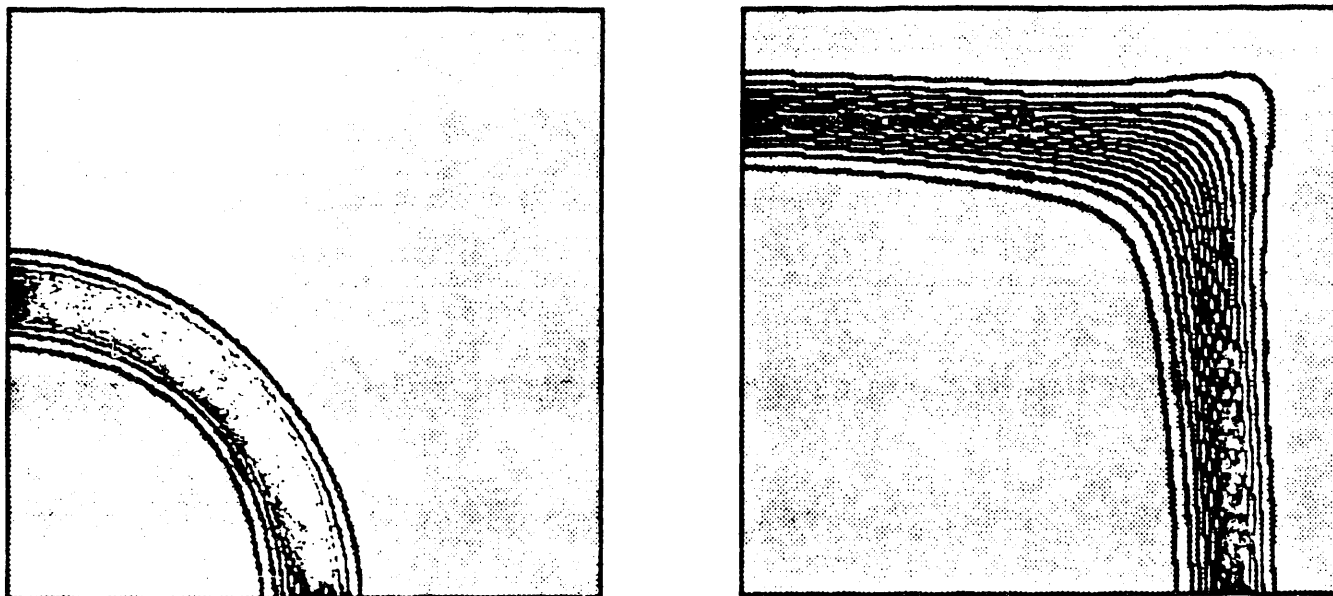


Figure 29.

# OSMG method

10 x 10 coarse grid - collocation  
625 x 625 one point upwinding

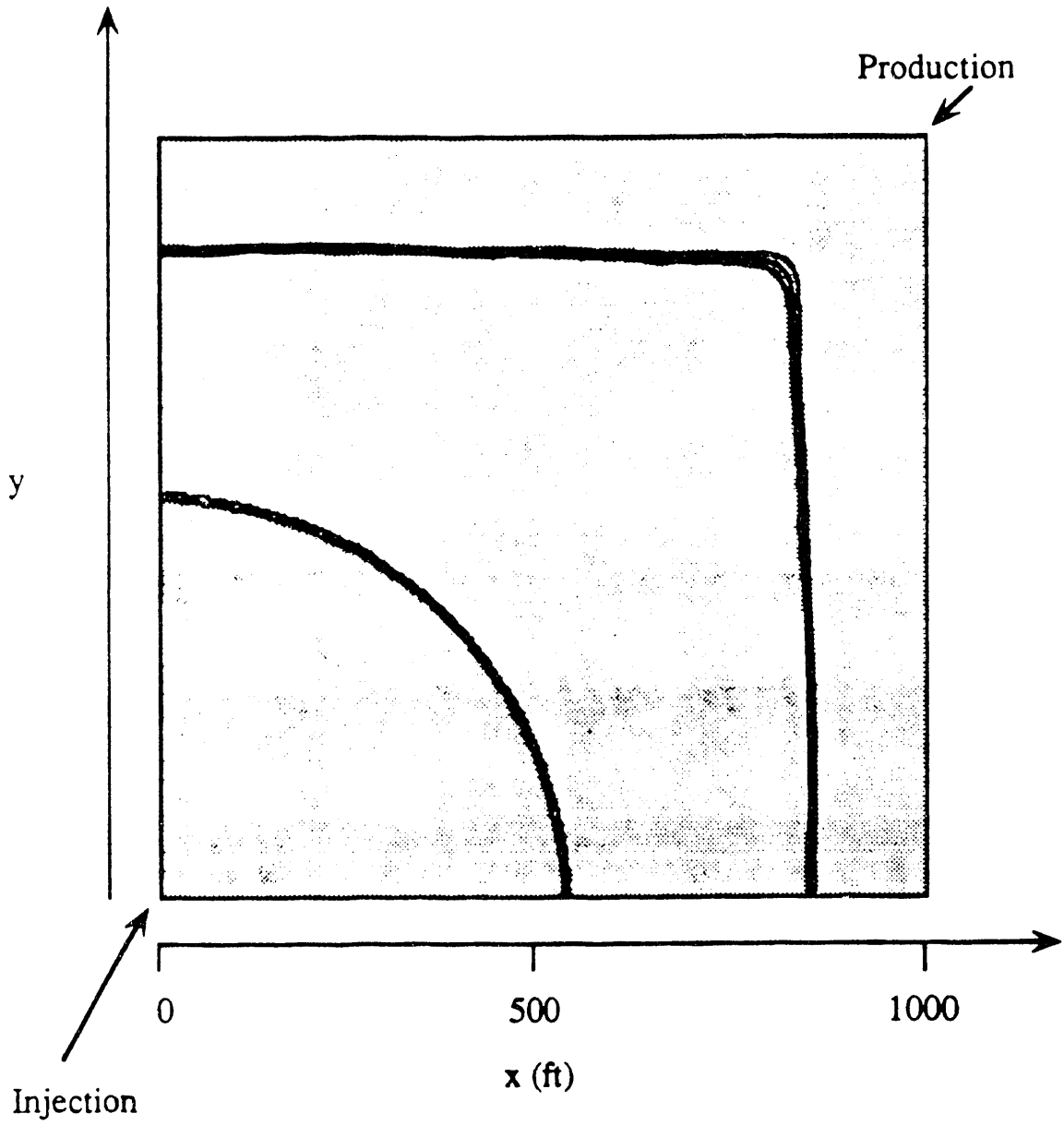
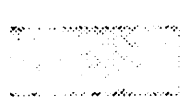
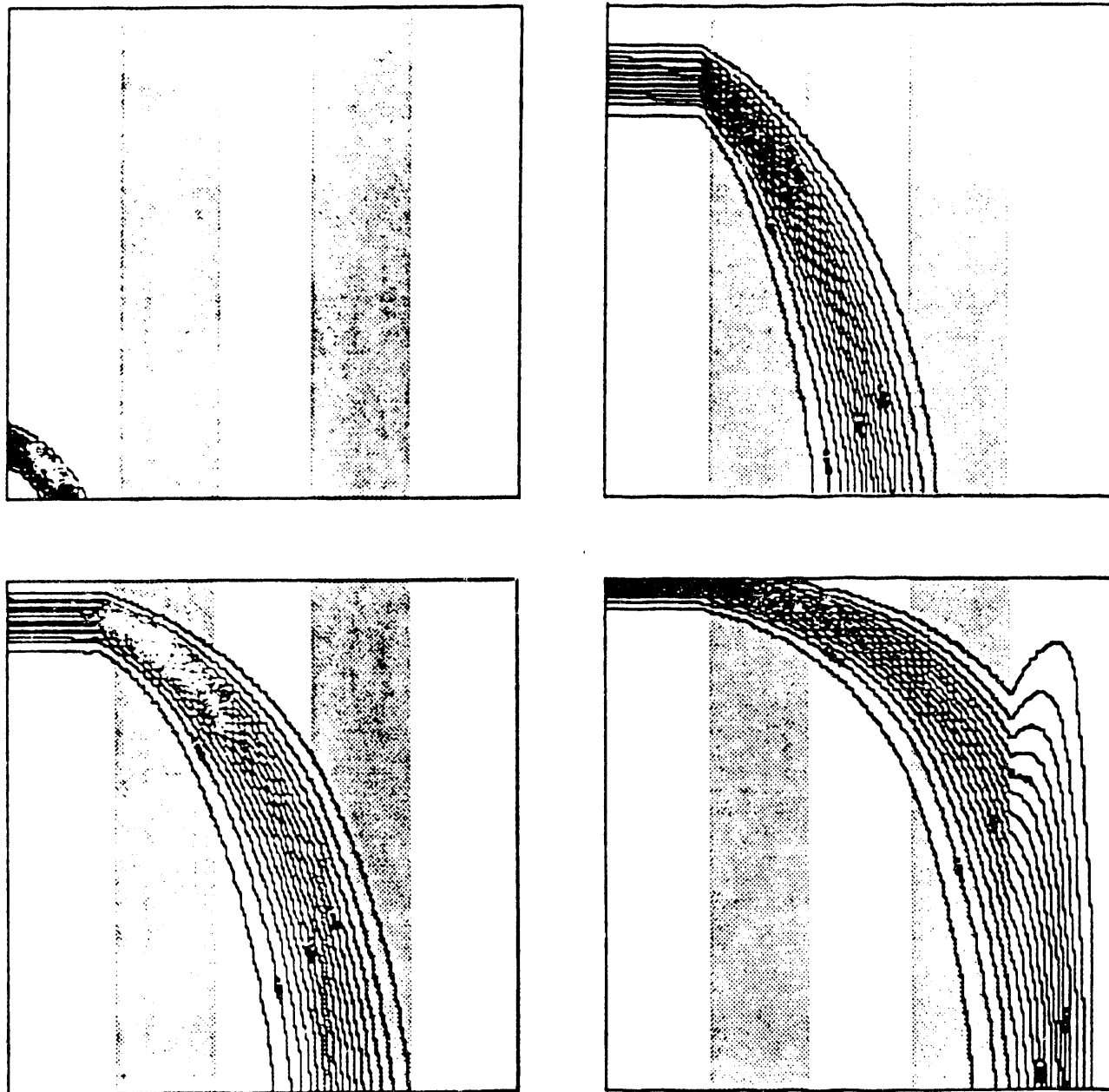


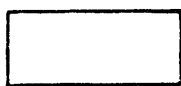
Figure 30.

Effect of heterogeneity:

IMPES 50 by 50



Low permeability bands



High permeability bands

Figure 31.

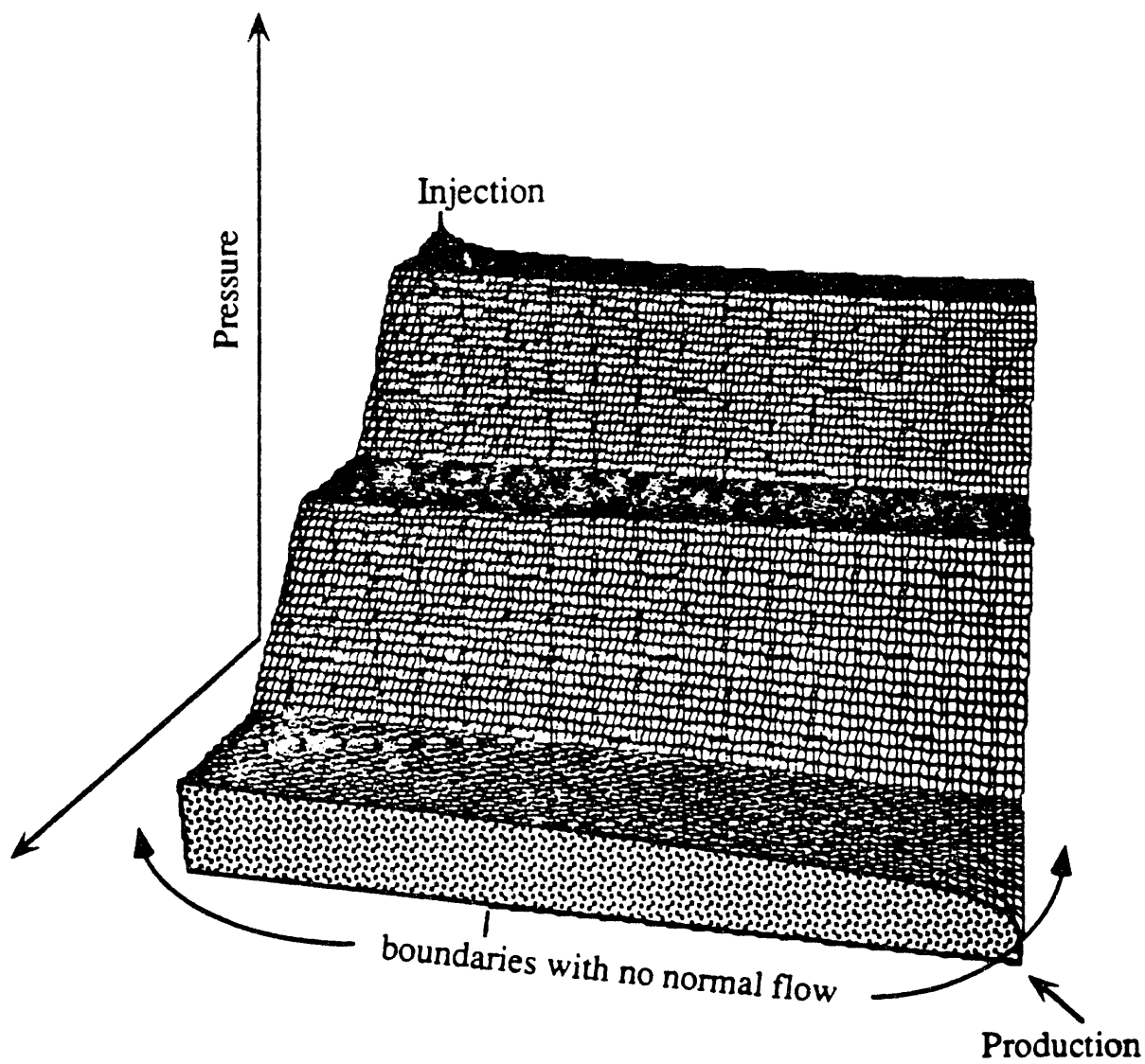
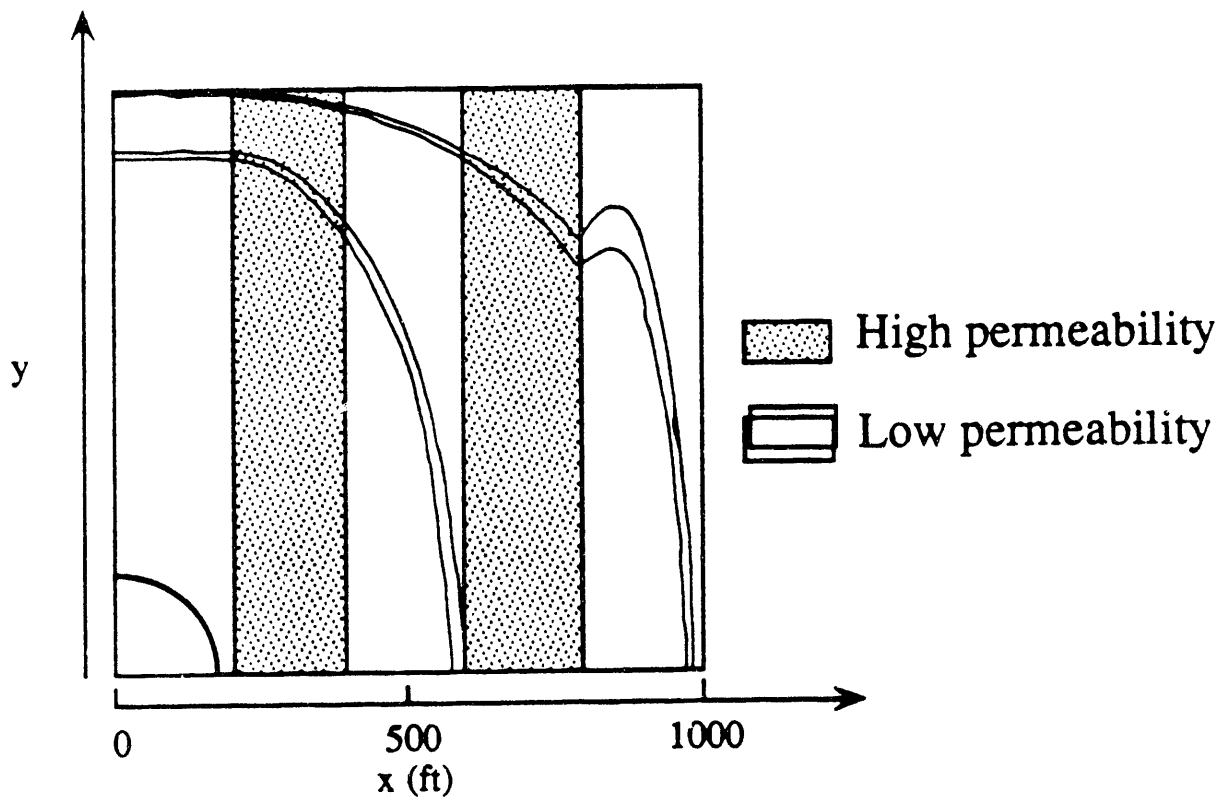


Figure 32.

# Concentration contour lines Miscible displacement



**Figure 33.**

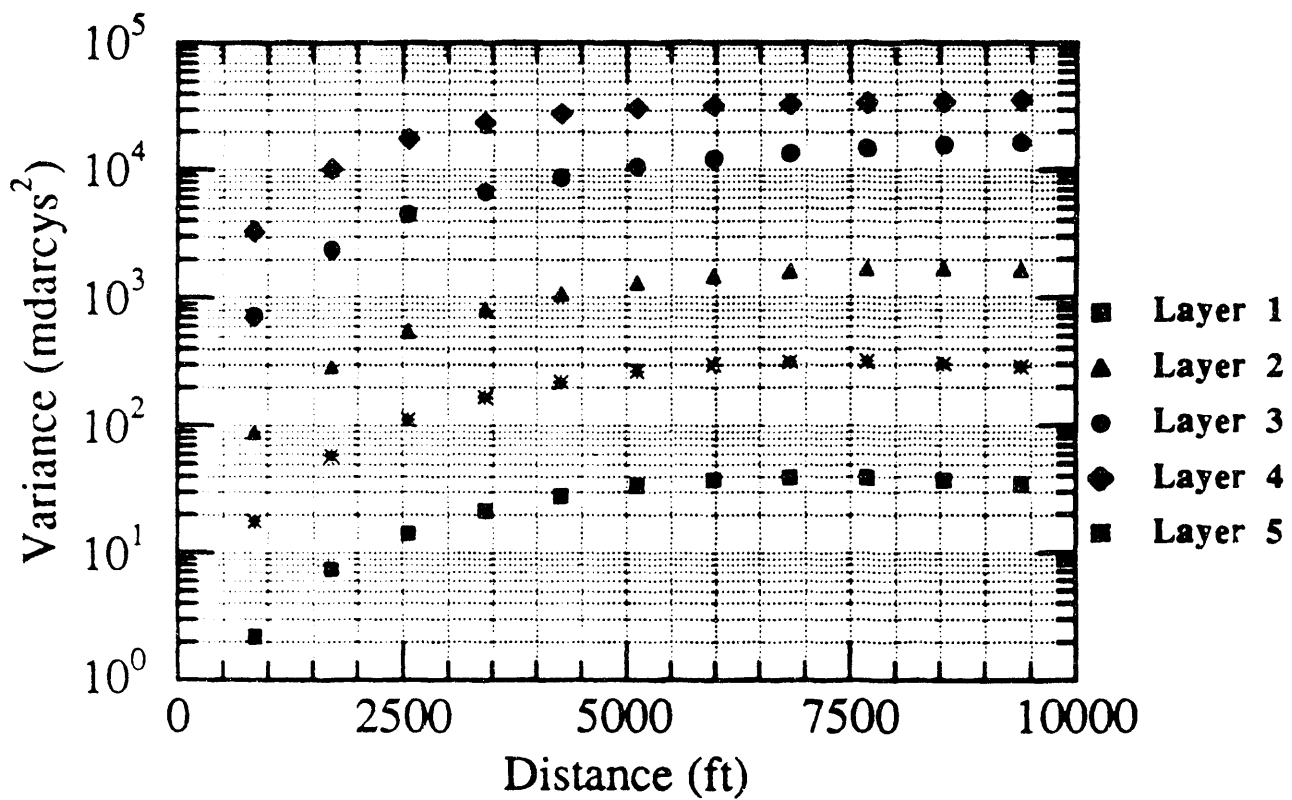


Figure 34. 2-D Semi-variogram for Five Layers of Real Permeability Data

Miscible displacement - real field data  
Contour lines

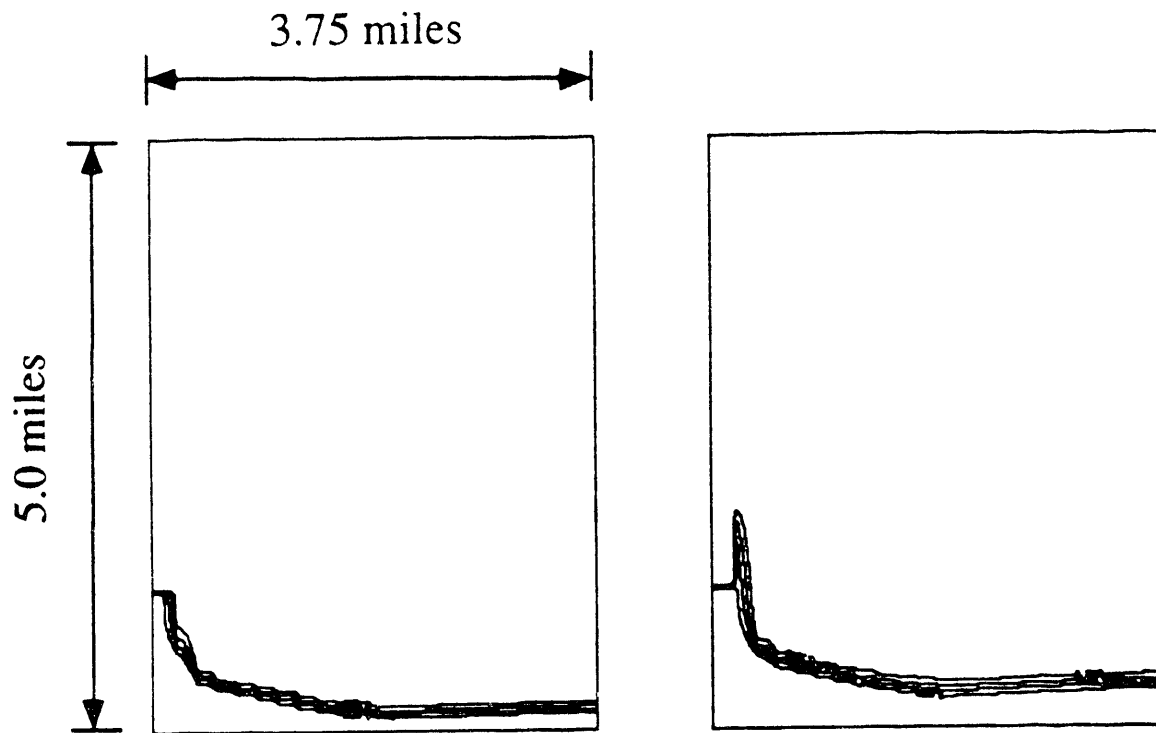


Figure 35.

### iPSC/2 (386) Speed-ups

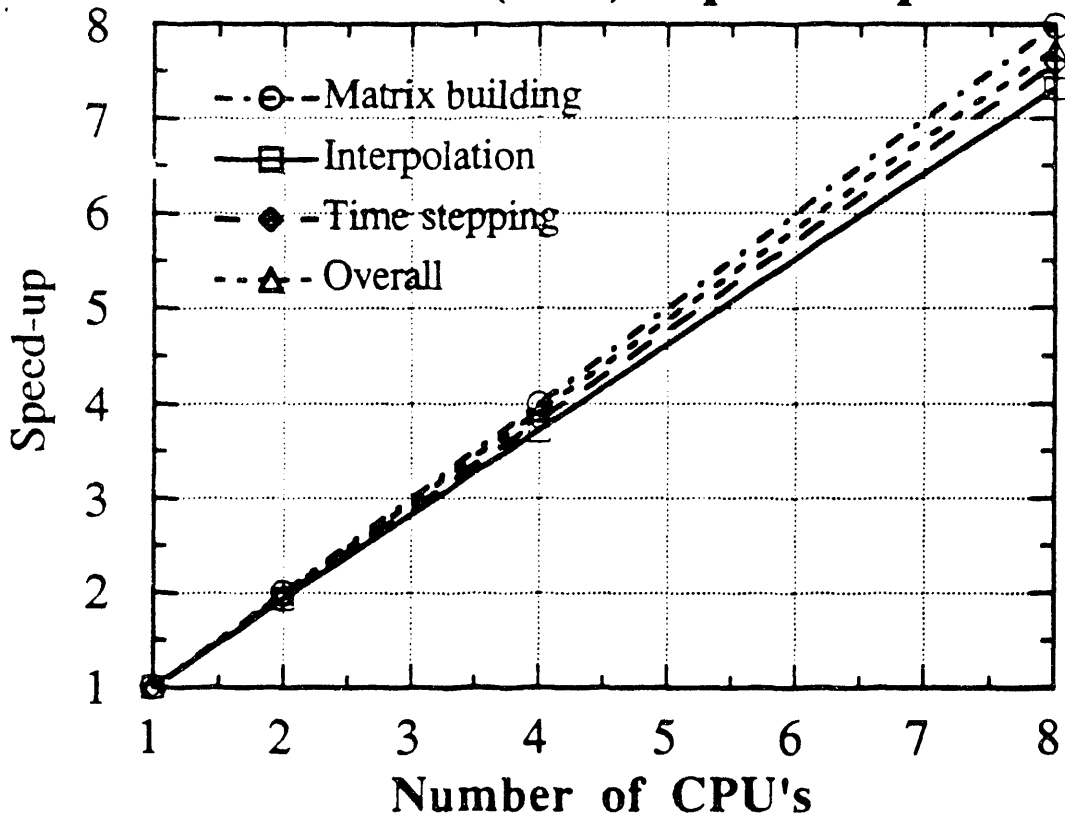


Figure 36. iPSc/2 Speedups for OSMG Method

**APPENDIX 1**

**FINAL OIL AND GAS  
RESERVOIR CANDIDATE LIST**

**STATE LANDS ENERGY  
RESOURCE OPTIMIZATION  
PROJECT**

Final Oil Candidate List

JACKSON BARRIER STRANDPLAIN SANDSTONE

	Cum. Prod MMSTB	Total Reservoir Wells Drilled 1986	RRC EOY Reservoir Producers 1987
Seventy-six, west	4.6	56	46
FRIO FLUVIAL/DELTAIC SANDSTONE (VICKSBURG)			
SUN	26	144	30
SUN (F-1-M 4950)	1.25	16	
Field total	27.25		
SAN ANDRES/GRAYBURG CARBONATE-SCBP			
Keystone-San Andres	2.5	86	76
PERMIAN SANDSTONE AND CARBONATE			
Keystone-Colby	70.63	1012	741
CLEAR FORK PLATFORM CARBONATE			
Keystone-Holt	38.8	166	159
DELAWARE SANDSTONE			
Tunstill	11.23	202	125
MIOCENE BARRIER/STRANDPLAIN SANDSTONE			
Powderhorn (5200 Sand)	4	9	5

NPC: 2063 RRC RES # : 82422001 GEOLOGICAL RESERVOIR CHARACTERISTICS

FIELD NAME SEVENTY-SIX, WEST RESERVOIR NAME:

PROVINCE: 220000 SUBPROVINCE: DISCOVERY YEAR: 1954 EIA CODE: 645723

BEG PLAY: 9 1009 JACKSON BARRIER/STRANDPLAIN SANDSTONE RRC DISTRICT: 4 STATE: 42 TEXAS

GAS PLAY:

GAS SUB-PLAY:

CURRENT OPERATOR: MAN-GAS, ARCO, TEXACO COUNTY: DUVAL ADDITIONAL COUNTIES:

---

PRODUCING FORMATION: COLE

DEPOSITIONAL SYSTEM: 152 BACK BARRIER AAPG GEOLOGICAL AGE CODE: 124

RESERVOIR FACIES:

LITHOLOGY: 1 SS TRAP TYPE: 7 NPP FRACTURED / FAULT : RESERVOIR DIP : 1.52 DEG CORE:

DEPTH TO TOP: 1.328 ft TVD: 1,328 ft CLAY CONTENT: -1.000 SHALE BREAK: 2

---

NPC: 2063 RRC RES #: 82422001

RESERVOIR INFORMATION

FIELD NAME: SEVENTY-SIX, WEST

RESERVOIR NAME:

PROVINCE: 220000

SUBPROVINCE:

DISCOVERY YEAR: 1954

BEG PLAY: 9 1009 JACKSON BARRIER/STRANDPLAIN SANDSTONE

RRC DISTRICT: 4

STATE: 42 TEXAS

GAS PLAY:

GAS SUB-PLAY:

PRODUCING FORMATION:

COLE

COUNTY: DUVAL

DEPOSITIONAL SYSTEM: 152 BACK BARRIER

DEPTH: 1,328 ft

GROSS PAY: 40ft

NET PAY: 15 ft

HEIGHT OF OIL COLUMN: 70 ft

GAS GRAVITY: . deg

AVERAGE POROSITY: 31.00%

AVERAGE PERMEABILITY: 1209.00 MD

PERM RANGE: 3,477 MD

API GRAVITY: 20.00 deg

INITIAL OIL SATURATION: 78.000 %	INITIAL WATER SATURATION: 22.000%	INITIAL GAS SATURATION: . %
CURRENT OIL SATURATION: 40.000 %	CURRENT WATER SATURATION: 40.000%	CURRENT GAS SATURATION: . %
RESIDUAL OIL SATURATION: 35.000 %	OIL VISCOSITY: 30.00 cp	FORMATION TEMPERATURE: 100 F

INITIAL FORMATION PRESSURE: 586 psi CURRENT FORMATION PRESSURE: 140 psi DYSKTRA-PARSONS COEFFICIENT: 0.72

INITIAL OIL FVF: 1.03 Res bbl/STB

MAJOR GAS CAP: N/D

FORMATION WATER SALINITY: 24000.00 PPM TDS

CURRENT OIL FVF: 1.00 Res bbl/STB

INITIAL GAS CAP/OIL RES:

INJECTION WATER SALINITY: -1.00 PPM TDS

INITIAL GOR: 300 SCF/BBL

CURRENT GOR: 13 SCF/BBL

FORMATION WATER RESISTIVITY: OHMS

BUBBLE POINT PRESSURE:

NPC: 2063                    RRC RES # : 82422001                    PRODUCTION DATA  
 FIELD NAME: SEVENTY-SIX, WEST                    RESERVOIR NAME:  
 PROVINCE: 220000                    SUBPROVINCE:                    DISCOVERY YEAR: 1954  
 BEG PLAY:            9 1009 JACKSON BARRIER/STRANDPLAIN SANDSTONE                    RRC DISTRICT: 4                    STATE: 42 TEXAS  
 GAS PLAY:  
 GAS SUB-PLAY:  
 PRODUCING FORMATION:                    COLE                    DEPTH: 1,328 ft  
 COUNTY:            DUVAL                    DEPOSITIONAL SYSTEM: 152 BACK BARRIER

OOIP:            3.136. M BBL    YEAR: 1986	PRIMARY RECOVERY:                    -1.000 M BBL/AC FT
CUM. OIL PROD: 4.603. M BBL    UNIT DATE: 1976	PRIMARY RECOVERY FACTOR:           -1.000
ANN. PRODUCTION: 64.100 M BBL    YEAR: SAME A/A	SECONDARY RECOVERY FACTOR:       -1.000
PRIMARY RECOVERY: -1.0 M BBL    YEAR: 1976	ULTIMATE RECOVERY FACTOR:       -1.000
ULT. RECOVERY:            M BBL    YEAR:	
CUM. GAS PROD:            MMSCF	

FIELD ACRES:            -1 ac                    PROVEN ACRES: 326 ac                    RESERVOIR ACRES: 320 ac  
 PRODUCTION TECHNOLOGY:                    DRIVE MECHANISM                    CURRENT DATE: -1  
 WELL SPACING: 20 ac    TOTAL WELLS: 47    PRODUCTION WELLS: 26    INJECTION WELLS: -1    FLD MULTIPLIER: -1.000  
 CUR. INJECTION RATE:    177 BD/WELL

**APPENDIX 2**  
**Data for the Seventy-Six, West Field**

**FIELD:** SEVENTY SIX, WEST, DUVAL COUNTY  
**B.E.G. PLATE:** JACKSON BARRIER/STRANDPLAIN SS  
**DEP. SYSTEM:** BACK BARRIER  
**TRAP:** UPDIP SS PINCH OUT  
**DRIVE:** SOLUTION GAS EXPANSION  
**DISCOVERY** 1-3-54  
**PRODUCTION FORMATION:** COLE  
**DEPTH:** 1,328 FT.  
**GROSS PAY:** 30-40 FT.  
**NET PAY:** 10-15 FT.  
**RESERVOIR DIP** 140 FT/MILE  
**OIL COLUMN:** 140 FT/MILE

**POROSITY = 31%      PERMEABILITY = 1,209 MD      APIG = 36**

**INITIAL:**       $S_o = 78$        $S_w = 22$   
**CURRENT:**       $S_o \cong 35-40$        $S_w \cong 30-40$   
**RESIDUAL:**       $S_o \cong 20-35$   
**RESERVOIR AREA:** 1,100 Ac.

**OOIP  $\cong$  10,000,000 bls**

**(1954-1967) PRIMARY RECOVERY:** 3,109,659; **FACTOR  $\cong$  0.3**  
**(1967-1988) SECONDARY RECOVERY:** 1,492,341; **FACTOR  $\cong$  0.15**  
**CUMULATIVE PRODUCTION:** 4,602,000 (1988)  
**ULTIMATE RECOVERY:** 5,000,000 bls.

**TARGET  $\cong$  1 - 1.5 X 10<sup>6</sup> bls.**

**Ulises Ricoy**  
**B. E. G./U. T.**  
**471-1534 Ext. 314**

\*U.S.GPO:1992-661-026/60046

**END**

**DATE  
FILMED**

**10 / 20 / 92**